공학박사 학위논문

Development of a Hybrid Stamp Coated with a Low-Surface-Energy, Diffusion-Blocking Layer for Organic Electronic Devices

낮은 표면 에너지와 확산 방지층으로 코팅된 하이브리드 도장의
개발 및 유기전자소자 제작에 대한 그 응용

2019년 8월

서울대학교 융합과학기술대학원
융합과학부 나노융합전공
차 석 균

Development of a Hybrid Stamp Coated with a Low-Surface-Energy, Diffusion-Blocking Layer for Organic Electronic Devices

지도교수 김 창 순

이 논문을 공학박사학위 논문으로 제출함.

2019년 7월

서울대학교 융합과학기술대학원
융합과학부 나노융합전공

차 석 균

차석균의 박사학위 논문을 인준함

2019 년 7 월

위 원 장 김 연 상 인

부위원장 김 창 순 인

위 원 송 윤 규 인

위 원 이 강 원 인

위 원 김 영 훈 인

Abstract

Development of a Hybrid Stamp Coated with a Low-Surface-Energy, Diffusion-Blocking Layer and Fabrication of Organic Electronic Devices

Sukgyun Cha

Program in Nano Science and Technology

The Graduate School of Convergence Science & Technology

Seoul National University

Since the pioneering work by Whitesides et al., termed “soft lithography”, poly(dimethylsiloxane) (PDMS) has been very widely used as a material composing a stamp from which various materials are transferred onto a target substrate. However, even more than 20 years after the first paper reporting this work, applications of PDMS-stamp-based materials transfer have been rather limited to simple cases where materials transfer alone is sufficient for their success and/or the quality of the transfer-bonded interfaces and the cleanliness of the transferred layers do not matter significantly. This is in part due to the following adverse properties of the PDMS stamp: absorption of small molecules by PDMS free volumes and contamination of the transferred layers by uncured oligomers in PDMS.

Here, I develop a hybrid stamp comprised of a PDMS bulk and a perfluoropolyether (PFPE) coating induced by a condensation reaction between not only PDMS and PFPE molecules but also adjacent PFPE molecules. A key role of the PFPE coating layer on the PDMS stamp is effective to prevent organic small molecules from being absorbed into the stamp and the uncured siloxane oligomers of the PDMS from migrating on a layer to be transferred. I prove the effectiveness and versatility of the PFPE-coated PDMS stamp by fabricating an organic light emitting diode whose organic-organic interface is formed by a transfer process and an organic hole-only device with a bottom electrode composed of a graphene bilayer transferred from the stamp. As a result, the mechanically bonded interfaces are sufficiently intimate at the molecular level compared to those of the same interface formed by thermal evaporation. Furthermore, the top surface of the transferred layer that was in contact with the stamp is enough to clean for injecting and extracting charge carriers. The PFPE-coated stamp demonstrated in this work is expected to be widely used in fabricating devices or systems that are especially difficult to realize using high-temperature or wet processes. An exciting example is full-color organic light-emitting device (OLED) displays with a resolution much higher than that of the current displays in smartphones, which is required for virtual reality applications but is difficult to fabricate using the current shadow mask-based patterning.

Keywords: PDMS stamps, PFPE coating, organic-pattern transfer, diffusion blocking layers, organic heterojunction

Student Number: 2013-31258

Contents

List of Figures

PDMS via the conventional wet-transfer method (using PMMA as a support layer).

Figure 2.3 Schematic illustration of the difference in the quality of support/graphene on PDMS, determined by wetting of the liquid bath, during the blow-drying process. (a) In the conventional wet-transfer case, sufficient wetting of a hydrophilic substrate by water provides conformal contact between graphene and the substrate without wrinkles when the sample is blow-dried using N_2 gas. (b) When a PDMS stamp, having a hydrophobic surface, is used instead of the hydrophilic substrate, water does not form a continuous layer between the graphene and the PDMS stamp, and consequently, the blow-drying process causes trapped water droplets to burst, followed by damaging the Au/graphene bilayer. (c) In our case, to prevent such problem, the surface tension of the liquid bath is decreased by mixing water with ethanol, resulting into sufficient wetting of the PDMS stamp by the mixture. As a result, a continuous layer of the mixture between the interfaces provides conformal contact comparable with the conventional wet-transfer case in (a).

Figure 2.4 Comparison of the quality of the transfer-printed graphene monolayer, determined by the surface tension of the liquid bath, water or the ethanol-water mixture. (a,b) Optical microscope images of the graphene on the SiO_2/Si substrate. The white arrow in (a) indicates the folded graphene induced by insufficient wetting. (c) Raman spectra of the graphene on the SiO_2/Si substrate. (d) Transmittances of the graphene on a glass substrate. Each line was obtained by averaging the transmittance of 5 samples.

Figure 2.5 Optical microscope image of the transferred graphene onto the PDMS stamp using water bath in our process.

Figure 2.6 Comparison photographs of the change in the quality of the Au/graphene bilayer on the PDMS stamp, determined by wetting of the liquid bath, during the blow-drying and heat treatment process. They were taken after scooping up the Au/graphene bilayer floated on (a) water bath and (b) the ethanol-water mixture bath with the PDMS stamp. (a) When water bath was used, water dewets in several locations, resulting into non-uniformly conformal contact between the graphene and the PDMS (the left photograph). Blow-drying N_2 gas not only removed most of water enclosed between the Au/graphene and the PDMS stamp, but also led to form winkles with water droplets trapped inside (the middle). After heat treatment, there were still the wrinkles, although the water droplets were removed (the right). (b) In the case of using the ethanol-water mixture bath, the mixture formed a continuous layer between the Au/graphene bilayer and the PDMS stamp, unlike the case of water bath (the left). Owing to the continuous layer, the mixture was mostly displaced by blow-drying process using N_2 gas, and then the Au/graphene bilayer were mildly corrugated (the middle). After heat treatment, the mild corrugation of the Au/graphene bilayer was flattened on the PDMS stamp with the globally conformal contact (the right).

Figure 2.7 Optical microscope images taken before and after stamping process of the graphene monolayer in the case of the elastomer stamp method. In this process, graphene on Cu foil is transferred by directly attaching it on the elastomer stamp, followed by etching away the Cu layer using the Cu etchant, and

consequently, it is printed on a target substrate. (a) The transferred graphene on the PDMS stamp with defects shaped like a dry earth. (b) The transfer-printed graphene on a glass substrate with defects far worse than that in (a).

Figure 2.8 Characterization of the transfer-printed pattern of a graphene monolayer onto fragile materials. (a,b) Optical microscope images of the patterned graphene on (a) MoO_3 and (b) PEDOT:PSS. The black and red arrows denote the fragile layer (MoO_3 or PEDOT:PSS) and the patterned graphene on the fragile layer, respectively. (c,d) Raman spectra of the patterned graphene on (c) MoO_3 and (d) PEDOT:PSS.

Figure 2.9 SEM image of the edge of the patterned graphene on MoO_3. The white and red arrows denote the MoO_3 layer and the patterned graphene on it, respectively. The pattern edge resolution is approximately 50 nm.

Figure 2.10 Morphological characterization of the transfer-printed graphene monolayer on the SiO_2/Si substrate. SEM images of the graphene before heat treatment in (a) and after heat treatment in (b). The white circle and arrow in (a) indicate graphene multilayer and wrinkle, respectively. (b) AFM image of the graphene used in (a). (d) Surface-height profile of the graphene along the white dotted line in (b).

Figure 2.11 Elemental characterization of the transfer-printed graphene. (a) STEM image of the region for the analysis. (b) EDX spectrum for element components on that region. Other signals besides C and Si peaks were measured from the TEM grid and the separation layer.

Figure 2.12 Schematic illustration of the patterning process. (a) CVD-grown graphene on Cu foil. (b) A patterned photoresist layer on the graphene/Cu obtained by the conventional photolithography process. (c) Etching away the graphene uncovered by photoresist via O_2 RIE process. (d) Removal of the patterned photoresist layer on the graphene/Cu by dipping in acetone.

Figure 2.13 Schematic illustration of the transferring process of the transfer-printed graphene onto the lacey carbon TEM grid for the element analysis using STEM-EDX. (a) Transfer-printed graphene on the SiO_2/Si substrate coated with PEDOT:PSS prepared by using our method. (b) Spin-coated PMMA layer onto the graphene/PEDOT:PSS/SiO_2/Si. (c) Dissolution of the PEDOT:PSS interlayer by dipping the PMMA/graphene/PEDOT:PSS/SiO_2/Si into clean water bath, and then the PMMA/graphene bilayer separated from the SiO_2/Si floating onto the water bath. (d) Scooping up the PMMA/graphene bilayer with the lacey carbon TEM grid. (e) Removal of the PMMA layer on the graphene/grid using acetone. (f) As a result, the transfer-printed graphene on the target substrate is transferred onto the lacey carbon TEM grid.

Figure 3.1 (a) Dip-coating of PFPE on a PDMS stamp. A PFPE thin layer is formed on a PDMS surface as a result of a condensation reaction between the hydroxyl groups in PFPE (b, c) and PDMS (d, e), as well as those in the adjacent PFPE molecules. As a result, PFPE molecules are strongly anchored to the PDMS surface and are linked with the adjacent PFPE molecules by Si–O–Si covalent bonding (f).

Figure 3.2 The thickness of a PFPE layer coated on a PDMS stamp for dipping times from 30 to 120 min. Each condition contains 5 samples.

Figure 3.3 Scanning electron microscopy images of a PFPE-coated PDMS stamp with a flat surface (a) and relief structures (b). (a) Side view, (b) top view. Scale bars are 2 and 50 μm, respectively.

Figure 3.4 Illustration of advantages of a PFPE-coated PDMS stamp

Figure 3.5 The PFPE coating on a PDMS stamp. (a,b) First, to hydrate the ethoxysilane end groups of PFPE into hydroxyl groups, a solution of ethoxysilane-terminated PFPE was diluted in IPA at 0.1 wt %, into which water (0.4 wt %) and acetic acid (0.1 wt %) were added. After keeping the solution in an atmosphere for 30 min, a PDMS stamp whose surface was modified with hydroxyl groups, prepared by UV-ozone treatment, was immersed in the solution and then stored for 2 h (c). (d) To remove excess PFPE, the stamp was sonicated twice in IPA for 5 min each time, after which it was rinsed with water. (e) Finally, the stamp was placed on a hot plate at 100 ˚C for 10 min to remove the residual IPA inside, and then was further heated at 150 ˚C for 15 min.

Figure 4.1 (a) Illustration of the transfer of an Alq_3 layer patterned into the Seoul National University logo from a stamp onto an NPB layer on an ITO-coated glass substrate. (b, c) Photoluminescence (PL) images of the stamps (top) and the substrates (bottom) obtained by placing them on an UV lamp with a center wavelength of 365 nm. The PFPE-coated and uncoated PDMS stamps

were used in (b) and (c), respectively. The images to the left and the right of the gray arrows correspond to the samples before and after the transfer, respectively. Note that the samples used for the ″before″ images in (b) and (c) were taken out of the glovebox for imaging only and were not used in the transfer processes yielding the ″after″ images. Scale bars: 1 cm. (d, e) Schematic diagrams showing the results of the transfer processes when (d) the PFPE-coated stamp and (e) the uncoated stamp were used.

Figure 4.2 Photoluminescence spectra of the stamps and the substrates after transferring an unpatterned 50-nm-thick Alq_3 layer on a PFPE-coated or uncoated PDMS stamp onto a 50-nm-thick NPB layer on an ITO-coated glass substrate. The excitation wavelength is 350 nm in (a) and 420 nm in (b).

Figure 4.3 Photoluminescence spectra of an Alq_3 layer and an NPB layer, both 50 nm in thickness, deposited on a glass substrate by thermal evaporation in vacuum. The excitation wavelength is 350 nm.

Figure 4.4 Thickness of an NPB layer on an ITO-coated glass substrate diffused into a PFPE-coated or uncoated PDMS stamp after being in contact with the stamp under a pressure of 2 MPa for a different duration from 5 to 40 min. The measurement was performed following the experiment described in Ref. 30 as follows: (i) a 100-nm-thick NPB layer was deposited onto an ITO-coated glass substrate by thermal evaporation; (ii) a PFPE-coated or PDMS stamp was brought into contact with the NPB layer, followed by storing the samples at 23 ˚C or 60 ˚C under a pressure of 2 MPa for a varying contact time; (iii) the stamp was carefully peeled off from the substrate; (iv) a step height of the NPB layer

was measured near the boundary of the contacted region. When the uncoated stamp was used, the number of molecules diffused from the substrate into the stamp, which increased with contact time, significantly increased with temperature. When the PFPE-coated stamp was used, in contrast, the thickness of the NPB layer on the substrate remained unchanged even after 40 min at 60 ˚C.

Figure 4.5 AFM height images of the ITO-coated glass substrate coated with the NPB layer onto which the patterned Alq_3 layer on (a) a PDMS stamp and (b) a PFPE-coated PDMS stamp were transferred. Scale bars: 2 μm. The profiles shown below were measured along the white dotted lines in the height images.

Figure 4.6 AFM height images of the ITO-coated glass substrate coated with the NPB layer in a region that was in direct contact with (a) a PDMS stamp and (b) a PFPE-coated PDMS stamp (in a region not covered with the Alq_3 patterns) during the transfer process. Scale bars: 2 μm. The profiles shown below were measured along the white dotted lines in the height images.

Figure 4.7 (a) Current density–voltage (*J*–*V*) and (b) external quantum efficiency–current density (η_{ext}–*J*) characteristics of organic light-emitting devices fabricated by transferring Alq_3 layers using uncoated (blue triangles) and PFPE-coated PDMS stamps (red squares), compared with those of a control device, where all layers were vacuum deposited (black circles). The device structure is glass substrate/ITO/50 nm NPB/50 nm Alq_3/0.5 nm LiF/100 nm Al.

Figure 4.8 (a) Current density–voltage (*J*–*V*) and (b) external quantum efficiency–current density (η_{ext}–*J*) characteristics of organic light-emitting devices fabricated by transferring Alq_3 layers using uncoated (blue lines, $OLED_{PDMS}$) and PFPE-coated PDMS stamps (red lines, $OLED_{PFPE}$), compared with those of control devices where all layers were vacuum-deposited (black lines, $OLED_{CTRL}$). For each type of OLEDs, 30 devices (6 devices per substrate) were fabricated. All 30 devices were operational in the cases of $OLED_{CTRL}$ and $OLED_{PFPE}$, whereas only 19 devices were not short-circuited for $OLED_{PDMS}$. The much higher yield of $OLED_{PFPE}$ than that of $OLED_{PDMS}$ is attributed to the capability of the PFPE layer to block diffusion of small molecules into the stamp and of the PDMS oligomers onto the target substrate.

Figure 4.9 X-ray photoelectron spectra of a graphene monolayer on a PET film transferred from (a) an uncoated PDMS stamp and (b) a PFPE-coated PDMS stamp. The insets show narrow-scan XPS spectra of the Si2p peak at 102 eV.

Figure 4.10 (a,b) Scanning electron microscopy and (c,d) atomic force microscopy images of a graphene monolayer transferred from (a,c) an uncoated PDMS stamp and (b,d) a PFPE-coated PDMS stamp. Scale bars in (a,b) and (c,d) are 25 and 2 μm, respectively.

Figure 4.11 XPS spectra of the I3d peaks at 629.9 eV and 618.4 eV for a graphene monolayer on a PET film transferred from (a) a PFPE-coated PDMS stamp and (b) an uncoated PDMS stamp. (c) XPS spectrum of a graphene mon-

olayer on a PET film transferred from a PFPE-coated PDMS stamp in a binding-energy range including 686 eV corresponding to the F1s electron.

Figure 4.12 Current density–voltage (*J*–*V*) characteristics of organic hole-only devices whose graphene bottom electrodes were formed by using a PDMS stamp (blue triangles) and a PFPE-coated PDMS stamp (red squares). *J* was not allowed to exceed ~3×104 mA cm^{-2} by the instrument setting. The device structure is shown in the inset.

Figure 4.13 Current density–voltage (*J*–*V*) characteristics of NPB hole-only devices whose graphene bottom electrodes were formed by using a PDMS stamp (blue) and a PFPE-coated PDMS stamp (red). *J* was not allowed to exceed ~3×104 mA cm^{-2} by the instrument setting.

Figure 4.14 Optical microscopy images of the top surfaces of NPB hole-only devices whose graphene bottom electrodes were formed by using (a) a PDMS stamp and (b) a PFPE-coated PDMS stamp (b). Scale bar: 40 μm.

Figure 4.15 Illustration of the transfer-printing of organic small molecule layers on a PFPE-coated PDMS stamp with relief structures from the stamp onto an organic small molecule layer on an ITO-coated glass substrate. (a) A thermally deposited organic-small molecule layers on the PFPE-coated PDMS stamp with relief structures (a) and the ITO-coated glass substrate (b). (c) Placing the structure-faced stamp onto the substrate, and then keeping it on a hot plate at 75 ˚C with a pressure of ~0.5 MPa for 15 min. (d) Peeling off the stamp

from the molecules/substrate. (e) Consequentially, the molecule patterns on the relief structures were transfer-printed onto the target substrate.

Figure 4.16 Optical microscope images of patterned $Be(bq)_2$:$Ir(phq)_2acac$ layers (thickness: 40 nm) on a 40-nm-thick NPB layer. The diameter of the patterns is 200 μm.

Figure 4.17 The device structure and the schematic energy-level diagram of the red phosphorescent OLED are shown in (a) and (b), respectively. (c) Normalized electroluminescence spectrum of the OLED (c).

Figure 4.18 (a) Current density–voltage (J–V) and (b) external quantum efficiency–current density (η_{ext}–J) characteristics of organic light-emitting devices fabricated by transfer-printing 50 nm $Be(bq)_2$:$Ir(phq)_2acac$ patterns (blue triangles) and 5 nm NPB/50 nm $Be(bq)_2$:$Ir(phq)_2acac$ patterns (green squares) using PFPE-coated PDMS stamps with relief structures, compared with those of control devices where all layers were vacuum-deposited (red circles). The inset shows EL images of the device at 6 V.

Figure 4.19 Organic patterns formed by a transfer-printing process. (a,c) Optical microscope images and (b,d) photoluminescence images of patterns of $Be(bq)_2$:$Ir(phq)_2acac$.

Figure 5.1 Summarization of further studies

List of Publications

[1] **S. Cha**, M. Cha, S. Lee, J. H. Kang, and C. Kim, Low-temperature, dry transfer-printing of a patterned graphene monolayer, *Scientific Reports*, **5**, 17877 (2015).

[2] **S. Cha** and C. Kim, Poly(dimethylsiloxane) stamp coated with a low-surface-energy, diffusion-blocking, covalently bonded perfluoropolyether layer and Its application to the fabrication of organic electronic devices by layer transfer, *ACS Applied Materials & Interfaces*, **10**, 24003 (2018).

Chapter 1 Introduction

1.1 Overview

1.1.1 Limitations of PDMS as a stamp in a contact transfer process

Contact transfer is a very powerful process that can form patterns and/or layers of various materials, such as polymers [1,2], metals [3,4], 2D materials [5–7], quantum dots (QDs) [8,9], nanoparticles (NPs) [10,11], nanowires [12,13], supramolecules [14], and deoxyribonucleic acids (DNAs) [15], on a target substrate under low-temperature and dry conditions (Fig. 1.1). In many such studies, poly(dimethylsiloxa-ne) (PDMS) is the most widely used material for stamps due to its low Young's modulus and surface energy, which makes it suitable for large area transfer of microstructures. However, absorbing organic small molecules, such as organic semiconductors and solvents, into free volumes of the PDMS [8,16–19] and/or contamination of a transferred layer by uncured siloxane oligomers of the PDMS [20–23] still remain serious problems in not only the contact transfer process, but also the others such as microfluidics and cell-culture systems.

For example, when nanoscale organic patterns, which is difficult to fabricate by conventionally thermal evaporating through a fine metal mask (FMM), is required, it can be easily and inexpensively fabricated by transferring organic layers formed on a patterned stamp onto a target substra-

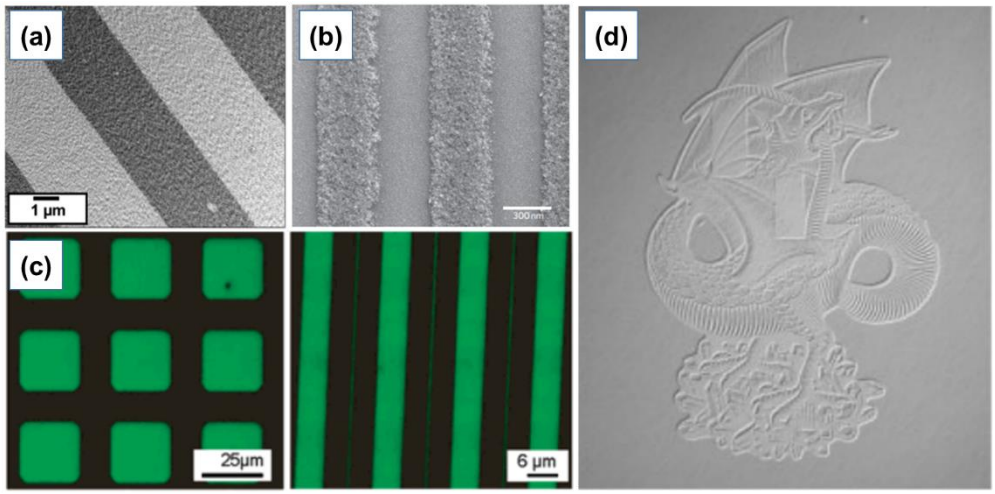

Figure 1.1 Examples of transferring of various materials using a contact transfer process. (a) nanoparticles (NPs) [10], (b) quantum dots (QDs), (c) deoxyribonucleic acids (DNAs) [15], (d) metals [3].

te. However, the PDMS can not be used as a stamp owing to the absorbing property. As another example, when materials, such as QDs, NPs, and nanowires, dispersed in organic solvents are coated on a surface of the PDMS stamp and then transferred onto a target substrate, the solvents can swell the stamp, preventing the materials from forming a continuous close-packed layer or periodically positioned ones on it. Therefore, the range of a solvent that can be used is very limited. Although a layer on the PDMS stamp is fully transferred onto a target substrate, the transferred layer can be severely degraded in its optical properties, such as photoluminescence (PL), and/or its electrical properties, such as charge carrier transport, by the PDMS oligomer present on it.

1.1.2 Previous studies to overcome problems with PDMS

Attempts have been made to form a layer on the PDMS that can block unwanted migration of the molecules in both directions perpendicular to the surface, because a cause of those problems — namely, absorbing organic small molecules and remaining the PDMS oligomers — is fundamentally their migration. For example, when organic layers on a patterned PDMS stamp are transfer-printed onto a target substrate, in order to avoid the organic layers from being degraded by the PDMS oligomers, the organic layers and the PDMS surface were decoupled by depositing Cr/Au bilayer before the organic layers were formed on the stamp [24]. However, extremely high Young's modulus of the metal bilayer prevents the layers to

be transferred on the stamp and the substrate from forming a conformal contact during the transfer process [25], so that the metal is not suitable. As another example, to avert swelling PDMS by absorbing solvents, Kim et al. deposited a parylene-C layer on the PDMS by chemical vapor deposition (CVD) before forming QDs dispersed in chloroform on it and then transfer-printing them [8]. However, since the parylene-C–PDMS interface is bonded by weak van der Waals interactions, the interface may be delaminated during peel-off of the stamp from the substrate, thereby leaving Parylene-C as an unwanted residue on the transferred layer. This possible concern is probably growing when transferring a layer with higher surface energy in comparison with that of the PDMS. In practice, when transferring graphene on a fluorine-resin-coated PDMS, whose interface is also bonded by van der Waals interactions, onto a target substrate, the whole coating layer is present on the transferred graphene after separating the stamp from the substrate [21,26]. Thus, to remove the coating layer, the transferred graphene and its underlying substrate are exposed to a high-temperature or wet process. Even though the coating layer has advantageous properties such as blocking of diffusion, low surface energy, and low Young's modulus, the weakly fixed layer on the PDMS is particularly unsuitable for transferring layers that are easily degraded to a wet or high-temperature process, such as organic semiconductors.

1.2 Common elements to understand a contact transfer process

1.2.1 Conditions for a reliable contact-transfer process

The contact transfer process is a method used to transfer a layer and/or patterns on a stamp onto a target substrate. In this process, the adhesion energy (G) between two contacting layers depends on two parameters: the chemical properties of the surface represented by the work of adhesion (W); the mechanical properties represented by $\phi(v, T)$ in which T is the temperature of the bulk in contact and v is a spend at which to disconnect. Therefore, one can express G as:

$$G = W(1 + \phi(v, T)) \tag{1.1}$$

In the contact transfer process, transferring materials on a stamp onto a substrate can be fundamentally achieved by the difference in the work of adhesion at the interface between the layer to be transferred and a stamp (and a substrate). The work of adhesion (W_{a-b}) between two materials 'a', 'b' is expressed as:

$$W_{a-b} = \gamma_a + \gamma_b - \gamma_{a-b} \tag{1.2}$$

where, γ_a, γ_b, and γ_{a-b} are the surface energy of material 'a', the surface energy of material 'b', and the interfacial free energy between materials 'a' and 'b'. The work of adhesion at the interface made of the same material is expressed as follows, and this force is called the cohesion.

$$W_a = 2\gamma_a \tag{1.3}$$

The surface energy value of each material can be obtained by measuring the contact angle between liquid and the surface of the material, and is expressed by the following Young's equation:

$$\gamma_s - \gamma_{sl} = \gamma_l \cos\theta \tag{1.4}$$

where, γ_s, γ_{sl}, γ_l, and θ are the solid surface free energy, the solid/liquid interfacial free energy, the liquid surface free energy, and the contact angle. The contact angle that satisfies equ. 1.4 can not be obtained without paying close attention to the measurement. Therefore, the measurement conditions required for the calculation of surface energy are as follows.

- The measured contact angle must be Young's angle. It is recommended that Young's contact angle be measured once a droplet has been formed on the solid surface, and then the volume of the droplet is finely grown using a syringe.
- The liquid used for the measurement shall be very pure.
- There should be no absorption or reactivity between the liquid and solid used. In particular, in the case of polymer, the polymer should not cause swelling in the liquid. Therefore, careful attention should be paid to the selection of liquids.
- The surface of solid should be very uniform. If it is non-uniform, measurement of Young's contact angle is impossible. In general, when the surface of solid is uneven, the contact angle actually measured is larger than

Young's contact angle.

- The surface energy of the liquid must be larger than that of the solid. If the calculated γ_s is greater than γ_l, the liquid must be selected again.

Owens et al. assume that γ_{sl} is the geometric mean of the force due to dispersion and polarity, and is expressed as:

$$\gamma_{sl} = \gamma_s + \gamma_l - 2\left(\gamma_s^{\mathrm{d}}\gamma_l^{\mathrm{d}}\right)^{0.5} - 2\left(\gamma_s^{\mathrm{p}}\gamma_l^{\mathrm{p}}\right)^{0.5} \tag{1.5}$$

γ_l^{d} and γ_l^{p} are the eigenvalue of the liquid used for the measurement, d and p are the parameters by the dispersion and polarity, respectively. By combining equations (3) and (4), the following equations can be obtained:

$$\gamma_l\,(1 + \cos\theta) = 2\left(\gamma_s^{\mathrm{d}}\gamma_l^{\mathrm{d}}\right)^{0.5} + 2\left(\gamma_s^{\mathrm{p}}\gamma_l^{\mathrm{p}}\right)^{0.5} \tag{1.6}$$

From this equ. 1.5, γ_s^{d} and γ_s^{p} can be obtained by solving the simultaneous equations obtained by measuring two kinds of liquids.

$$\gamma_{a-b} = \gamma_a + \gamma_b - \frac{4\left(\gamma_a^{\mathrm{d}}\gamma_b^{\mathrm{d}}\right)}{\gamma_a^{\mathrm{d}} + \gamma_b^{\mathrm{d}}} - \frac{4\left(\gamma_a^{\mathrm{p}}\gamma_b^{\mathrm{p}}\right)}{\gamma_a^{\mathrm{p}} + \gamma_b^{\mathrm{p}}} \tag{1.7}$$

From equ. 1.7, the interfacial free energy can be obtained and, as mentioned above, the surface energy of each materials can be obtained by using the contact angle between the solid and the liquid whose the value of surface energy is well known.

1.2.2 Stamp materials for a contact transfer process

- Poly(dimethylsiloxane) (PDMS):

PDMS is the most widely used material for fabricating stamps and offers numerous attractive properties that are well suited for a contact transfer process.

When fabricating structures whose feature size is in micro range, the mechanical properties of PDMS is sufficient to make conformal contact even with rough surfaces but still shows enough mechanical stiffness, because Young's modulus of PDMS is typically around 1.5 MPa. This property can be a great advantage when transferring material onto a substrate that has a rough surface, such as indium tin oxides, and/or when dust-like materials are present on the substrate. For many applications, the surface energy of PDMS is sufficiently low. Above all, PDMS stamps with relief structures can be easily fabricated by thermally curing prepolymers, which is inexpensive and commercially available materials. However, the PDMS stamp has the disadvantage that not only the above-mentioned problems but also a somewhat lower Young's modulus are not suitable for making nano-sized structures.

- Perfluoropolyether (PFPE):

PFPE has sufficient mechanical properties for a high-resolution stamp, adequate flexibility for a conformal contact with a substrate, low shrinkage for precision and accuracy of a transferring process, stability to various chemicals and very low surface energy properties. Since a PFPE mold is fabricated in a photo-curable system, it has advantages for reducing the phenomenon of thermal shrinkage as compared with that fabricated in a thermal curing system such as a PDMS mold, and can also reduce the time required for mold production. However, since the price of PFPE is too high, it may not be suitable as a stamp material that is used many times.

- Poly(urethane acrylate) (PUA):

	PDMS	PFPE	PUA
Surface energy	○	◎	△
Conformal contact	◎	△	△
Residues	◎	△	◎
Fine pattern	X	◎	◎
Chemical resistance	△	◎	○
Cost	◎	X	○

Figure 1.2 Comparison of properties of widely used materials as a stamp material. ◎: excellent, ○: good, △: average, X: poor.

A noteworthy characteristic of PUA is that it has a high density of fine patterns below 100 nm due to its sufficiently high mechanical properties like PFPE. It also has excellent chemical resistance to various organic solvents. However, there is a disadvantage that additional processes are required to remove trapped polymer radicals and any remaining unsaturated acrylate in the mold.

1.3 Scope of this thesis

This thesis is describing the result of applying hybrid stamp for organic small molecular transfer process and applying it to fabrication of organic electronic device. In *Chapter* 2, the first study focuses on low-temperature and dry-type transfer processes that can form high-quality patterned graphenes on wet, high-temperature, and plasma-sensitive materials such as organic semiconductors. The second study (*Chapter* 3) is a development of a hybrid stamp consisting of a PDMS bulk and a PFPE coating layer induced by a condensation reaction between PDMS and perfluoropolyether (PFPE) molecules as well as adjacent PFPE molecules. In *Chapter* 4, the efficiency and versatility of the PFPE-coated PDMS stamp in the thin film transfer process were evaluated by using an organic hole-only having an organic light-emitting diode including an organic-organic interface formed by the transfer process and a lower electrode composed of a graphene double layer. Finally, in *Chapter 5*, I comprehensively summarized each chapter and briefly discuss the further studies of the PFPE-coated PDMS stamp through

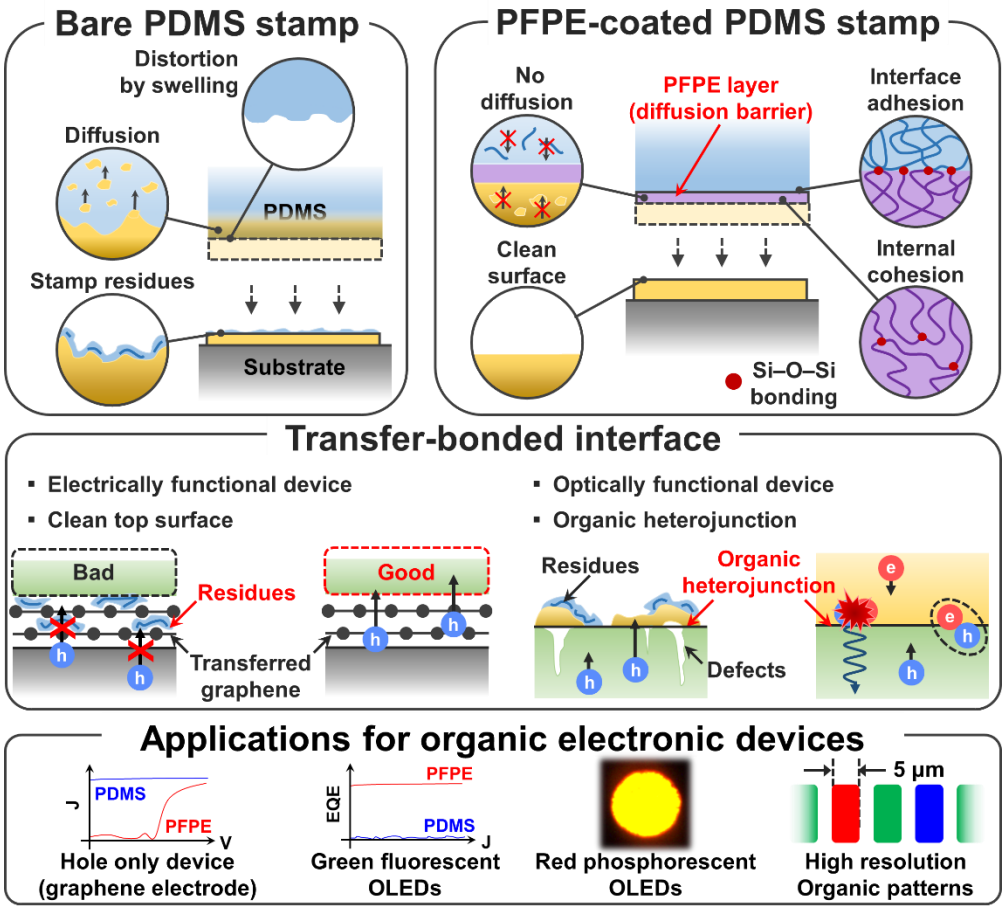

Figure 1.3. Summarization of my research

the identification of its advantages and disadvantages.

1.3.1 Development of a process for transferring of graphene patterns and the motivation for the need to coat a PFPE layer on PDMS

In *Chapter 2*, I demonstrate a low-temperature, dry process capable of transfer-printing a patterned graphene monolayer grown on Cu foil onto a target substrate using an elastomeric stamp. A challenge in realizing this is to obtain a high-quality graphene layer on a hydrophobic stamp made of PDMS, which is overcome by introducing two crucial modifications to the conventional wet-transfer method – the use of a support layer composed of Au and the decrease in surface tension of the liquid bath. Using this technique, patterns of a graphene monolayer were transfer-printed on poly(3,4-ethylenedioxythiophene):polystyrene sulfonate and MoO_3, both of which are easily degraded when exposed to an aqueous or aggressive patterning process. I discuss the range of application of this technique, which is currently limited by oligomer contaminants, and possible means to expand it by eliminating the contamination problem. These results have been published as ″Low-temperature, dry transfer-printing of a patterned graphene monolayer″ by S. Cha, M. Cha, S. Lee, J. H. Kang, and C. Kim, *Sci*. *Rep*., **5**, 17877 (2015).

1.3.2 Overcoming limitation of PDMS as a stamp in a contact transfer process

In *Chapter 3*, I demonstrate that a stamp composed of a PDMS bulk and

perfluoropolyether (PFPE) coating fabricated by a simple dip-coating method has the following properties that are ideal for the transfer patterning of various materials. Deposited by a condensation reaction between PDMS and PFPE molecules as well as the adjacent PFPE molecules, the PFPE coating has a strong adhesion to the PDMS surface and strong internal cohesion, while providing a low energy surface. Furthermore, it is also found that the PFPE molecules self-assembled and formed a dense and continuous film along the surface of the relief structure of the stamp. These results have been published as ″Poly(dimethylsiloxane) stamp coated with a low-surface-energy, diffusion-blocking, covalently bonded perfluoropolyether layer and its application to the fabrication of organic electronic devices by layer transfer″ by S. Cha and C. Kim, *ACS Applied Materials & Interfaces*, **10**, 24003 (2018).

1.3.3 Application of the PFPE-coated PDMS stamp to the fabrication of organic electronic devices

In *Chapter 4*, I found that a PFPE film coated on PDMS stamp serves as a bidirectional diffusion barrier: it effectively prevents organic small molecules deposited on the stamp from being absorbed into free volumes of PDMS; it also prevents PDMS oligomers from migrating onto the layer to be transferred, thereby avoiding the contamination of that layer. It is demonstrated that morphological and elemental characterization of the surfaces of the transferred organic semiconductor and graphene layers

confirms a successful transfer with a high degree of surface cleanliness. The quality of interfaces mechanically bonded using the PFPE-coated stamps and the cleanliness of the transferred layers are remarkably high that the electronic functions of a transfer-bonded organic heterojunction are comparable to those of the same interface formed by vacuum deposition, and that the charge transport across the transfer-bonded graphene–graphene and graphene–MoO_3 interfaces is efficient. These results have been published as ″Poly(dimethylsiloxane) stamp coated with a low-surface-energy, diffusion-blocking, covalently bonded perfluoropolyether layer and its application to the fabrication of organic electronic devices by layer transfer″ by S. Cha and C. Kim, *ACS Applied Materials & Interfaces*, **10**, 24003 (2018). Additionally, I show that the characteristics of the phosphorescent OLEDs fabricated by transfer-printing of organic patterns are comparable to those of the control device, where all layers were thermally deposited in vacuum. This result is the first demonstration of fabricating a highly efficient phosphorescent OLED, which is composed of a commercially useful structure, by forming a pattern through a contact transfer process. I also demonstrated that the transfer-printing process using the PFPE-coated PDMS stamp can be used to provide a possible way for fabricating high-resolution organic patterns.

1.4 References

[1] W. M. Lackowski, P. Ghosh, and R. M. Crooks, Micron-scale patterning of hyperbranched polymer films by micro-contact printing, *J. Am. Chem. Soc.*, **121**, 1419 (1999).

[2] Y. Ka, H. Hwang, and C. Kim, Hybrid organic tandem solar cell comprising small-molecule bottom and polymer:fullerene top subcells fabricated by thin-film transfer, *Sci. Rep.*, **7**, 1942 (2017).

[3] H. Schmid, H. Wolf, R. Allenspach, H. Riel, S. Karg, B. Michel, and E. Delamarche, Preparation of metallic films on elastomeric stamps and their application for contact processing and contact printing, *Adv. Funct. Mater.*, **13**, 145 (2003).

[4] C. Kim, M. Shtein, and S. R. Forrest, Nanolithography based on patterned metal transfer and its application to organic electronic devices, *Appl. Phys. Lett*, **80**, 4051 (2002).

[5] K. S. Kim, Y. Zhao, H. Jang, S. Y. Lee, J. M. Kim, K. S. Kim, J. -H. Ahn, P. Kim, J. Y. Choi, and B. H. Hong, Large-scale pattern growth of graphene films for stretchable transparent electrodes, *Nature*, **457**, 706 (2009).

[6] G. -H. Lee, Y. -J. Yu, X. Cui, N. Petrone, C. -H. Lee, M. S. Choi, D. -Y. Lee, C. Lee, W. J. Yoo, K. Watanabe, T. Taniguchi, C. Nuckolls, P. Kim, and J. Hone, Flexible and transparent MoS_2 field-effect transistors on hexagonal boron nitride-graphene hetero-structures, *ACS Nano*, **7**, 7931 (2013).

[7] G. Plechinger, F. Mooshammer, A. Castellanos-Gomez, G. Steele, C. Schu¨ller, and T. Korn, Optical spectroscopy of interlayer coupling in artificially stacked MoS_2 layers, *2D Mater*., **2**, 034016 (2015).

[8] L. Kim, P. O. Anikeeva, S. A. Coe-Sullivan, J. S. Steckel, M. G. Bawendi, and V. Bulović, Contact printing of quantum dot light-emitting devices, *Nano Lett*., **8**, 4513 (2008).

[9] T. -H. Kim, K. -S. Cho, E. K. Lee, S. J. Lee, J. Chae, J. W. Kim, D. H. Kim, J. -Y. Kwon, G. Amaratunga, S. Y. Lee, B. L. Choi, Y. Kuk, J. M. Kim, and K. Kim, Full-colour quantum dot displays fabricated by transfer printing, *Nat*. *Photonics*, **5**, 176 (2011).

[10] T. Kraus, L. Malaquin, H. Schmid, W. Riess, N. D. Spencer, and H. Wolf, Nanoparticle printing with single-particle resolution, *Nat*. *Nanotechnol*., **2**, 570 (2007).

[11] V. Santhanam and R. P. Andres, Microcontact printing of uniform nanoparticle arrays, *Nano Lett*., **4**, 41 (2004).

[12] T. Takahashi, K. Takei, J. C. Ho, Y. -L. Chueh, Z. Fan, and A. Javey, Monolayer resist for patterned contact printing of aligned nanowire arrays, *J*. *Am*. *Chem*. *Soc*., **131**, 2102 (2009).

[13] C. H. Lee, D. R. Kim, and X. Zheng, Fabricating nanowire devices on diverse substrates by simple transfer-printing methods, *Proc*. *Natl*. *Acad*. *Sci*. *U.S.A*., **107**, 9950 (2010).

[14] C. M. Bruinink, C. Nijhuis, M. Peter, B. Dordi, O. Crespo-Biel, T. Auletta,

A. Mulder, H. Schonherr, G. Vancso, J. Huskens, and D. Reinhoudt, Supramolecular microcontact printing and dip-pen nanolithography on molecular printboards, *Chem*. *Eur*. *J*., **11**, 3988 (2005).

[15] S. A. Lange, V. Benes, D. P. Kern, J. H. Ho¨rber, and A. Bernard, Microcontact printing of DNA molecules, *Anal*. *Chem*., **76**, 1641 (2004).

[16] K. Glasmästar, J. Gold, A. S. Andersson, D. S. Sutherland, and B. Kasemo, PDMS absorption of small molecules and consequences in microfluidic applications, *Lab Chip*, **6**, 1484 (2006).

[17] R. Hawaldar, P. Merino, M. R. Correia, I. Bdikin, J. Grácio, J. Méndez, J. A. Martin-Gago, and M. K. Singh, Convenient method for modifying poly(dimethylsiloxane) to be airtight and resistive against absorption of small molecules, *Anal. Chem.*, **82**, 5965–5971 (2010).

[18] J. P. Rolland, E. C. Hagberg, G. M. Denison, and K. R. Carter, and J. M. De Simone, Patterned removal of molecular organic films by diffusion, *Langmuir*, **27**, 9073−9076 (2011).

[19] J. Choi, D. Kim, P. J. Yoo, and H. H. Lee, Simple detachment patterning of organic layers and its application to organic light-emitting diodes, *Adv. Mater.*, **17**, 166−171 (2005).

[20] S. Yunus, C. de Crombrugghe de Looringhe, C. Poleunis, and A. Delcorte, Diffusion of oligomers from polydimethylsiloxane stamps in microcontact printing: Surface analysis and possible application, *Surf. Interface Anal.*, **39**, 922−925 (2007).

[21] J. Song, F. -Y. Kam, R. -Q. Png, W. -L. Seah, J. -M. Zhuo, G. -K. Lim, P. K. Ho, and L. -L. Chua, A general method for transferring graphene onto soft surfaces, *Nat. Nanotechnol.*, **8**, 356–362 (2013).

[22] K. Glasmästar, J. Gold, A. -S. Andersson, D. S. Sutherland, and B. Kasemo, Silicone transfer during microcontact printing, *Langmuir*, **19**, 5475–5483 (2003).

[23] S. Cha, M. Cha, S. Lee, J. H. Kang, and C. Kim, Low-temperature, dry transfer-printing of a patterned graphene monolayer, *Sci. Rep.*, **5**, 17877 (2015).

[24] C. Kim, Y. Cao, W. O. Soboyejo, and S. R. Forrest, Patterning of active organic materials by direct transfer for organic electronic devices, *J. Appl. Phys.*, **97**, 113512 (2005).

[25] Y. Cao, C. Kim, S. R. Forest, and W. Soboyejo, Effects of dust particles and layer properties on organic electronic devices fabricated by stamping, *J. Appl. Phys.*, **98**, 033713 (2005).

[26] J. H. Beck, R. A. Barton, M. P. Cox, K. Alexandrou, N. Petrone, G. Olivieri, S. Yang, J. Hone, and I. Kymissis, Clean graphene electrodes on organic thin-film devices via orthogonal fluorinated chemistry, *Nano Lett.*, **15**, 2555–2561 (2015).

Chapter 2 Low-Temperature, Dry Transfer-Printing of a Patterned Graphene Monolayer

2.1 Introduction

Graphene, a one-atom-thick layer of carbon atoms arranged in a hexagonal lattice, has outstanding electrical [1,2] and mechanical [3,4] properties, as well as high optical transmittance [5]. For this reason, many electronic and photonic devices employing graphene, as either an active layer or a transparent electrode, have been demonstrated, such as light-emitting diodes (LEDs) [6,7], solar cells [8,9], field-effect transistors (FETs) [10], photodetectors [11], touch screens [12], terahertz wave modulators [13–15], and Schottky junction devices [16,17]. In many such demonstrations, a graphene layer has been deposited by transferring it onto a device substrate following the conventional wet-transfer method, where a graphene–polymer bilayer floating on a water bath is scooped by the substrate [18]. And when the patterning of graphene layers is required, it has mostly been performed after graphene transfer, typically using photolithography followed by reactive-ion etch (RIE) [19,20]. However, this method of obtaining patterned graphene layers — the wet-transfer and subsequent patterning process — has only a limited range of applications, where graphene layers must be deposited and patterned, when necessary, prior to deposition of any material that is too fragile to withstand a wet, high-temperature, or plasma

process. Notable, practically important examples of such materials are organic semiconductors [21] and organometal trihalide perovskite compounds [22].

Attention, therefore, has been focused on development of dry-transfer techniques [23]. For example, a graphene layer grown on a Cu layer on a donor substrate can be directly transferred onto a target substrate, by delaminating the graphene–Cu interface when the target substrate in contact with the graphene layer is peeled off from the donor substrate [24]. However, for selective delamination, the target substrate needs to be coated with an epoxy adhesion layer, which makes this technique unsuitable for high-performance electronic devices: for example, it cannot be applied to fabrication of an LED with a top graphene electrode, since the adhesion layer in this case would be placed in the device interior, just beneath the graphene electrode, impeding efficient charge injection. Another approach is to transfer-print a graphene layer coated with a 'self-release' layer from an elastomeric stamp onto a target substrate [25], where reliable transfer is achieved by choosing an appropriate self-release layer that assures the selective delamination at the interface between that and the elastomer. Although the transfer process itself is dry, removing the self-release layer transferred along with the graphene is typically achieved with an organic solvent, ultimately limiting applications of this method. Jung et al. demonstrated a technique capable of transferring graphene monolayers without an adhesion or a self-release layer [26]. In this mechano-electro-thermal process, complete transfer, instead, requires application of high temperature (≥160 ˚C) and voltage (≥600 V) while a graphene layer grown on Cu foil is pressed

onto a target substrate.

In this chapter, I demonstrate a low-temperature, dry transfer process capable of transfer-printing a patterned graphene monolayer onto a target substrate that can be damaged or degraded by a wet, plasma or high-temperature process. In this process, a graphene monolayer on Cu foil, which is grown by chemical vapor deposition (CVD) and then patterned using a conventional lithographic process, is transferred onto a stamp made of poly(dimethylsiloxane) (PDMS), and subsequently transfer-printed from the stamp onto the target substrate. The graphene transfer from Cu foil to PDMS is achieved using the conventional wet-transfer process [18], with the following two modifications: the use of Au, instead of poly(methylmethacrylate) (PMMA), as a material for the support layer, and the decrease in surface tension of the liquid bath using a water-ethanol mixture. These modifications are critical in preventing defect formation in a graphene monolayer during its transfer onto a PDMS stamp, thereby leading to a minimum sheet resistance of 573 Ω/sq for a graphene monolayer transfer-printed onto a glass substrate. Furthermore, I demonstrate transfer-printing of patterned graphene monolayers on poly(3,4-ethyenedioxythiophene):polystyrene sulfonate (PEDOT:PSS) and MoO_3, which are representative examples of organic electronic materials and practically important metal oxides [27], respectively, that are usually damaged or degraded when exposed to aqueous or aggressive patterning processes. The morphological and elemental characterizations of the surfaces of transfer-printed graphene show

the existence of contaminants that are likely to be siloxane oligomers transferred from the PDMS stamp. I discuss the current range of application of this technique and possible means to expand it by eliminating the contamination problem.

2.2 Results and discussion

2.2.1 The low-temperature and dry transfer process for a CVD-grown graphene monolayer

A graphene monolayer on Cu foil was grown in a CVD system consisting of a tubular quartz reactor and a furnace. Experimental details described in Ref. 12 were closely followed except the following: Cu foil was annealed under a 5 SCCM flow of H_2 at 20 mTorr, and during growth, the reactor was filled with a mixture of CH_4 and H_2 at a total pressure of 150 mTorr, whose flow rates are 35 and 5 SCCM, respectively.

To transfer a graphene monolayer onto a target substrate that can be damaged or degraded by a wet or high-temperature process (Fig. 2.1), I first transfer a CVD-grown graphene onto a PDMS stamp following the conventional wet-transfer method (a to f): by scooping up, with the PDMS stamp, a graphene–support bilayer floating on liquid. After the support layer is removed by chemical etching, the graphene is transfer-printed on a target substrate (g to h). The first part of this process (a to f), although seemingly

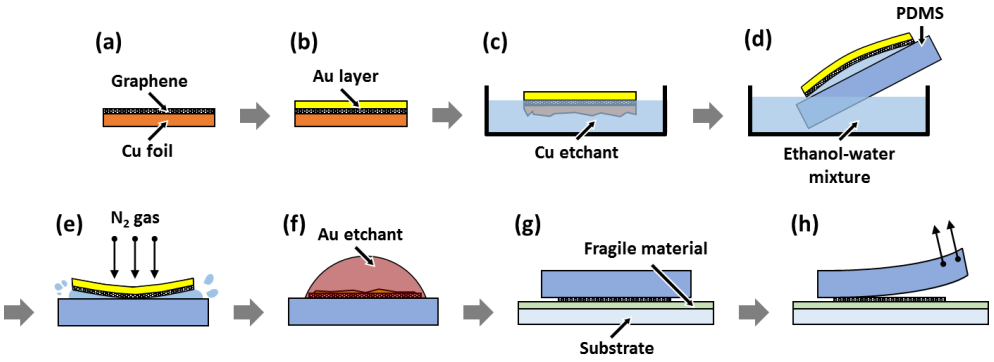

Figure 2.1 Schematic illustration of the low-temperature and dry transfer process for a CVD-grown graphene monolayer. (a) A CVD-grown graphene monolayer on Cu foil. (b) A thermally deposited Au layer onto the as-grown graphene monolayer on Cu foil. (c) Etching away Cu foil by floating it on a Cu etchant bath. (d) Scooping up the Au/graphene bilayer floated on the ethanol-water mixture bath with a PDMS stamp. (e) Blow-drying the Au/graphene bilayer on the PDMS stamp using N_2 gas, followed by baking it. (f) Etching away the Au layer on the graphene/PDMS using an Au etchant. (g) Placing the graphene-faced stamp onto a target substrate coated with fragile material, and then baking it. (h) Peeling off the PDMS stamp from the graphene/substrate. Consequentially, the graphene monolayer on Cu foil was transferred onto the target substrate.

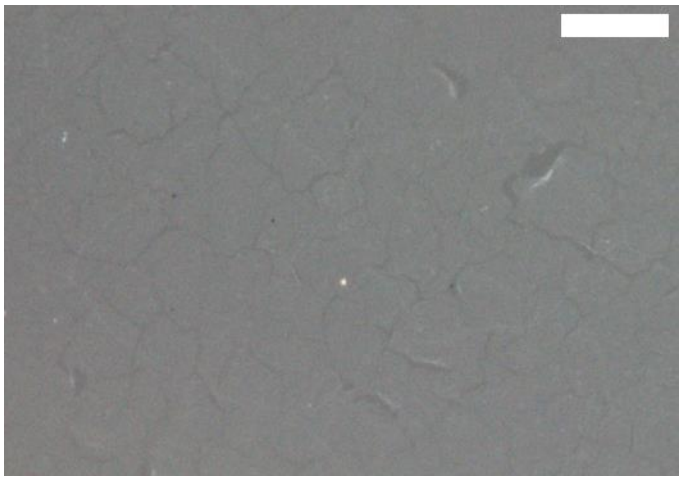

Figure 2.2 Optical microscope image of the transferred graphene onto the PDMS via the conventional wet-transfer method (using PMMA as a support layer).

similar to the conventional wet-transfer technique [18], has two distinct features, which are crucial to obtain a high-quality graphene monolayer on a target substrate.

First, as a support layer material, I use thermally deposited Au, instead of PMMA, which is most widely used for this purpose in the wet-transfer method [28]. PDMS, the material chosen for a stamp owing to its mechanical and chemical properties suitable for various transfer-printing techniques [29], swells when immersed in an organic solvent [30] that can dissolve the PMMA support layer, such as acetone and chloroform. When this occurs, the graphene monolayer cracks, creating a large number of defects (Fig. 2.2). On the contrary, the use of a Au support layer allows one to obtain a high-quality graphene monolayer on PDMS, since Au can be removed using an aqueous etchant, which does not swell PDMS.

Second, for the liquid on which the graphene–Au bilayer floats and from which it is scooped with a PDMS stamp [Fig. 2.1(d)], I use an ethanol–water mixture, instead of water commonly used in the conventional wet-transfer technique. This is to decrease the surface tension of the liquid. In the conventional case, after the graphene–support bilayer is scooped with a hydphilic substrate [as in Fig. 2.1(d)], a thin layer of water is present throughout the graphene–substrate interface, providing sufficient lubrication at that interface. As a result, when the sample is blow-dried using a N_2 gun, the graphene and substrate form a conformal contact without wrinkles throughout the substrate, as the water is laterally displaced [Fig. 2.3(a)].

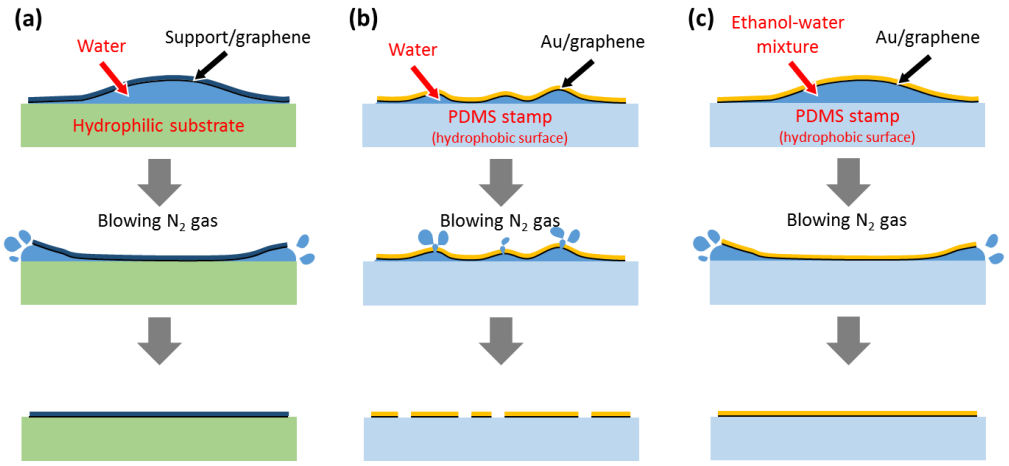

Figure 2.3 Schematic illustration of the difference in the quality of support/graphene on PDMS, determined by wetting of the liquid bath, during the blow-drying process. (a) In the conventional wet-transfer case, sufficient wetting of a hydrophilic substrate by water provides conformal contact between graphene and the substrate without wrinkles when the sample is blow-dried using N_2 gas. (b) When a PDMS stamp, having a hydrophobic surface, is used instead of the hydrophilic substrate, water does not form a continuous layer between the graphene and the PDMS stamp, and consequently, the blow-drying process causes trapped water droplets to burst, followed by damaging the Au/graphene bilayer. (c) In our case, to prevent such problem, the surface tension of the liquid bath is decreased by mixing water with ethanol, resulting into_sufficient wetting of the PDMS stamp by the mixture. As a result, a continuous layer of the mixture between the interfaces provides conformal contact comparable with the conventional wet-transfer case in (a).

Since the surface of a PDMS stamp is hydrophobic, which is favorable for reliable transfer of a graphene monolayer onto a target substrate via stamping (g to h in Fig. 2.1), the use of water bath in Fig. 2.1(d) leads to a discontinuous lubrication layer between the bilayer and substrate, as schematically shown in Fig. 2.3(b). Therefore, blow-drying in this case results into bursting of trapped water droplets, tearing the graphene monolayer. This can be effectively prevented by using an ethanol–water mixture as the liquid bath, which sufficiently wets the PDMS surface to provide a continuous lubrication layer [Fig. 2.3(c)].

When patterning of graphene is required, a conventional patterning process, such as O_2 RIE of graphene using photoresist patterned by photolithography as an etch mask [19,20], is performed before Step (b) in Fig. 2.1. Then, performing the remaining processes [Step (b) to (h)], one can obtain a patterned graphene monolayer on a target substrate. This pre-transfer patterning of graphene allows one to avoid possible damage to the fragile material that is likely to occur, when a process such as photolithography [19,20], RIE [19,20], or laser ablation [31] is performed after the graphene is transferred to the target substrate.

2.2.2 Effect of surface on the quality of transfer-printed graphene monolayers

To show that the surface tension of a liquid used in Step (d) in Fig. 2.1 is a critical factor determining the quality of transfer-printed graphene, I transfer-

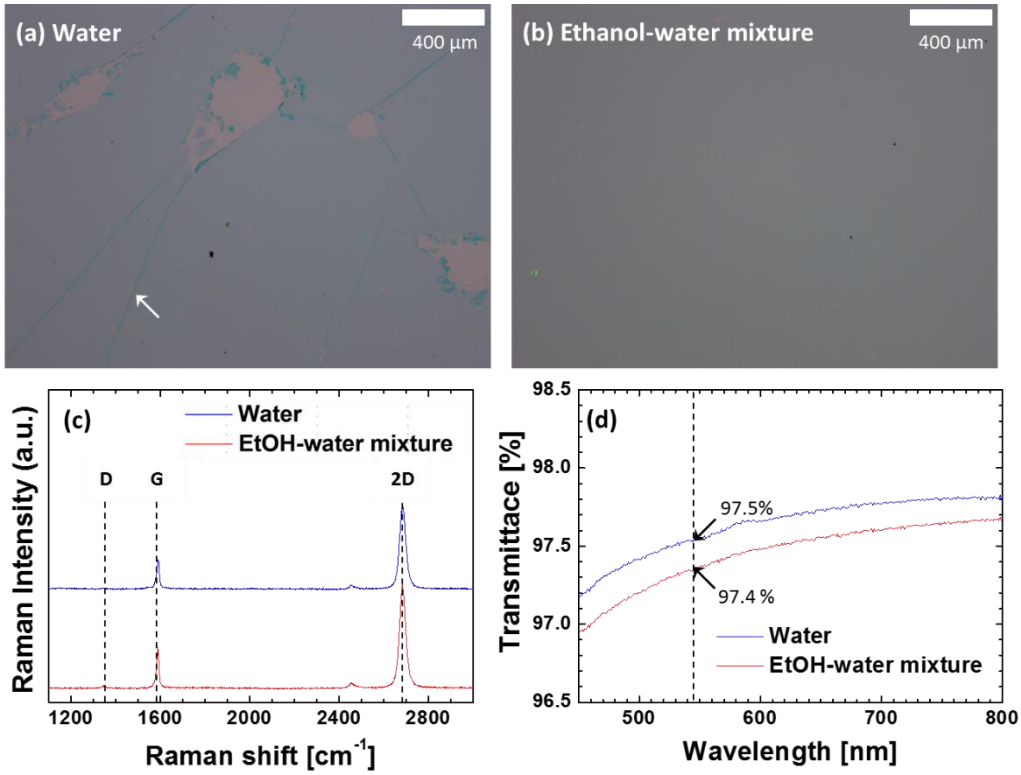

Figure 2.4 Comparison of the quality of the transfer-printed graphene monolayer, determined by the surface tension of the liquid bath, water or the ethanol-water mixture. (a,b) Optical microscope images of the graphene on the SiO_2/Si substrate. The white arrow in (a) indicates the folded graphene induced by insufficient wetting. (c) Raman spectra of the graphene on the SiO_2/Si substrate. (d) Transmittances of the graphene on a glass substrate. Each line was obtained by averaging the transmittance of 5 samples.

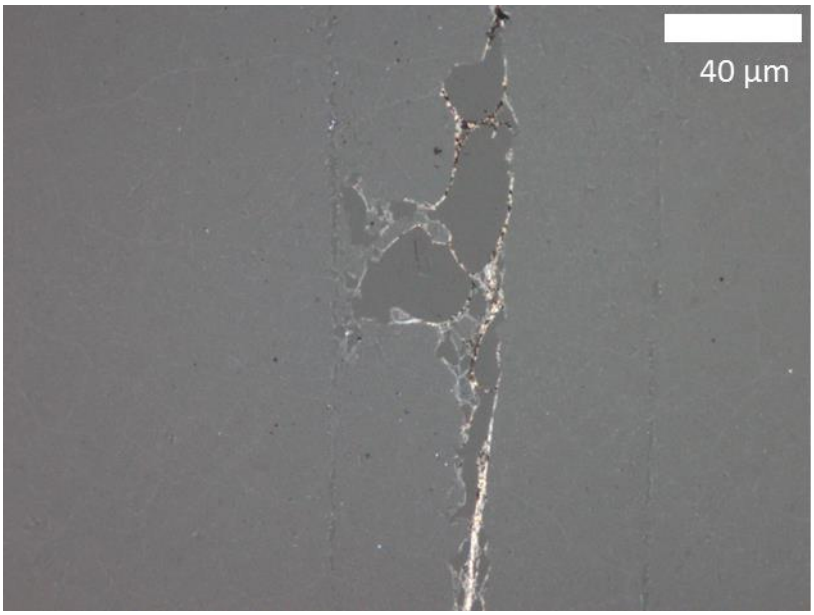

Figure 2.5 Optical microscope image of the transferred graphene onto the PDMS stamp using water bath in our process.

printed a graphene monolayer on a Si substrate coated with a 285-nm-thick SiO_2 layer following a process described in Fig. 2.1, while varying the liquid bath: in one set of experiments, I used water, and in the other, a water–ethanol mixture (30% water and 70% ethanol by volume). When water bath was used, although the entire graphene sheet (1.3 cm by 1.3 cm) was seemingly well-transferred, a closer observation revealed that there are randomly distributed irregular-shaped holes where graphene is absent, as shown in Fig. 2.4(a). The density of these defects is approximately 10 cm^{-2}, which was obtained by counting the number of defects distributed over the whole sample area using an optical microscope. When the PDMS stamp was observed by an optical microscope after Step (f) in Fig. 2.1, it was found that similar defects, albeit smaller in size, were present (Fig. 2.5), indicating that the defects are formed while transferring the graphene layer onto the PDMS surface and are exacerbated during the transfer-printing onto the substrate. As described in the Section 2.2.1, the defects arise from insufficient wetting of the PDMS surface by water. Since PDMS is hydrophobic and water has high surface tension (~72 dyn/cm at 23 ˚C [32]), immediately after a graphene–Au bilayer is scooped by a PDMS stamp, water dewets the PDMS surface in several locations, making the bilayer form contacts to the PDMS surface that is only locally conformal [Figs 2.3(b) and 2.6(a)]. As the sample is blow-dried using a N_2 gun, these locally conformal contacts laterally expand, generating narrow wrinkles with water droplets trapped inside, as shown in the right image of Fig. 2.6(a). I speculate that further application of N_2 pressure causes the water droplets to burst,

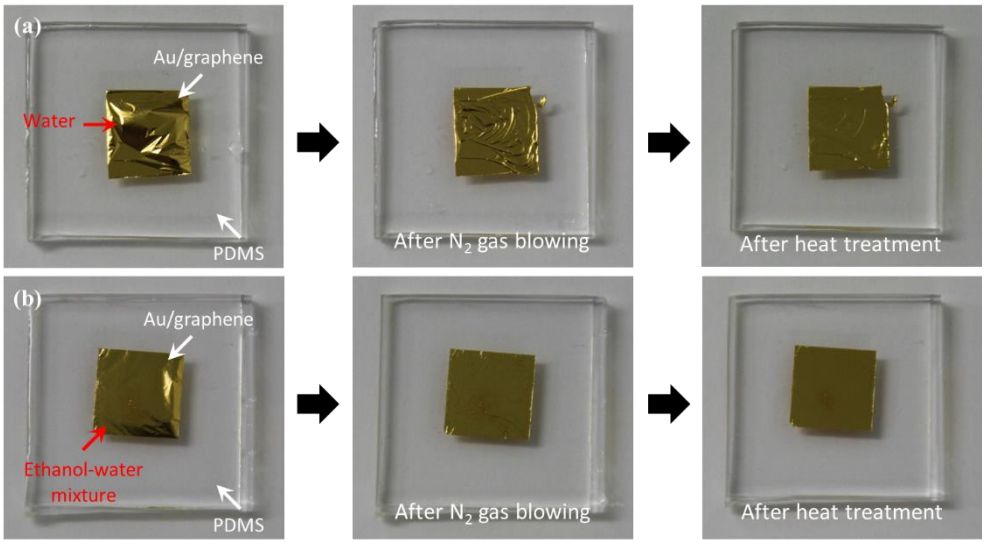

Figure 2.6 Comparison photographs of the change in the quality of the Au/graphene bilayer on the PDMS stamp, determined by wetting of the liquid bath, during the blow-drying and heat treatment process. They were taken after scooping up the Au/graphene bilayer floated on (a) water bath and (b) the ethanol-water mixture bath with the PDMS stamp. (a) When water bath was used, water dewets in several locations, resulting into non-uniformly conformal contact between the graphene and the PDMS (the left photograph). Blow-drying N_2 gas not only removed most of water enclosed between the Au/graphene and the PDMS stamp, but also led to form winkles with water droplets trapped inside (the middle). After heat treatment, there were still the wrinkles, although the water droplets were removed (the right). (b) In the case of using the ethanol-water mixture bath, the mixture formed a continuous layer between the Au/graphene bilayer and the PDMS stamp, unlike the case of water bath (the left). Owing to the continuous layer, the mixture was mostly displaced by blow-drying process using N_2 gas, and then the Au/graphene bilayer were mildly corrugated (the middle).

resulting into defects such as that shown in Fig. 2.5. In fact, as shown in Fig. 2.4(a), the locations of many defects in the graphene transferred onto the substrate seem to coincide with the intersection of the wrinkles, where relatively large water droplets are expected to form: the linear regions in Fig. 2.4(a) indicated by the white arrow are where the graphene monolayer is folded, which results from the wrinkles in the graphene–Au bilayer. In contrast, when the ethanol–water mixture was used, its lower surface tension (~25 dyn/cm at 23 ˚C [32]) allows a continuous lubrication layer to form between the graphene and PDMS surfaces, providing effective "decoupling" of the bilayer from the PDMS surface. Therefore, no wrinkles, except a few with much smaller heights, were observed in the graphene–Au bilayer on the PDMS stamp [Fig. 2.6(b)]. I found that mild baking at 40 ˚C removes these wrinkles, resulting into the flat graphene–Au bilayer that is globally conformal to the PDMS stamp, and consequently, successful transfer-printing of the graphene monolayer was achieved without defects, as shown in Fig. 2.4(b).

The sheet resistance (R_{sh}) was measured for graphene monolayers transfer-printed on glass substrates, through the van der Pauw method [33] using a source meter (2400, Keithley) and a multimeter (34410A, Agilent). The size of the graphene monolayers are approximately 1.3 cm by 1.3 cm, and the R_{sh} values were obtained with an injected current of 1 mA. In the following, a graphene monolayer transfer-printed onto a final substrate from a PDMS stamp onto which a graphene–Au bilayer was scooped from a bath of water and the ethanol–water mixture are referred to as G_{water} and $G_{EtOH–water}$, respectively. For

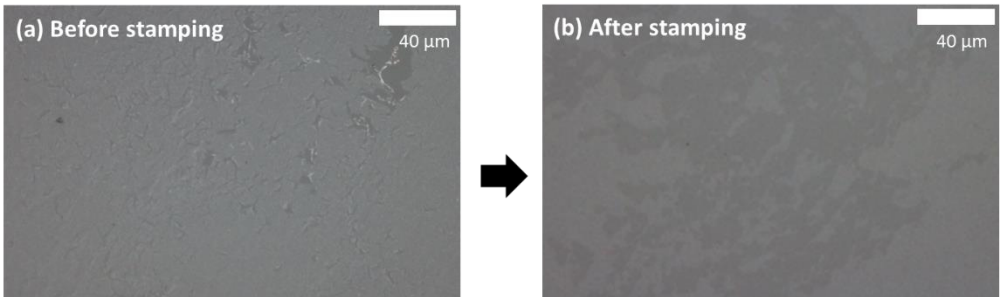

Figure 2.7 Optical microscope images taken before and after stamping process of the graphene monolayer in the case of the elastomer stamp method. In this process, graphene on Cu foil is transferred by directly attaching it on the elastomer stamp, followed by etching away the Cu layer using the Cu etchant, and consequently, it is printed on a target substrate. (a) The transferred graphene on the PDMS stamp with defects shaped like a dry earth. (b) The transfer-printed graphene on a glass substrate with defects far worse than that in (a).

G_{water}, the sheet resistance, averaged over five samples ($\acute{R}_{sh}$) is 3119 Ω/sq, with a minimum equal to 2664 Ω/sq. In contrast, for $G_{EtOH–water}$, $\acute{R}_{sh}$ is 914 Ω/sq, with a minimum being 573 Ω/sq. Figure 2.4(c) shows Raman spectra, which is obtained by using a confocal Raman microscope (inVia, Renishaw) with an excitation wavelength of 514.5 nm emitted from an Ar laser, of graphene monolayers shown in Fig. 2.4(a,b), where for G_{water} they were obtained from defect-free regions. The spectra show that, for both cases, (i) each Raman peak occurs at the same location (D: 1344 cm^{-1}, 2D: 2686 cm^{-1}, G: 1588 cm^{-1}), (ii) the height of the D peaks is negligible, and (iii) the 2D/G peak ratios are larger than 2.7, confirming that the transfer-printed graphene is indeed a monolayer [34]. This result indicates that significantly larger values of R_{sh} for G_{water}, in comparison to that for $G_{EtOH–water}$, are due not to the properties of graphene in defect-free regions, but to large-scale defects as shown in Fig. 2.4(a), which has been prevented by decreasing the surface tension in the case of $G_{EtOH–water}$.

Figure 2.4(d) shows the optical transmission spectra of G_{water} and $G_{EtOH–water}$ transfer-printed on a 0.7-mm-thick glass substrate, averaged over five samples for each case. The spectra were measured by using an ultraviolet–visible spectrophotometer (Lambda 35, Perkin Elmer). Transmittance (T), plotted on the y-axis, is the intensity of the optical beam transmitted through a glass/graphene sample normalized to that transmitted through a glass substrate. The size of the optical beam at the sample location was approximately 2 mm by 8 mm. For both G_{water} and $G_{EtOH–water}$, the values of T are consistent with what was previously measured for a graphene monolayer on a quartz substrate [12]. The

value of T for G_{water} is slightly higher than that for $G_{EtOH–water}$, primarily because the absence of graphene in the defects in G_{water} allow more light to be transmitted. Under this hypothesis, the ratio of total area of the defects to the entire area of the graphene sheet (α) can be estimated as $\alpha = (T_{water} - T_{EtOH–water}) / (1 - T_{EtOH–water})$, where T_{water} and $T_{EtOH–water}$ are transmittance of G_{water} and $G_{EtOH–water}$, respectively. The value of α calculated at each wavelength in Fig. 2.4(d) ranges from 6% to 8%, which is consistent with our estimation based on optical microscope images.

As expected, successful transfer-printing of graphene requires a defect-free graphene monolayer that is globally conformal to a PDMS stamp. The technique achieves this with the water–ethanol mixture, which provides a continuous lubrication layer, and with a Au support layer, which allows for its removal without swelling PDMS. Alternatively, one may attempt to obtain a defect-free graphene monolayer on a PDMS stamp by pressing the stamp onto a graphene layer grown on Cu foil and then etching away the Cu foil by floating the Cu/graphene/PDMS on a bath of a Cu etchant. Since the surface of Cu foil commonly used in CVD growth of graphene typically has corrugations on the micron scale [28], the PDMS attached to the graphene in this case is in contact with the graphene only partially. As a result, subsequent processes such as N_2 blow-dry and transfer-printing tend to cause defects in the graphene layer, as shown in Fig. 2.7. In fact, it was previously reported that R_{sh} of a transfer-printed graphene monolayer by this approach was 4 kΩ/sq, even with a self-release layer inserted for reliable graphene transfer [25].

2.2.3 Characterizations of graphene monolayer patterns transfer-printed on materials that can be damaged by a wet process

To fabricate practical electronic devices where graphene is used as active layers or electrodes, the patterning of graphene is required. The developed technique, described in Fig. 2.1, can achieve this with a simple modification: the process begins with a patterned graphene on Cu foil in Step (a), instead of an unpatterned graphene layer. In current demonstration, I first prepared a patterned graphene monolayer on Cu foil by etching unpatterned graphene grown on Cu foil by O_2 RIE using a photoresist etch mask patterned by photolithography. Next, the patterned graphene was transfer-printed on a Si/SiO_2 substrate coated with MoO_3 or PEDOT:PSS, both of which are susceptible to degradation when exposed to an aqueous condition or aggressive patterning process. Figure 2.8(a,b) are optical micrographs of the substrates, where patterned graphene monolayers were transfer-printed in regions indicated by the arrows, showing that the patterns defined on photomasks were replicated in the transfer-printed graphene monolayers. The widths of the smallest features — lines in Fig. 2.8(a) and arcs in Fig. 2.8(b) — are 10 μm and 15 μm, respectively, which are identical, within the resolution of the optical imaging system used (~0.5 μm), to those of the corresponding features on the photomask. A closer observation of the pattern edge using a field-emission scanning electron microscope (FE-SEM; JSM-6700F, JEOL) revealed that it is not straight on the nanoscale, with an “edge resolution” of 50 nm, which is probably attributed to

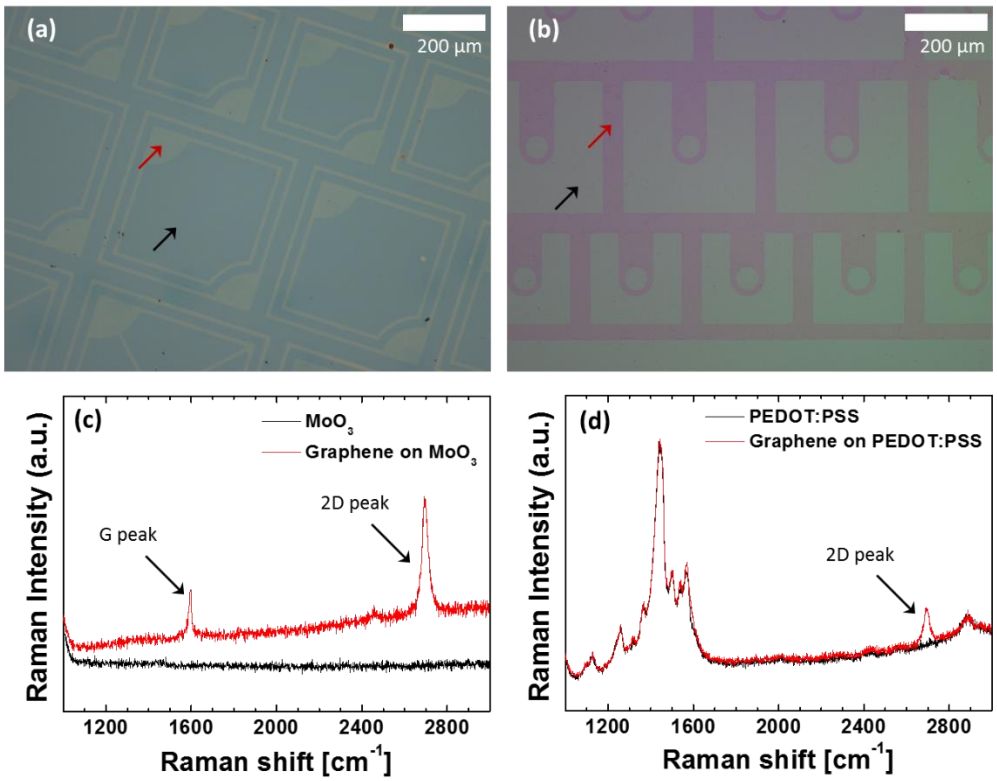

Figure 2.8 Characterization of the transfer-printed pattern of a graphene monolayer onto fragile materials. (a,b) Optical microscope images of the patterned graphene on (a) MoO_3 and (b) PEDOT:PSS. The black and red arrows denote the fragile layer (MoO_3 or PEDOT:PSS) and the patterned graphene on the fragile layer, respectively. (c,d) Raman spectra of the patterned graphene on (c) MoO_3 and (d) PEDOT:PSS.

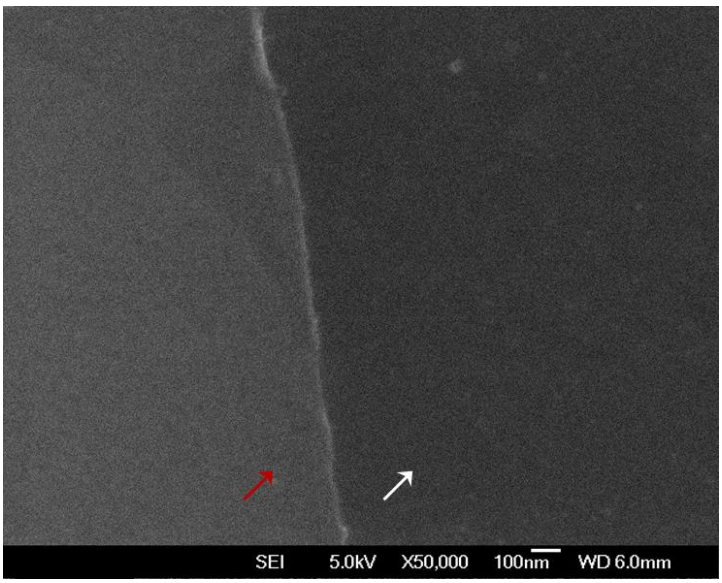

Figure 2.9 SEM image of the edge of the patterned graphene on MoO_3. The white and red arrows denote the MoO_3 layer and the patterned graphene on it, respectively. The pattern edge resolution is approximately 50 nm.

the edge resolution of the photomask patterns and/or limitation of the photolithography process (Fig. 2.9). From this, together with the fact that previously demonstrated transfer-printing-based patterning techniques can create patterns whose size is well below 100 nm [35], I expect that our technique is capable of creating sub-micrometer graphene patterns, if a nanopatterning process, for example electron-beam [36], nanoimprint [37], or nanosphere [38] lithography, is employed, instead of photolithography. Raman spectra obtained from the graphene transfer-printed on the MoO_3 show the distinct G and 2D peaks, with the 2D/G intensity ratio of 2.5, and the negligible D peak, suggesting that the quality of the graphene is comparable to that in Fig. 2.4(b). For the case of the graphene transfer-printed onto the PEDOT:PSS, the peaks associated with graphene, except the 2D peak, cannot be identified due to the overlap with Raman spectra of PEDOT:PSS.

2.2.4 Morphological characterizations of transfer-printed graphene monolayers

Next, I observed the surface of the transfer-printed graphene on a Si/SiO_2 substrate, using a FE-SEM and an atomic force microscope (AFM; Dimension Edge, Bruker). As shown in Fig. 2.10(a), irregularly shaped dark patches, as enclosed by a white circle, are randomly distributed throughout the surface. Also shown are the dark lines, as marked by the white arrow. These two features, patches and lines, are commonly found in the transferred graphene CVD-grown on Cu foil — with the former and latter attributed to graphene

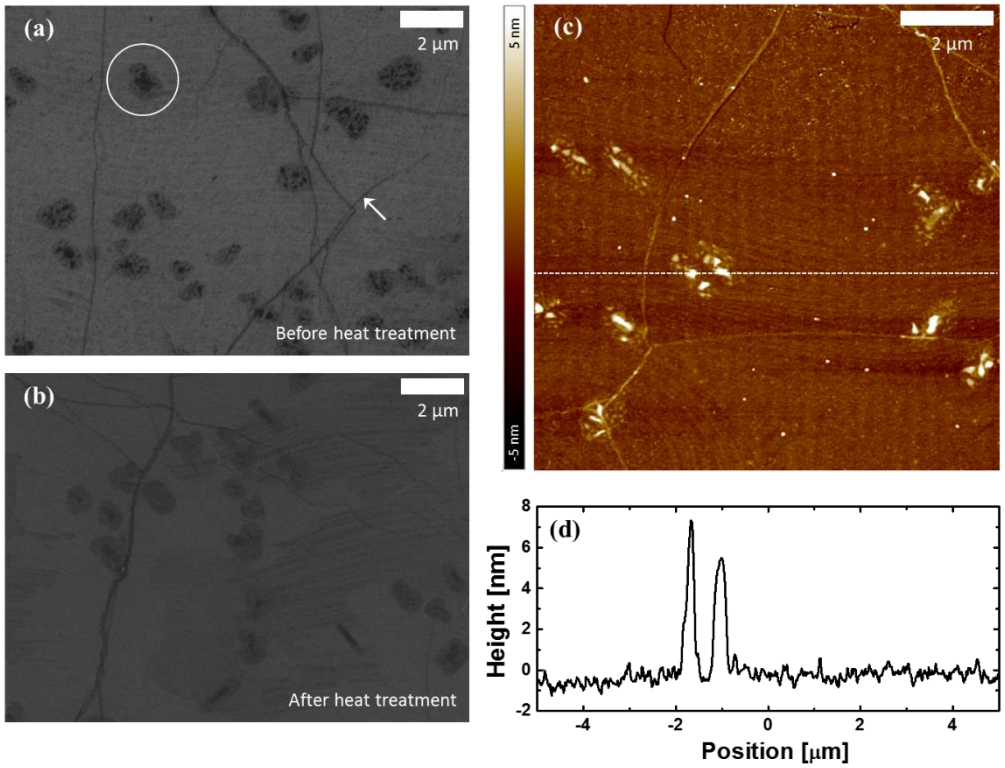

Figure 2.10 Morphological characterization of the transfer-printed graphene monolayer on the SiO_2/Si substrate. SEM images of the graphene before heat treatment in (a) and after heat treatment in (b). The white circle and arrow in (a) indicate graphene multilayer and wrinkle, respectively. (b) AFM image of the graphene used in (a). (d) Surface-height profile of the graphene along the white dotted line in (b).

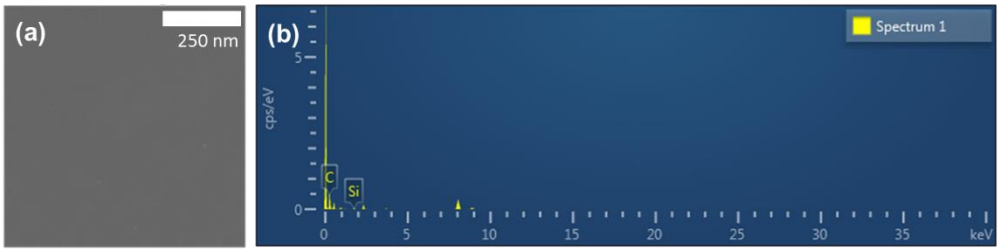

Figure 2.11 Elemental characterization of the transfer-printed graphene. (a) STEM image of the region for the analysis. (b) EDX spectrum for element components on that region. Other signals besides C and Si peaks were measured from the TEM grid and the separation layer.

multilayers and wrinkles, respectively [28] — and hence are not caused by our transfer technique. It is also shown that in the patches, there are darker spots with diameters of approximately 150 nm. The surface profile measured using an AFM along the white dotted line in Fig. 2.10(c) shows that the spots have heights as high as approximately 7 nm [Fig. 2.10(d)]. To identify the origin of the dark spots, elemental analysis was carried out using a scanning transmission electron microscope capable of energy dispersive x-ray spectroscopy (STEM-EDS; JEM-2100F, JEOL). In order to prepare a sample for this analysis, a graphene layer was transfer-printed from a PDMS stamp onto a Si/SiO_2 substrate coated with a PEDOT:PSS separation layer, and then transferred onto a lacey carbon TEM grid using the conventional wet-transfer method (see the 2.4.3 Section for the experimental detail). An EDS spectrum obtained from a region shown in Fig. 2.11(a) shows that, in addition to carbon, silicon atoms are present on the graphene surface [Fig. 2.11(b)]. Given many previous reports showing that uncured siloxane oligomers were present on PDMS surfaces [25,39], it is highly likely that the dark spots on the graphene surface are siloxane residues that have been transferred from the PDMS stamp. This speculation was further supported by the fact that the dark spots can be eliminated by annealing the sample at 400 ˚C under H_2 and Ar, as shown in Fig. 2.10(b) [40]. The AFM measurements [Fig. 2.10(c,d)] show that the surface in the background, that is, regions away from the patches and lines, is much rougher than that of a clean graphene surface [41], suggesting that the oligomer residues are also present throughout the surface, not only on the multilayer regions.

The morphological and elemental characterizations of the surface of transfer-printed graphene discussed above help determine the range of application of the technique in its current form. Since the oligomer residues are likely to be present only on the top surface, that is, the graphene surface that used to be in contact with the PDMS, our technique can be applied to fabrication of (i) devices where only the bottom surface of the graphene electrode is involved in injection or collection of charge carriers, such as LEDs and solar cells, made of organic semiconductors [42] or organometal trihalide perovskite compounds [43], with top graphene electrodes, and (ii) devices whose graphene electrodes are used to establish electric fields without charge carrier transport, such as thin-film transistors with graphene gate electrodes [44] and terahertz wave modulators [13–15]. Meanwhile, when charge carrier injection or collection occurs in both sides of the graphene layer, such as in tandem LEDs and solar cells where it is part of the interlayers, this technique is not applicable. Therefore, expanding the range of application of our technique by eliminating the oligomer contamination, possibly with the following modification, is important future work: replacing PDMS with other stamp material that can be completely cured; or depositing a blocking layer on the PDMS surface to prevent possible transfer of uncured oligomers onto the graphene surface, with a potential candidate being a pressure sensitive adhesive layer [45,46].

2.3 Conclusions

In summary, I have developed a low temperature, dry process capable of transfer-printing a patterned graphene monolayer grown on Cu foil on a target substrate. Two features distinct from the conventional wet-transfer method [18] — the use of a support layer composed of Au, instead of PMMA, and the decrease in surface tension of the liquid bath on which a graphene–Au bilayer floats — allow one to obtain a graphene monolayer on a PDMS stamp without defects that would otherwise arise. Subsequently, the graphene is transfer-printed from the stamp onto a target substrate. The characteristics of a graphene monolayer transfer-printed using our technique are comparable to those obtained with the conventional wet-transfer method, with a sheet resistance as low as 573 Ω/sq and optical transmittance of 97.4% at 550 nm. In addition, with pre-transfer patterning of graphene on Cu foil using conventional patterning processes, this technique is capable of creating graphene monolayer patterns on materials that are easily degraded when exposed to high-temperature processes, organic solvents, or aqueous chemicals. As an example, using photolithography followed by reactive-ion etch to pattern graphene monolayers on Cu foil and then transfer-printing them, I have obtained graphene monolayer patterns on MoO_3 and PEDOT:PSS, with the smallest feature size and edge resolution of ~10 μm and 50 nm, respectively. Immediate application areas of this technique include organic electronic devices whose top electrodes are composed of graphene.

Moreover, by eliminating siloxane oligomer residues on graphene using alternate stamp material, the technique can be further applied to devices whose graphene electrodes are in their interiors, such as tandem LEDs and solar cells. Finally, with possible appropriate modification, it may also be applied to dry-transfer of other two-dimensional materials, including boron nitride [47] and molybdenum disulfide [48].

2.4 Methods

2.4.1 Low-temperature, dry transfer-printing process

Low-temperature, dry transfer of graphene monolayers was carried out by following processes described in Fig. 2.1. To form a support layer on a graphene monolayer on Cu foil, a 200-nm-thick Au layer was deposited by thermal evaporation in high vacuum (1 Å/s, ~10^{-7} Torr) (b). To etch away the Cu foil, the Cu/graphene/Au multilayer was floated on an ammonium persulfate solution, prepared by dissolving 10 g of ammonium persulfate (Sigma Aldrich) in 500 mL of water (c). After the etch was completed, the graphene–Au bilayer was scooped with a glass slide, and then transferred on a bath of water to remove residual ammonium persulfate. Next, the graphene–Au bilayer was moved onto a bath composed of an ethanol–water mixture (70 vol % ethanol and 30 vol % water), from which the bilayer was scooped by and transferred onto a PDMS stamp (d). The sample was then blow-dried using a N_2 gun (e), and was further dried on a hot plate at 40 ˚C for more than 4 h. The Au support layer

was etched using an ammonium iodide solution (LAE-202, Cowon Innotech. Inc.) (f), after which the PDMS/graphene sample was rinsed with water. After water droplets on the sample were blown away using a N_2 gun, the graphene-coated PDMS stamp was gently pressed onto a target substrate, inducing intimate contact throughout the substrate area (g). Before separation of the stamp from the substrate, the sample was stored at room temperature for 1 h under a pressure of 9.9 kPa, and then placed on a hot plate at 70 ˚C for 10 min without application of pressure. Finally, the stamp was carefully peeled off from the substrate (h), resulting in the transfer-printed graphene monolayer on the target substrate.

2.4.2 Transfer-printing of patterned graphene layers

In this process, a graphene monolayer on Cu foil was first patterned using conventional photolithography and reactive-ion etch, as described in Fig. 2.12. A 1.5-μm-thick photoresist (AZ GXR-601, 14 cP) was spin-coated on a Cu/graphene sample, and then patterned by photolithography. The patterned graphene on Cu foil was obtained, when the graphene in the areas not covered by the photoresist was etched by reactive ion etch in O_2 (100 W, 0.1 Torr, 20 s, 50 SCCM). Performing the processes described in Fig. 2.1 with this sample, instead of unpatterned graphene on Cu foil, I transfer-printed a patterned graphene monolayer on a target substrate coated with a 75-nm-thick PEDOT:PSS or a 20-nm MoO_3 layer. The target substrate was a 500-μm-thick Si substrate pre-coated with a 285-nm-thick thermal SiO_2 layer, and the PEDOT:PSS (He-

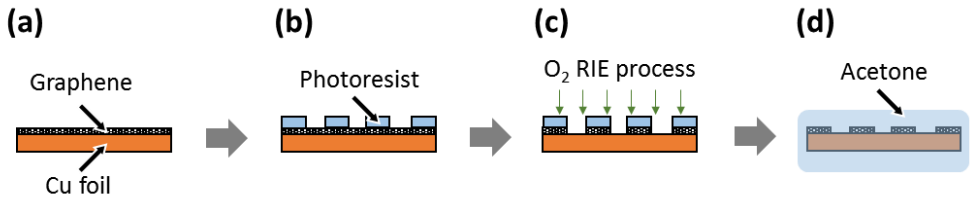

Figure 2.12 Schematic illustration of the patterning process. (a) CVD-grown graphene on Cu foil. (b) A patterned photoresist layer on the graphene/Cu obtained by the conventional photolithography process. (c) Etching away the graphene uncovered by photoresist via O_2 RIE process. (d) Removal of the patterned photoresist layer on the graphene/Cu by dipping in acetone.

raeus) and MoO_3 (LTS Chemical Inc.) layers were deposited by spin-coating (3000 rpm, 30 s) and thermal evaporation in high vacuum (1 Å/s, ~10^{-7} Torr), respectively.

2.4.3 Sample preparation for the elemental analysis

Samples for the elemental analysis were prepared following the processes described in Fig. 2.13. After a graphene monolayer was transfer-printed from a PDMS stamp onto a PEPOT:PSS layer using our transfer method (a), a layer of PMMA was deposited on the graphene layer by spin coating at 3000 rpm for 30 s (b). The PMMA solution was prepared by dissolving PMMA (138 mg, Sigma Aldrich) into chlorobenzene (3 mL, Sigma Aldrich). The sample was then immersed into a water bath, separating the PMMA–graphene bilayer from the Si/SiO_2 substrate as the PEDOT:PSS layer was dissolved (c). Next, the bilayer was transferred to another water bath and kept floating on it for more than 24 h to ensure that PEDOT:PSS remaining on the graphene surface was removed. Then, the bilayer was scooped with a lacey carbon TEM grid (Ted Pella, Inc.) (d), after which the grid was placed on a hot plate at 40 ˚C for more than 2 h. Finally, the PMMA layer was removed by acetone (e), resulting in the graphene monolayer on the TEM grid (f).

2.4.4 Preparation of PDMS stamps

The base and curing agent of PDMS (Sylgard 184, Dow Corning) were thoroughly mixed in a weight ratio of 10:1, and then degassed in a low-vacuum chamber. The mixture, the amount of which is such that the resulting thickness

of the PDMS stamp is ~2 mm, was poured onto a bare Si wafer. Next, the mixture was cured on a hot plate at 80 ˚C for ~24 h.

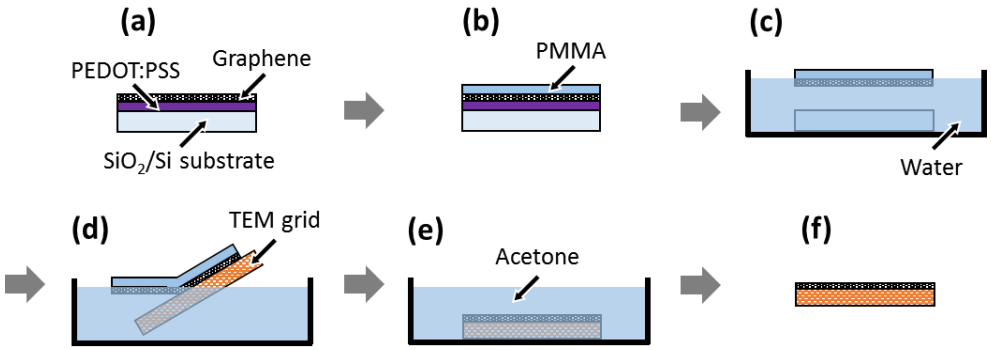

Figure 2.13 Schematic illustration of the transferring process of the transfer-printed graphene onto the lacey carbon TEM grid for the element analysis using STEM-EDX. (a) Transfer-printed graphene on the SiO_2/Si substrate coated with PEDOT:PSS prepared by using our method. (b) Spin-coated PMMA layer onto the graphene/PEDOT:PSS/SiO_2/Si. (c) Dissolution of the PEDOT:PSS interlayer by dipping the PMMA/graphene/PEDOT:PSS/SiO_2/Si into clean water bath, and then the PMMA/graphene bilayer separated from the SiO_2/Si floating onto the water bath. (d) Scooping up the PMMA/graphene bilayer with the lacey carbon TEM grid. (e) Removal of the PMMA layer on the graphene/grid using acetone. (f) As a result, the transfer-printed graphene on the target substrate is transferred onto the lacey carbon TEM grid.

2.5 References

[1] K. S. Novoselov, A. K. Geim, S. V. Morozov, D. Jiang, Y. Zhang, S. V. Dubonos, I. V. Grigorieva, and A. A. Firsov, Electric field effect in atomically thin carbon films, *Science*, **306**, 666 (2004).

[2] A. H. Castro Neto, F. Guinea, N. M. R. Peres, K. S. Novoselov, and A. K. Geim, The electronic properties of graphene, *Rev*. *Mod*. *Phys*., **81**, 109 (2009).

[3] F. Liu, P. Ming, and J. Li, Ab initio calculation of ideal strength and phonon instability of graphene under tension, *Phys*. *Rev*. *B*, **76**, 064120 (2007).

[4] C. Lee, X. Wei, J. W. Kysar, and J. Hone, Measurement of the elastic properties and intrinsic strength of monolayer graphene, *Science*, **321**, 385 (2008).

[5] R. R. Nair, P. Blake, A. N. Grigorenko, K. S. Novoselov, T. J. Booth, T. Stauber, N. M. R. Peres, and A. K. Geim, Fine structure constant defines visual transparency of graphene, *Science*, **320**, 1308 (2008).

[6] J. Meyer, P. R. Kidambi, B. C. Bayer, C. Weijtens, A. Kuhn, A. Centeno, A. Pesquera, A. Zurutuza, J. Robertson, and S. Hofmann, Metal oxide induced charge transfer doping and band alignment of graphene electrodes for efficient organic light emitting diodes, *Sci*. *Rep*., **4**, 5380 (2014).

[7] B. J. Kim, C. Lee, Y. Jung, K. H. Baik, M. A. Mastro, J. K. Hite, C. R. Jr. Eddy, and J. Kim, Large-area transparent conductive few-layer graphene electrode in GaN-based ultra-violet light-emitting diodes, *Appl*. *Phys*. *Lett*.,

99, 143101 (2011).

[8] Y. Wang, S. W. Tong, X. F. Xu, B. Özyilmaz, and K. P. Loh, Interface engineering of layer-by-layer stacked graphene anodes for high-performance organic solar cells, *Adv*. *Mater*., **23**, 1514 (2011).

[9] H. Park, P. R. Brown, V. Bulović, and J. Kong, Graphene as transparent conducting electrodes in organic photovoltaics: studies in graphene morphology, hole transporting layers, and counter electrodes, *Nano Lett*., **12**, 133 (2012).

[10] C. Di, D. Wei, G. Yu, Y. Liu, Y. Guo, and D. Zhu, Patterned graphene as source/drain electrodes for bottom-contact organic field-effect transistors, *Adv*. *Mater*., **20**, 3289 (2008).

[11] D. Baierl, B. Fabel, P. Lugli, and G. Scarpa, Efficient indium-tin-oxide (ITO) free top-absorbing organic photodetector with highly transparent polymer top electrode, *Org*. *Electron*., **12**, 1669 (2011).

[12] S. Bae, H. Kim, Y. Lee, X. Xu, J. S. Park, Y. Zheng, J. Balakrishnan, T. Lei, H. R. Kim, Y. I. Song, Y. J. Kim, K. S. Kim, B. Özyilmaz, J. H. Ahn, B. H. Hong, and S. Iijima, Roll-to-roll production of 30-inch graphene films for transparent electrodes, *Nat*. *Nanotechnol*., **5**, 574 (2010).

[13] B. Sensale-Rodriguez, R. Yan, M. M. Kelly, T. Fang, K. Tahy, W. S. Hwang, D. Jena, L. Liu, and H. G. Xing, Broadband graphene terahertz modulators enabled by intraband transitions, *Nat*. *Commun*., **3**, 780 (2012).

[14] W. Gao, J. Shu, K. Reichel, D. V. Nickel, X. He, G. Shi, R. Vajtai, P. M. Ajayan, J. Kono, D. M. Mittleman, and Q. Xu, High-contrast terahertz

wave modulation by gated graphene enhanced by extraordinary transmission through ring apertures, *Nano Lett*., **14**, 1242 (2014).

[15] Q. Li, Z. Tian, X. Zhang, R. Singh, L. Du, J. Gu, J. Han, and W. Zhang, Active graphene-silicon hybrid diode for terahertz waves, *Nat*. *Commun*., **6**, 7082 (2015).

[16] H. Yang, J. Heo, S. Park, H. J. Song, D. H. Seo, K. E. Byun, P. Kim, I. Yoo, H. J. Chung, and K. Kim, Graphene barristor, a triode device with a gate-controlled Schottky barrier, *Science*, **336**, 1140 (2012).

[17] S. Tongay, M. Lemaitre, X. Miao, B. Gila, B. R. Appleton, and A. F. Hebard, Rectification at graphene-semiconductor interfaces: zero-gap semiconductor-based diodes, *Phys*. *Rev*. *X*, **2**, 01102 (2012).

[18] X. Li, W. Cai, J. An, S. Kim, J. Nah, D. Yang, R. Piner, A. Velamakanni, I. Jung, E. Tutuc, S. K. Banerjee, L. Colombo, and R. S. Ruoff, Large-area synthesis of high-quality and uniform graphene films on copper foils, *Science*, **324**, 1312 (2009).

[19] W. H. Lee, J. Park, S. H. Sim, S. B. Jo, K. S. Kim, B. H. Hong, and K. Cho, Transparent flexible organic transistors based on monolayer graphene electrodes on plastic, *Adv*. *Mater*., **23**, 1752 (2011).

[20] R. Shi, H. Xu, B. Chen, Z. Zhang, and L. M. Peng, Scalable fabrication of graphene devices through photolithography, *Appl*. *Phys*. *Lett*., **102**, 113102 (2013).

[21] S. R. Forrest, The path to ubiquitous and low-cost organic electronic appliances on plastic, *Nature*, **428**, 911 (2004).

[22] H. J. Snaith, Perovskites: the emergence of a new era for low-cost, high-efficiency solar cells, *J. Phys. Chem. Lett.*, **4**, 36233630 (2013).

[23] J. Kang, D. Shin, S. Bae, and B. H. Hong, Graphene transfer: key for applications, *Nanoscale*, **4**, 5527 (2012).

[24] T. Yoon, W. C. Shin, T. Y. Kim, J. H. Mun, T. S. Kim, and B. J. Cho, Direct measurement of adhesion energy of monolayer graphene as-grown on copper and its application to renewable transfer process, *Nano Lett.*, **12**, 1448 (2012).

[25] J. Song, F. Y. Kam, R. Q. Png, W. L. Seah, J. M. Zhuo, G. K. Lim, P. K. H. Ho, and L. L. Chua, A general method for transferring graphene onto soft surfaces, *Nat. Nanotechnol.*, **8**, 356 (2013).

[26] W. Jung, D. Kim, M. Lee, S. Kim, J. H. Kim, and C. S. Han, Ultraconformal contact transfer of monolayer graphene on metal to various substrates, *Adv. Mater.*, **26**, 6394 (2014).

[27] C. Girotto, E. Voroshazi, D. Cheyns, P. Heremans, and B. P. Rand, Solution-processed MoO_3 thin films as a hole-injection layer for organic solar cells, *ACS Appl. Mater. Interfaces*, **3**, 3244 (2011).

[28] X. Li, Y. Zhu, W. Cai, M. Borysiak, B. Han, D. Chen, R. D. Piner, L. Colomba, and R. S. Ruoff, Transfer of large-area graphene films for high-performance transparent conductive electrodes, *Nano Lett.*, **9**, 4359 (2009).

[29] Y. Xia and G. M. Whitesides, Soft lithography, *Angew. Chem. Int. Ed.*, **37**, 550 (1998).

[30] J. N. Lee, C. Park, and G. M. Whitesides, Solvent compatibility of poly(dimethylsiloxane)-based microfluidic devices, *Anal. Chem.*, **75**, 6544 (2003).

[31] G. Kalita, L. Qi, Y. Namba, K. Wakita, and M. Umeno, Femtosecond laser induced micropatterning of graphene film, Mater. Lett., **65**, 1569 (2011).

[32] C. Hansen, New simple method to measure polymer surface tension, *Pigm. Resin Technol.*, **27**, 374 (1998).

[33] L. J. van der Pauw, A method of measuring specific resistivity and Hall effect of discs of arbitrary shape, *Philips Tech. Rev.*, **13**, 1 (1958).

[34] A. C. Ferrari, J. C. Meyer, V. Scardaci, C. Casiraghi, M. Lazzeri, F. Mauri, S. Piscanec, D. Jiang, K. S. Novoselov, S. Roth, and A. K. Geim, Raman spectrum of graphene and graphene layers, *Phys. Rev. Lett.*, **97**, 187401 (2006).

[35] C. Kim, M. Shtein, and S. R. Forrest, Nanolithography based on patterned metal transfer and its application to organic electronic devices, *Appl. Phys. Lett.*, **80**, 4051 (2002).

[36] F. Withers, T. H. Bointon, M. Dubois, S. Russo, and M. F. Craciun, Nanopatterning of fluorinated graphene by electron beam irradiation, *Nano Lett.*, **11**, 3912 (2011).

[37] X. Liang, Y. S. Jung, S. Wu, A. Ismach, D. L. Olynick, S. Cabrini, and J. Bokor, Formation of bandgap and subbands in graphene nanomeshes with sub-10 nm ribbon width fabricated via nanoimprint lithography, Nano Lett., **10**, 2454 (2010).

[38] L. Liu, Y. Zhang, W. Wang, C. Gu, X. Bai, and E. Wang, Nanosphere lithography for the fabrication of ultranarrow graphene nanoribbons and on-chip bandgap tuning of graphene, *Adv. Mater.*, **23**, 1246 (2011).

[39] K. Glasmastar, J. Gold, A. -S. Andersson, D. S. Sutherland, and B. Kasemo, Silicone transfer during microcontact printing, *Langmuir*, **19**, 5475 (2003).

[40] M. J. Allen, V. C. Tung, L. Gomez, Z. Xu, L. M. Chen, K. S. Nelson, C. Zhou, R. B. Kaner, and Y. Yang, Soft transfer printing of chemically converted graphene, *Adv. Mater.*, **21**, 2098 (2009).

[41] A. Pirkle, J. Chan, A. Venugopal, D. Hinojos, C. W. Magnuson, S. Mc Donnell, L. Colombo, E. M. Vogel, R. S. Ruoff, and R. M. Wallace, The effect of chemical residues on the physical and electrical properties of chemical vapor deposited graphene transferred to SiO_2, *Appl. Phys. Lett.*, **99**, 122108 (2011).

[42] J. H. Beck, R. A. Barton, M. P. Cox, K. Alexandrou, N. Petrone, G. Olivieri, S. Yang, J. Hone, and I. Kymissis, Clean graphene electrodes on organic thin-film devices via orthogonal fluorinated chemistry, *Nano Lett.*, **15**, 2555 (2015).

[43] P. You, Z. Liu, Q. Tai, S. Liu, and F. Yan, Efficient semitransparent perovskite solar cells with graphene electrodes, *Adv. Mater.*, **27**, 3632 (2015).

[44] J. K. Park, S. M. Song, J. H. Mun, and B. J. Cho, Graphene gate electrode for MOS structure-based electronic devices, *Nano Lett.*, **11**, 5383 (2011).

[45] T. Choi, S. J. Kim, S. Park, T. Y. Hwang, Y. Jeon, and B. H. Hong, Roll-

to-roll continuous patterning and transfer of graphene via dispersive adhesion, *Nanoscale*, **7**, 7138 (2015).

[46] S. J. Kim, T. Choi, B. Lee, S. Lee, K. Choi, J. B. Park, J. M. Yoo, Y. S. Choi, J. Ryu, P. Kim, J. Hone, and B. H. Hong, Ultraclean patterned transfer of single-layer graphene by recyclable pressure sensitive adhesive films, *Nano Lett*., **15**, 3236 (2015).

[47] C. Zhang, S. Zhao, C. Jin, A. L. Koh, Y. Zhou, W. Xu, Q. Li, Q. Xiong, H. Peng, and Z. Liu, Direct growth of large-area graphene and boron nitride heterostructures by a co-segregation method, *Nat*. *Commun*., **6**, 6519 (2015).

[48] Y. Shi, W. Zhou, A. Y. Lu, W. Fang, Y. H. Lee, A. L. Hsu, S. M. Kim, K. K. Kim, H. Y. Yang, L. J. Li, J. C. Idrobo, and J. Kong, Van der Waals epitaxy of MoS_2 layers using graphene as growth templates, *Nano Lett*., **12**, 2784 (2012).

Chapter 3 Polydimethylsiloxane (PDMS) Stamp Coated with a Low-Surface-Energy, Diffusion-Blocking, Covalently Bonded Perfluoropolyether (PFPE) Layer

3.1 Introduction

Polydimethylsiloxane (PDMS) is optically transparent, mechanically flexible, and biocompatible. It is easy to fabricate nanostructures and patterns, and has the advantage of easy surface modification. As a result, many researchers have been used PDMS as a core material for a long time for various applications such as stamps or molds for soft lithography [1], chips for microfluidics [2], chambers for cell-culture systems [2], and substrates for stretchable electronics.

Although many studies have been carried out, it has been found that organic small molecules such as organic semiconductors and solvents that are in contact with the surface of PDMS are absorbed into the free volume of the PDMS or various undesirable phenomena generated by the uncured siloxane oligomer of PDMS have been reported in a number of existing studies. This is particularly problematic in soft lithography such as μ-contact printing (μ-CP) and micromolding in capillaries (MIMICs) where the PDMS stamp and the material to be patterned must be in contact. For example, a nanoscale organic pattern that is difficult to fabricate by conventional methods of thermal depo-

sition through a fine metal mask (FMM) can be easily and inexpensively produced by transferring organic small molecules thermally deposited on a patterned stamp surface onto a target substrate, PDMS can not be used due to its property of absorbing organic small molecules. Another important example is that when the solution containing the substance to be transferred is coated on the surface of the stamp and transferred onto the target substrate, the solvent should not be absorbed by the PDMS to swell the PDMS and the PDMS surface and wettability should be good. The type of solvent is very limited. Although the substance to be transferred on the PDMS stamp is fully transferred onto the target substrate, the undesired PDMS oligomer on the transferred material surface is another problem.

In this chapter, I demonstrate a simple method of forming a perfluoropolyether (PFPE) coating on a PDMS stamp, with the following properties ideal for transfer patterning of various materials: it prevents the diffusion of both organic molecules into the stamp and uncured siloxane oligomers in PDMS onto the layer to be transferred; it has a low surface energy, allowing a reliable transfer; the internal cohesion of the PFPE layer and its adhesion to the stamp are strong, leaving no PFPE residues on the substrate after the transfer. To obtain the PFPE coating, the end groups of PFPE and the surface of the PDMS stamp were first modified by hydrolysis and UV-ozone treatment, respectively. Then, the stamp was dip-coated, inducing a condensation reaction between the modified end groups of PFPE and pendant groups of PDMS, as well as that between the modified end groups of the adjacent PFPE molecules.

3.2 Results and discussion

3.2.1 Dip-coating process for depositing a PFPE layer on a PDMS stamp

A dip-coating process for depositing a PFPE layer on a PDMS stamp is schematically illustrated in Fig. 3.1. First, the end groups [$-Si(OC_2H_5)_3$] of PFPE dissolved in isopropanol (IPA) are hydrated into $-Si(OH)_3$ by adding water for the hydrolysis and acetic acid for the catalysis [Fig. 3.1(b,c)] [3]. When a PDMS stamp whose surface is treated with UV-ozone [Fig. 3.1(d,e)] is immersed in the IPA solution containing hydrated PFPE molecules, a PFPE coating is formed on the PDMS surface as a result of a condensation reaction between the hydroxyl groups in PFPE and PDMS, as well as between those in the adjacent PFPE molecules, as shown in Fig. 3.1(f). As described below in detail, the PFPE layer on the PDMS surface is found to function as a bidirectional diffusion barrier: it effectively prevents organic small molecules deposited on the stamp from being absorbed into free volumes of PDMS; it also prevents PDMS oligomers from migrating onto the layer to be transferred, thereby avoiding the contamination of that layer. In addition, since both the PFPE−PDMS and PFPE−PFPE bonds are strong Si−O−Si covalent bonds, as shown in Fig. 3.1(f), PFPE molecules are not present on the surface of the layer transferred onto a target substrate. Therefore, a process for removing the residues of the diffusion barrier layer, which is typically a high temperature or wet process, is not necessary, making the PFPE-coated PDMS stamp particu-

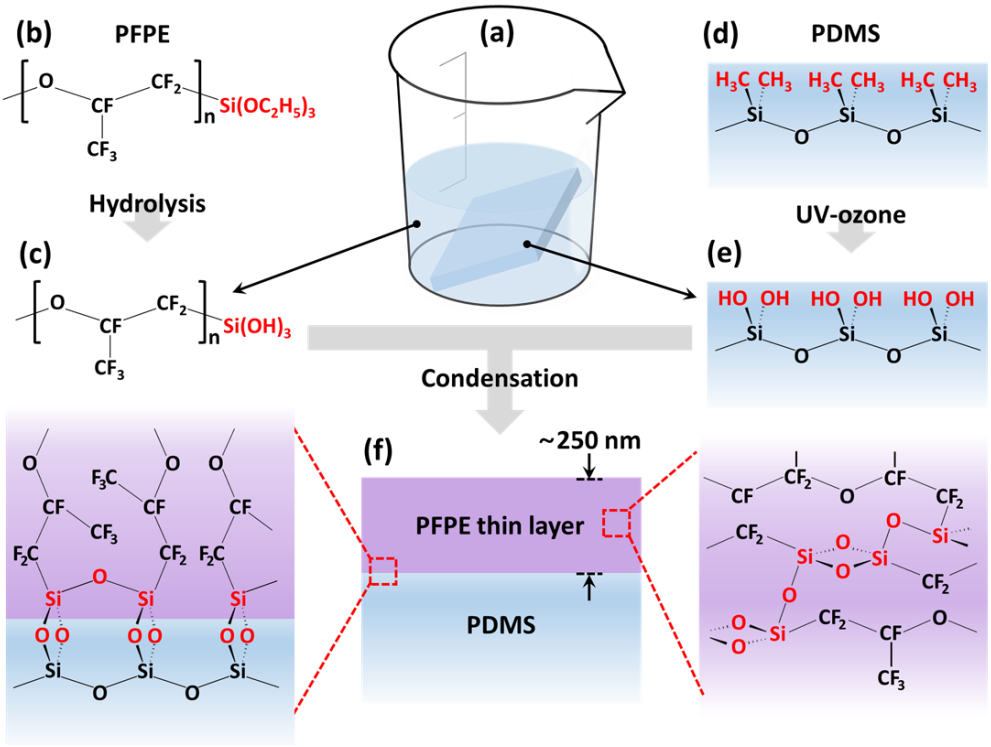

Figure 3.1 (a) Dip-coating of PFPE on a PDMS stamp. A PFPE thin layer is formed on a PDMS surface as a result of a condensation reaction between the hydroxyl groups in PFPE (b, c) and PDMS (d, e), as well as those in the adjacent PFPE molecules. As a result, PFPE molecules are strongly anchored to the PDMS surface and are linked with the adjacent PFPE molecules by Si–O–Si covalent bonding (f).

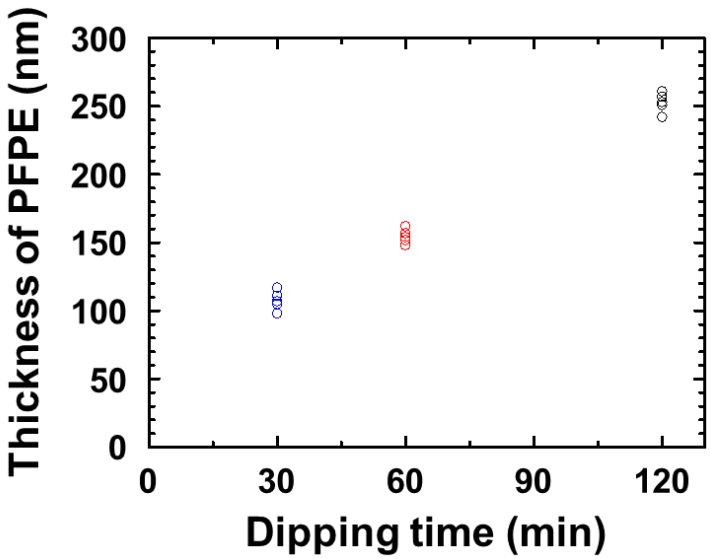

Figure 3.2 The thickness of a PFPE layer coated on a PDMS stamp for dipping times from 30 to 120 min. Each condition contains 5 samples.

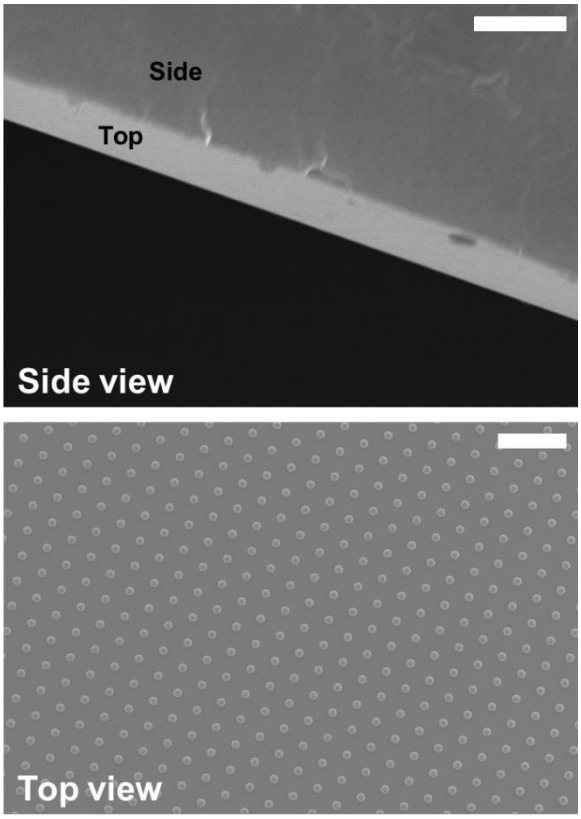

Figure 3.2 The thickness of a PFPE layer coated on a PDMS stamp for dipping times from 30 to 120 min. Each condition contains 5 samples.

larly suitable for transferring materials, such as organic semiconductors, organometal halide perovskites, and ionic gels, that can be damaged by such processes. Since the surface energy of PFPE (17.7 mN m^{-1}) [4] is smaller than that of PDMS (~23.5 mN m^{-1}) [5], the PFPE coating in our case also serves as an adhesion-reduction layer, enhancing the reliability of the materials transfer. In fact, owing to its low surface energy, PFPE has been previously used as a stamp material [4,6]. In those demonstrations, however, stamps were entirely composed of PFPE, whose Young's modulus (9.5 MPa) [7] is much higher than that of PDMS (2.4 MPa) [7], and are therefore inferior to those made of PDMS in terms of conformity in contact. In contrast, the thickness of the PFPE coating in our case, which can be readily controlled by varying the dipping time and the concentration of PFPE, is only ~250 nm, thus preserving the conformity provided by PDMS while taking advantage of the low surface energy of PFPE. When the dipping time decreased, the thickness of a PFPE layer coated on a PDMS stamp is decreased (Fig. 3.2).

3.3 Conclusions

In this chapter, I have developed a hybrid stamp composed of a PDMS bulk and PFPE coating obtained by simple dip-coating inducing a condensation reaction between PDMS and PFPE molecules as well as that between the adjacent PFPE molecules. The PFPE-coated stamp has the following properties ideal for material transfer techniques: the ability to prevent diffusion of small

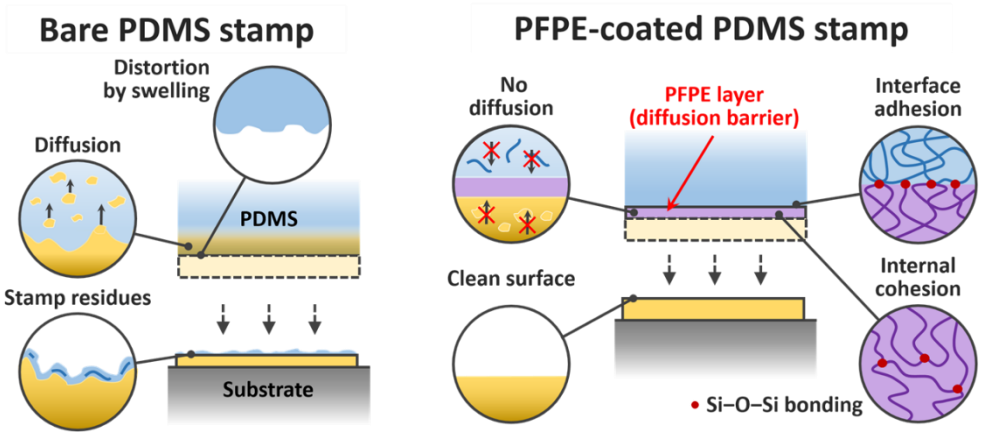

Figure 3.4 Illustration of advantages of a PFPE-coated PDMS stamp

molecules, low surface energy, strong internal cohesion of the PFPE layer, and strong adhesion at the PFPE−PDMS interface.

3.4 Methods

3.4.1 Preparation of PDMS stamps

The base and curing agent of PDMS (Sylgard 184, Dow Corning) were thoroughly mixed in a weight ratio of 10:1, and then degassed in a low-vacuum chamber. The mixture, the amount of which is such that the resulting thickness of the PDMS stamp is ~2 mm, was poured onto a bare Si wafer. Next, the mixture was cured on a hot plate at 80 ˚C for ~24 h.

3.4.2 PFPE dip-coating of PDMS stamps

The PFPE coating on a PDMS stamp, shown in Fig. 3.1, was obtained as follows (Fig. 3.5). First, to hydrate the ethoxysilane end groups of PFPE into hydroxyl groups as shown in Fig. 3.1(b,c), a solution of ethoxysilane-terminated PFPE (Fluorolink S10, Solvay Solexis) was diluted in IPA at 0.1 wt %, into which water (0.4 wt %) and acetic acid (0.1 wt %) were added. After keeping the solution in an atmosphere for 30 min, a PDMS stamp whose surface was modified with hydroxyl groups, prepared by UV-ozone treatment [Fig. 3.1(d,e)], was immersed in the solution and then stored for 2 h. During this process, the PFPE coating was formed on the PDMS surface via a condensation reaction between the hydroxyl groups of PFPE and PDMS and, also, between

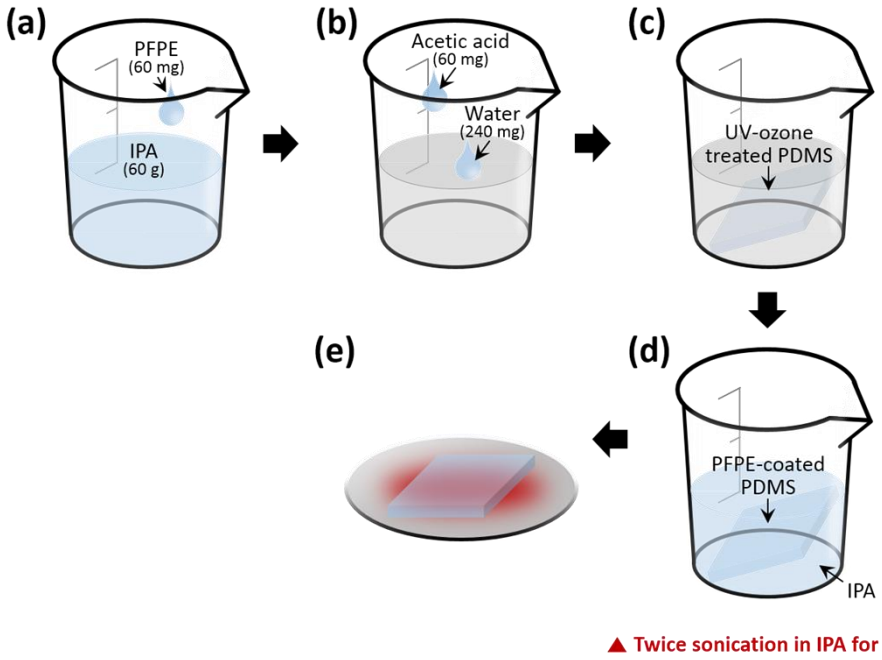

Figure 3.5 The PFPE coating on a PDMS stamp. (a,b) First, to hydrate the ethoxysilane end groups of PFPE into hydroxyl groups, a solution of ethoxysilane-terminated PFPE was diluted in IPA at 0.1 wt %, into which water (0.4 wt %) and acetic acid (0.1 wt %) were added. After keeping the solution in an atmosphere for 30 min, a PDMS stamp whose surface was modified with hydroxyl groups, prepared by UV-ozone treatment, was immersed in the solution and then stored for 2 h (c). (d) To remove excess PFPE, the stamp was sonicated twice in IPA for 5 min each time, after which it was rinsed with water. (e) Finally, the stamp was placed on a hot plate at 100 ˚C for 10 min to remove the residual IPA inside, and then was further heated at 150 ˚C for 15 min.

those of the neighboring PFPEs [Fig. 3.1(f)]. To remove excess PFPE, the stamp was sonicated twice in IPA for 5 min each time, after which it was rinsed with water. Finally, the stamp was placed on a hot plate at 100 ˚C for 10 min to remove the residual IPA inside, and then was further heated at 150 ˚C for 15 min.

3.5 References

[1] J. N. Lee, C. Park, and G. M. Whitesides, Solvent compatibility of poly (dimethylsiloxane)-based microfluidic devices, *Anal. Chem.*, **75**, 6544 (2003).

[2] L. J. Millet, M. E. Stewart, J. V. Sweedler, R. G. Nuzzo, and M. U. Gillette, Microfluidic devices for culturing primary mammalian neurons at low densities, *Lab Chip*, **7**, 987 (2007).

[3] V. Vespini, S. Coppola, M. Todino, M. Paturzo, V. Bianco, S. Grilli, and P. Ferraro, Forward electrohydrodynamic inkjet printing of optical micro-lenses on microfluidic devices, *Lab Chip*, **16**, 326 (2016).

[4] S. H. Sung, H. Yoon, J. Lim, and K. Char, Reusable stamps for printing sub-100 nm patterns of functional nanoparticles, *Small*, **8**, 826 (2012).

[5] J. P. Rolland, E. C. Hagberg, G. M. Denison, K. R. Carter, and J. M. De Simone, High-resolution soft lithography: enabling materials for nano-technologies, *Angew. Chem., Int. Ed.*, **43**, 5796 (2004).

[6] H. Park, H. Cho, J. Kim, J. W. Bang, S. Seo, Y. Rahmawan, D. Y. Lee, and K. -Y. Suh, Multiscale transfer printing into recessed microwells and on curved surfaces via hierarchical perfluoropolyether stamps., *Small*, **10**, 52 (2014).

[7] M. Domenichini, R. Sahai, P. Castrataro, R. Valsecchi, C. Tonelli, F. Greco, and P. Dario, Fabrication of layered polydimethylsiloxane/perfluoropoly-

ether microfluidic devices with solvent compatibility and valve functionality, *Microfluid. Nanofluid.*, **15**, 753 (2013).

Chapter 4 Application of the PFPE-coated PDMS Stamp to the Fabrication of Organic Electronic Devices by Layer Transfer

4.1 Introduction

A stamp-based material transfer is a versatile, low temperature, and dry process that can be used to deposit and pattern various materials such as polymers [1,2], metals [3,4], two-dimensional (2D) materials [5–7], quantum dots (QDs) [8,9], nanoparticles (NPs) [10,11], nanowires [12,13], supramolecules [14], and DNAs [15] onto target substrates. Poly(dimethylsiloxane) (PDMS), the most widely used material for stamps, has low Young's modulus and surface energy, which makes it suitable for large area transfer of microstructures composed of materials including NPs [11], 2D materials [16], and QDs [17]. However, PDMS has undesirable properties limiting its widespread use in material transfer techniques. Attempts to pattern an organic semiconductor layer by transferring it from a patterned PDMS stamp onto a substrate very often fail, since organic molecules deposited on the PDMS stamp are absorbed into free volumes in PDMS. When transferring a layer of materials such as polymers, QDs, NPs, or nanowires that are spin-coated on a PDMS stamp, organic solvent molecules absorbed into PDMS can swell the stamp, degrading the quality of the layer [8,18]. Furthermore, uncured siloxane oligomers in PDMS have been

found to contaminate the transferred layers [19–22], which degrades their optical and electrical properties, such as luminescence yield, and efficiency of injection and extraction of charge carriers.

Attempts have been made to form a coating on a PDMS stamp that can function as a diffusion-blocking layer. For example, when arrays of organic light-emitting devices (OLEDs) were fabricated by transferring an organic bilayer from a patterned PDMS stamp onto a substrate coated with an organic layer, the organic bilayer and the PDMS surface were decoupled by inserting a Cr/Au bilayer between them [23]. Although the Cr/Au bilayer proved effective in preventing the diffusion of both the organic molecules into the stamp and the PDMS oligomers onto the organic layer, very high Young's modulus of the metal bilayer resulted in an incomplete transfer in the substrate regions with step heights. Kim et al. deposited a layer of parylene-C on a PDMS stamp by a chemical vapor deposition (CVD) method to prevent absorption by the stamp of chloroform used in spin coating QDs on the stamp [8]. Because the parylene-C layer is bonded to the PDMS surface by weak van der Waals interactions, it can delaminate from the stamp and transfer onto a target substrate along with the layer designed to be transferred. In fact, this unwanted transfer occurs when transferring a graphene layer using a PDMS stamp spin-coated with a fluorinated resin with a low surface energy [20,24] necessitating a wet or high temperature process to remove the transferred resin. Consequently, this method cannot be applied in situations involving materials (e.g., organic small

molecules [22], polymers [25], ionic gels [26], and organometal halide perovskites [27]) that can degrade or dissolve when exposed to a wet or high temperature process.

In this chapter, I demonstrate the effectiveness and versatility of the PFPE-coated stamp by fabricating two types of electronic devices that have a mechanically bonded interface in their interiors, representative of applications where, in addition to layer transfer itself, high quality of the transfer-bonded interface and a high degree of cleanliness of the top surface of the transferred layer are required. In the first example, a layer of tris-(8-hydroxyquinoline)aluminum (Alq_3) was transferred onto a layer of N,N′-bis(naphthalene-1-yl)-N,N′-bis(phenyl)-benzidine (NPB) via weak Alq_3–NPB van der Waals adhesion, and an OLED employing this bilayer is shown to have a performance comparable to a control device fabricated by sequential vacuum depositions. In the second application, I fabricated an organic hole-only device composed of NPB, whose bottom electrode is a graphene bilayer formed by sequential transfer depositions of a graphene monolayer from a stamp. Using the PFPE-coated stamp, the charge transport between the graphene layers and hole injection from the graphene electrode into an adjacent MoO_3 layer were significantly enhanced, relative to the case when an uncoated-PDMS stamp was used. These results indicate that the PFPE-coated stamp prepared by the simple dip-coating may greatly expand the application range of stamp-based material transfer techniques, by making them applicable to cases where mechanically

bonded interfaces between weakly interacting surfaces need to be electronically functional and the additional layers or device(s) need to be placed on top of the transferred layers. This new capability dramatically broadens the technological relevance of stamp-based transfer in the fabrication of electronically active multilayer devices.

4.2 Results and discussion

4.2.1 Transfer-printing of a patterned layer composed of organic small molecules from the PFPE-coated stamp to a target substrate

Although the PFPE-coated PDMS stamp may be broadly used to transfer various materials such as 2D materials (e.g., graphene, boron nitride, and molybdenum disulfide), metal and metal oxide NPs, and QDs onto a target substrate, the advantageous properties of the PFPE coating described above blocking of diffusion, low surface energy, high adhesion to the stamp, high internal strength enable the transfer of patterned films of organic semiconductors in particular. To show this, I transferred a patterned layer of Alq_3 onto a layer of NPB on an indium tin oxide (ITO)-coated glass substrate using the PFPE-coated PDMS stamp, as shown in Fig. 4.1(a), and compared the result with that obtained with a PDMS stamp without a PFPE coating. The Alq_3 layer on the stamp was patterned into the Seoul National University (SNU) logo by a shadow mask. The Alq_3 and NPB layers, both 50 nm in thickness, were deposited using thermal evaporation in vacuum (~10^{-7} Torr). After the stamp was

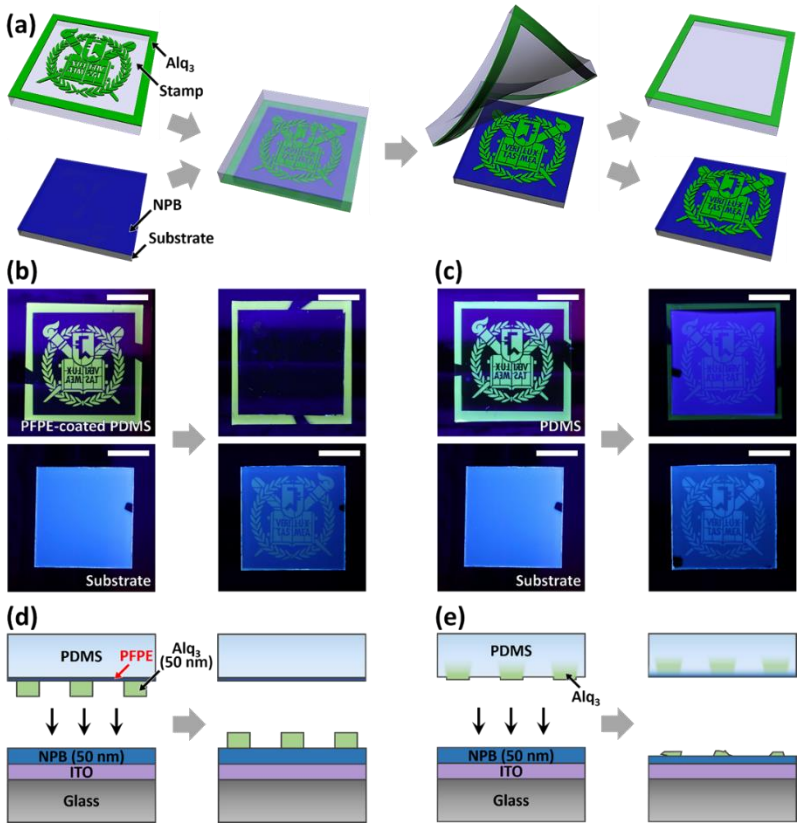

Figure 4.1 (a) Illustration of the transfer of an Alq_3 layer patterned into the Seoul National University logo from a stamp onto an NPB layer on an ITO-coated glass substrate. (b, c) Photoluminescence (PL) images of the stamps (top) and the substrates (bottom) obtained by placing them on an UV lamp with a center wavelength of 365 nm. The PFPE-coated and uncoated PDMS stamps were used in (b) and (c), respectively. The images to the left and the right of the gray arrows correspond to the samples before and after the transfer, respectively. Note that the samples used for the ″before″ images in (b) and (c) were taken out of the glovebox for imaging only and were not used in the transfer processes yielding the ″after″ images. Scale bars: 1 cm. (d, e) Schematic diagrams showing the results of the transfer processes when (d) the PFPE-coated stamp and (e) the uncoated stamp were used.

placed onto the substrate, the conformal contact between them was induced by applying gentle pressure with tweezers. They were then placed on a hot plate at 60 ˚C with a pressure of ~2 MPa for 10 min, after which the stamp was carefully peeled off from the substrate. The transfer process was performed in a glovebox connected to a vacuum thermal evaporator so that the stamp and the substrate remained in a nitrogen atmosphere after organic depositions.

Photoluminescence (PL) images of the stamps (top) and the substrates (bottom), obtained by placing them on a UV lamp with a center wavelength of 365 nm, are shown in Fig. 4.1(b,c), corresponding to the experiments where the PFPE-coated and uncoated PDMS stamps, respectively, were used. Also, shown in Fig. 4.1(d,e) are schematics summarizing the results of the transfer processes in both cases confirmed by analyses based on the PL images and spectra, as discussed below. The PL images were obtained using a UV lamp (UVItec Ltd.,) and a digital camera (500D, Canon) with a long-pass filter (400 nm). When the PFPE-coated stamp was used [Fig. 4.1(b)], the green SNU logo on the stamp (top left) was completely transferred onto the substrate (bottom right) as originally intended, and consequently no PL was observed after the transfer in the region of the stamp that was in contact with the substrate (top right, note that purplish blue patterns are the emission of the lamp itself). When the PDMS stamp was used, although the SNU logo appears to have been transferred onto the substrate [Fig. 4.1(c), bottom right], it is also visible on the stamp [Fig. 4.1(c), top right]. Furthermore, in addition to the substrate, the en-

tire area of the stamp that was in contact with the substrate appears blue, suggesting that the NPB layer on the substrate was in part transferred onto the stamp.

For further clarification, I measured the PL spectra of the stamps and substrates using a spectrophotometer (FS-2, Sinco), after the same transfer processes yielding the results shown in Fig. 2(b,c) were performed with unpatterned Alq_3 layers. In this measurement, I used two different excitation wavelengths (λ_{ex}): 350 nm, where the absorption of NPB is significantly larger than that of Alq_3 [Fig. 4.2(a)] and 420 nm, where Alq_3 absorbs more strongly than NPB [Fig. 4.2(b)]. When the PFPE-coated stamp was used, the spectra of the stamp (orange) for both λ_{ex} show negligible PL signals with no identifiable peak across the entire wavelength range. The PL spectra of the substrate show that in the case of λ_{ex} = 420 nm, a strong PL signal of Alq_3 with a peak at 520 nm is clearly visible [Fig. 4.2(b), red], and that for λ_{ex} = 350 nm, the spectrum [Fig. 4.2(a), red]resembles that of NPB (Fig. 4.3) with an increased long wavelength tail due to the PL of Alq_3 (Fig. 4.3). When the PDMS stamp was used, the PL spectra of the stamp show a strong NPB signal with a peak at 411 nm [Fig. 4.2(a), green] and an Alq_3 signal with a peak at 505 nm [Fig. 4.2(b), green], consistent with the PL image shown in Fig. 4.1(c). Note that the positions of these peaks were blue-shifted compared to those of the PL peaks of NPB and Alq_3 neat films, located at 435 [28] and 520 nm [29], respectively. Considering the previous reports that small molecules in contact with a PDMS stamp are found to be diffused into free volumes of PDMS [30], I attribute the

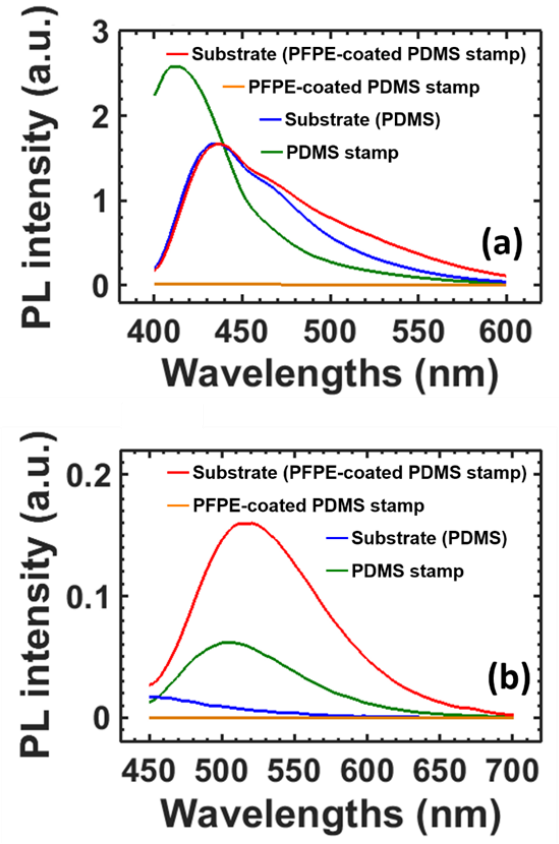

Figure 4.2 Photoluminescence spectra of the stamps and the substrates after transferring an unpatterned 50-nm-thick Alq_3 layer on a PFPE-coated or uncoated PDMS stamp onto a 50-nm-thick NPB layer on an ITO-coated glass substrate. The excitation wavelength is 350 nm in (a) and 420 nm in (b).

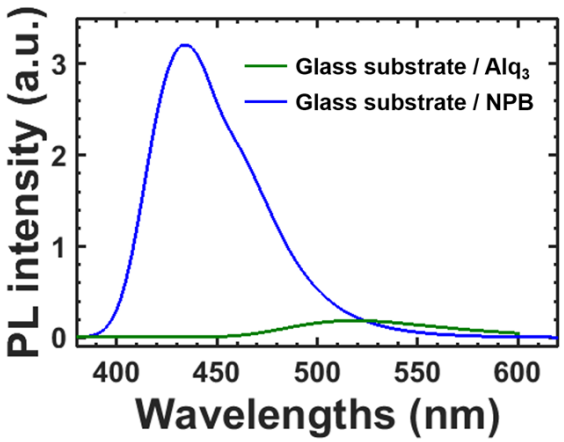

Figure 4.3 Photoluminescence spectra of an Alq_3 layer and an NPB layer, both 50 nm in thickness, deposited on a glass substrate by thermal evaporation in vacuum. The excitation wavelength is 350 nm.

blue-shifted PLs to the so-called solid-state solvation effect [31]: because of the diffusion of NPB (Alq_3) molecules into the PDMS stamp, which is facilitated by heat treatment during the transfer process and is effectively prevented in the case of the PFPE-coated stamp (Fig. 4.4), NPB (Alq_3) molecules on the two types of stamps are surrounded by materials with different polarizabilities neighboring NPB (Alq_3) molecules and PDMS molecules in the cases of the PFPE-coated and uncoated stamps, respectively. Because of the diffusion into the stamp, only a very small amount of Alq_3 molecules was transferred onto the substrate, which is evident from the negligible Alq_3 PL in the PL spectrum of the substrate after the transfer process [Fig. 4.2(b), blue]. From the PL spectra, together with the PL images shown in Fig. 4.1(b,c), the results of the transfer processes are schematically summarized in Fig. 4.1(d,e). When the PFPE-coated stamp was used, the patterned Alq_3 layer was completely transferred, as originally intended [Fig. 4.1(d)]. In contrast, unblocked diffusion of Alq_3 and NPB molecules in the case of the uncoated stamp resulted in a very small amount of Alq_3 molecules transferred onto the substrate, along with an unwanted partial transfer of the NPB layer from the substrate to the stamp in the entire region of the substrate that was in contact with bare PDMS [Fig. 4.1(e)].

Next, surface characterization using an atomic force microscope (AFM; Dimension Edge, Bruker) was performed on the transfer-printed substrates — those shown in the bottom right panels of Fig. 4.1(b,c). Figure 4.5(a) shows a height image (top) and a profile along a white dotted line in the image (bottom) of the top surface of the Alq_3 layer transferred from the uncoated PDMS stamp,

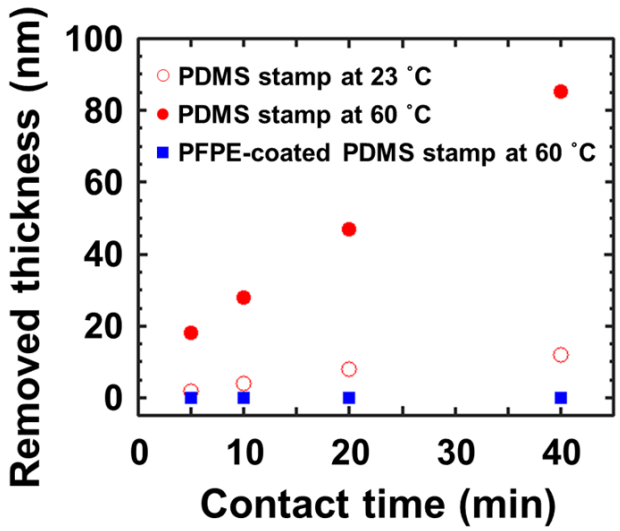

Figure 4.4 Thickness of an NPB layer on an ITO-coated glass substrate diffused into a PFPE-coated or uncoated PDMS stamp after being in contact with the stamp under a pressure of 2 MPa for a different duration from 5 to 40 min. The measurement was performed following the experiment described in Ref. 30 as follows: (i) a 100-nm-thick NPB layer was deposited onto an ITO-coated glass substrate by thermal evaporation; (ii) a PFPE-coated or PDMS stamp was brought into contact with the NPB layer, followed by storing the samples at 23 ˚C or 60 ˚C under a pressure of 2 MPa for a varying contact time; (iii) the stamp was carefully peeled off from the substrate; (iv) a step height of the NPB layer was measured near the boundary of the contacted region.

corresponding to the region of the SNU logo appearing light blue in Fig. 4.1(c). The surface is found to be much rougher than a typical Alq_3 thin film deposited by thermal evaporation in vacuum [32], with a root-mean-square (RMS) roughness of 16.4 nm and a maximum peak-to-valley height in the line scan of ~75 nm. This suggests that, because of the diffusion of Alq_3 molecules into the free volumes of PDMS, the transferred Alq_3 "layer" is not continuous but rather composed of randomly distributed small domains. In contrast, when the PFPE-coated stamp was used, the surface roughness is comparable to a typical vacuum-deposited Alq_3 film [32]: the RMS roughness and the maximum peak-to-valley height are, respectively, 1.4 and ~6 nm, more than 10 times smaller than the corresponding values for the case of the uncoated PDMS [Fig. 4.5(b)]. An undesirable feature arising from the molecular diffusion is also evident in the NPB layer that was in contact with the bare PDMS, corresponding to the regions in dark blue in Fig. 4.1(c). An AFM measurement on this region reveals that holes with a diameter of several hundred nanometers and a depth of 10 nm or more were randomly distributed throughout the NPB layer [Fig. 4.6(a)], which was formed presumably by the diffusion of NPB molecules into the nonuniformly distributed PDMS free volumes. In contrast, owing to the diffusion-blocking properties, the use of the PFPE-coated stamp prevents the unwanted substrate-to-stamp transfer of NPB molecules, with the roughness of the contacted NPB surface comparable to that of a vacuum-deposited NPB film [Fig. 4.6(b)] [32]. This prevention of the substrate-to-stamp transfer is a feature of the PFPE-coated stamp particularly important when a patterned layer of a

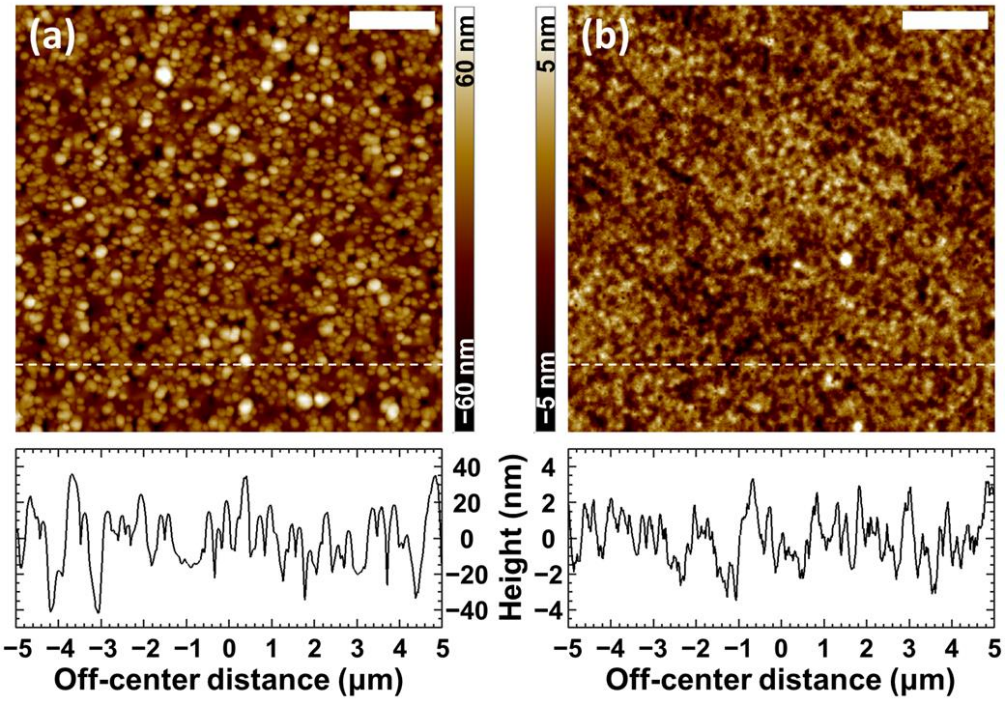

Figure 4.5 AFM height images of the ITO-coated glass substrate coated with the NPB layer onto which the patterned Alq_3 layer on (a) a PDMS stamp and (b) a PFPE-coated PDMS stamp were transferred. Scale bars: 2 μm. The profiles shown below were measured along the white dotted lines in the height images.

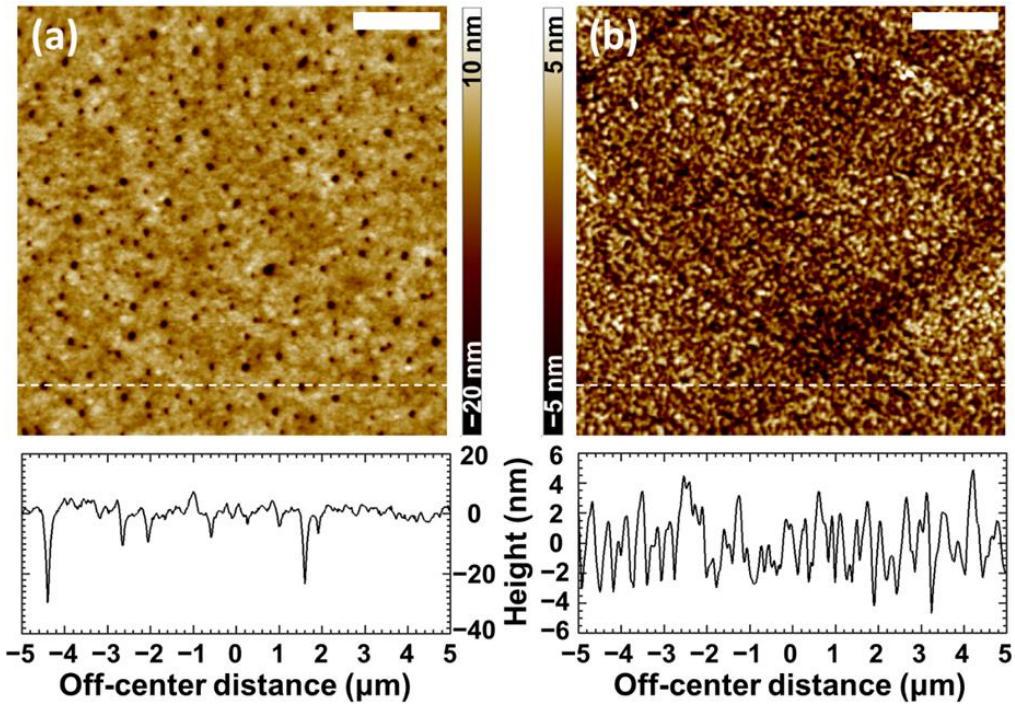

Figure 4.6 AFM height images of the ITO-coated glass substrate coated with the NPB layer in a region that was in direct contact with (a) a PDMS stamp and (b) a PFPE-coated PDMS stamp (in a region not covered with the Alq_3 patterns) during the transfer process. Scale bars: 2 μm. The profiles shown below were measured along the white dotted lines in the height images.

material — regardless of whether it is susceptible to diffusion into PDMS — is transfer printed onto an organic thin film from an unpatterned (i.e., without a surface relief) stamp, as in our demonstration, and, then, additional layers need to be deposited on the remaining region of the organic thin film. Practical examples include transfer deposition of layers of organic semiconductors or QDs onto an organic layer to integrate organic or QD light-emitting diodes emitting different colors onto a single substrate.

4.2.2 Fabrication of green fluorescent OLEDs by organic-layer transfer

For the PFPE-coated PDMS stamp to be widely used for the integration of organic electronic devices, a molecular interface formed by layer transfer needs to function like the same interface formed by successive vacuum depositions. To demonstrate this, I fabricated OLEDs whose structure is glass/ITO/50 nm NPB/50 nm Alq_3/0.5 nm LiF/100 nm Al, by performing the experiments described in Fig. 4.1(d,e), with unpatterned Alq_3 layers, followed by depositing the LiF/Al layer through a shadow mask with 2-mm-diameter circular openings by thermal evaporation in vacuum (~10^{-7} Torr). The devices fabricated using PFPE-coated and uncoated PDMS stamps are referred to as $OLED_{PFPE}$ and $OLED_{PDMS}$, respectively, and the current density–voltage (J–V) and the external quantum efficiency–current density (η_{ext}–J) characteristics of their representative devices were compared with those of the control device ($OLED_{CTRL}$), where all the layers were vacuum deposited (Fig. 4.7). The J–V and η_{ext}–J characteristics were obtained using

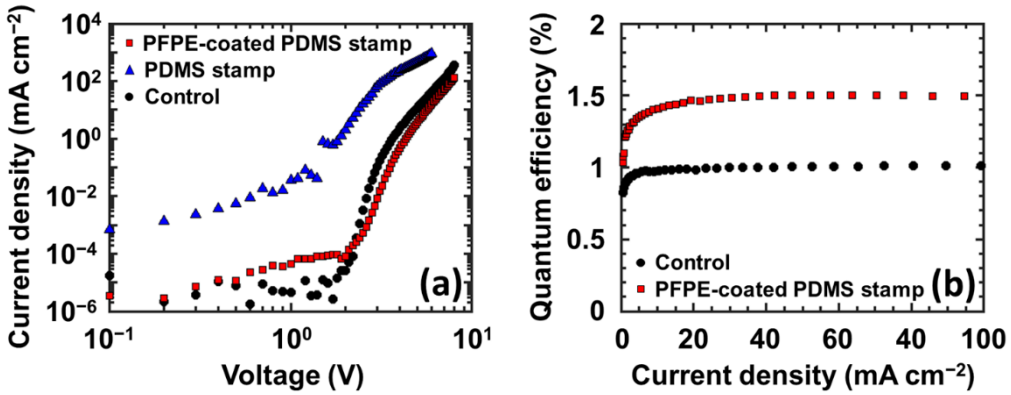

Figure 4.7 (a) Current density–voltage (*J*–*V*) and (b) external quantum efficiency–current density (η_{ext}–*J*) characteristics of organic light-emitting devices fabricated by transferring Alq_3 layers using uncoated (blue triangles) and PFPE-coated PDMS stamps (red squares), compared with those of a control device, where all layers were vacuum deposited (black circles). The device structure is glass substrate/ITO/50 nm NPB/50 nm Alq_3/0.5 nm LiF/100 nm Al.

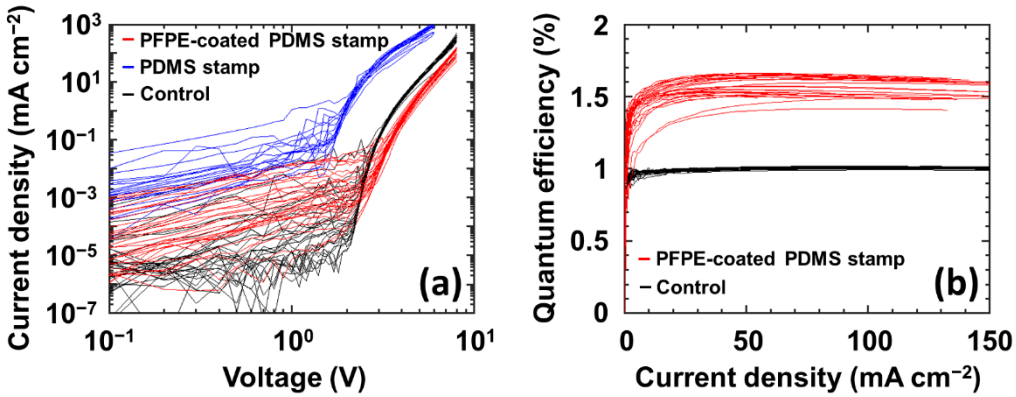

Figure 4.8 (a) Current density–voltage (*J*–*V*) and (b) external quantum efficiency–current density (η_{ext}–*J*) characteristics of organic light-emitting devices fabricated by transferring Alq_3 layers using uncoated (blue lines, $OLED_{PDMS}$) and PFPE-coated PDMS stamps (red lines, $OLED_{PFPE}$), compared with those of control devices where all layers were vacuum-deposited (black lines, $OLED_{CTRL}$). For each type of OLEDs, 30 devices (6 devices per substrate) were fabricated. All 30 devices were operational in the cases of $OLED_{CTRL}$ and $OLED_{PFPE}$, whereas only 19 devices were not short-circuited for $OLED_{PDMS}$. The much higher yield of $OLED_{PFPE}$ than that of $OLED_{PDMS}$ is attributed to the capability of the PFPE layer to block diffusion of small molecules into the stamp and of the PDMS oligomers onto the target substrate.

a source meter (2400, Keithley) and a Si photodiode (818-SL, Newport). Out of 30 devices fabricated for each type of OLEDs, all 30 devices were operational in the cases of $OLED_{CTRL}$ and $OLED_{PFPE}$, whereas only 19 devices were not short-circuited for $OLED_{PDMS}$. The *J*–*V* and η_{ext}–*J* characteristics of all operational OLEDs are shown in Fig. 4.8. As shown in Fig. 4.7(a), at a given *V*, $OLED_{PDMS}$ has a significantly larger value of *J* than the other devices: for example, the *J* values at 6 V are 902 mA cm^{-2} for $OLED_{PDMS}$ (blue triangles), 15 mA cm^{-2} for $OLED_{PFPE}$ (red squares), and 42 mA cm^{-2} for $OLED_{CTRL}$ (black circles). This is due to the molecular diffusion into the PDMS stamp as schematically described in Fig. 4.1(e), resulting in a very small amount of Alq_3 transferred onto the substrate and the NPB layer with a thickness much smaller than 50 nm: the thickness of the NPB–Alq_3 bilayer of $OLED_{PDMS}$ was 28 nm, whereas that of $OLED_{PFPE}$ is 100 nm. As a result, the intensity of the light output of $OLED_{PDMS}$ was too weak to be detected using a Si photodetector. In contrast, the characteristics of $OLED_{PFPE}$ are comparable to those of $OLED_{CTRL}$. For instance, V and η_{ext} corresponding to J = 10 mA cm^{-2} are, respectively, 5.7 V and 1.4% for $OLED_{PFPE}$ and 4.9 V and 1.0% for $OLED_{CTRL}$. The slightly higher driving voltage of $OLED_{PFPE}$ than that of $OLED_{CTRL}$ is likely to be due primarily to imperfections at the Alq_3–NPB interface, such as dust particles and adsorbed molecular contaminants, because the transfer experiments were performed in a glovebox. As shown in Fig. 4.7(b), $OLED_{PFPE}$ has higher ηext than $OLED_{CTRL}$ at all *J*. Since it is very unlikely that the internal quantum

efficiency of Alq_3 excitons is increased by the change in the Alq_3–NPB interfacial properties, I attributed the increased η_{ext} of $OLED_{PFPE}$ to the increased charge balance. The imperfections at the Alq_3–NPB interface in $OLED_{PFPE}$ may have decreased the number of holes reaching the cathode without forming excitons in the Alq_3 layer by impeding the hole transport to the Alq_3–NPB interface [29]. One may wonder whether the increases in the driving voltage and η_{ext} of $OLED_{PFPE}$ are entirely due to the extrinsic factors such as dust particles and adsorbed molecular contaminants or are also due to the intrinsic properties of the mechanically formed Alq_3–NPB molecular junction different from those of the same junction formed by sequential depositions in a vacuum. Answering this fundamental question requires further rigorous investigations. Nevertheless, this results indicate that the Alq_3–NPB interface transfer bonded using the PFPE-coated stamp is sufficiently intimate at the molecular level, and, to the best of my knowledge, are the first demonstration showing that a device with a small-molecule heterojunction formed by a layer transfer can have a performance comparable to that of the vacuum-deposited control device.

4.2.3 Characteristics of a transferred graphene monolayer using the PFPE-coated PDMS stamp

The diffusion-blocking properties of the PFPE film suggest that the contamination of the transferred layers by uncured siloxane oligomers, which was commonly observed when PDMS stamps were used, and thus limited their

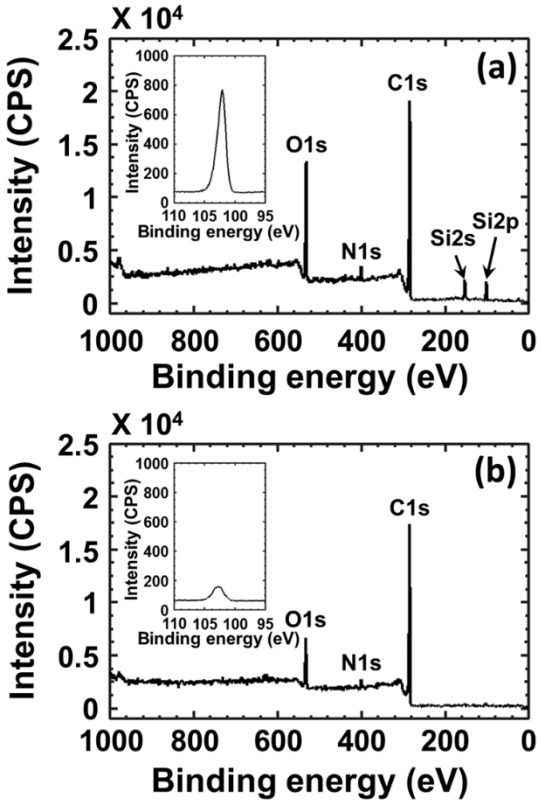

Figure 4.9 X-ray photoelectron spectra of a graphene monolayer on a PET film transferred from (a) an uncoated PDMS stamp and (b) a PFPE-coated PDMS stamp. The insets show narrow-scan XPS spectra of the Si2p peak at 102 eV.

applicability [19–22], can be effectively prevented using the PFPE-coated PDMS stamp. To confirm this, I carried out X-ray photoelectron spectroscopy (XPS; Sigma Probe, Thermo Scientific), scanning electron microscopy (SEM; JSM-6700F, JEOL), and AFM on graphene monolayers transferred onto substrates from uncoated and PFPE-coated PDMS stamps. To overcome the difficulties in obtaining a graphene monolayer on a hydrophobic PFPE or PDMS surface from a graphene monolayer grown on a Cu foil, I used a modified wet-transfer technique that uses a Au support layer and a low surface-tension liquid bath [22]. In the following, graphene monolayers transferred onto the substrates from the uncoated and PFPE-coated stamps are referred to as G_{PDMS} and G_{PFPE}, respectively. Figure 4.9(a) is the XPS spectrum of G_{PDMS} transferred on a poly(ethylene terephthalate) (PET) film. In addition to the C1s peak at 284 eV and the O1s peak at 531 eV, which have commonly been observed for graphene monolayers grown on Cu foils by CVD [33], the Si2s and Si2p peaks at 153 and 102 eV, respectively, were detected. The presence of the Si peaks indicates that G_{PDMS} is contaminated by uncured siloxane oligomers of PDMS, consistent with the previous studies [20,22,24]. In contrast, the XPS spectrum of G_{PFPE} on a PET substrate [Fig. 4.9(b)] appears to be free of the Si peaks, with a much smaller intensity of the O1s peak compared with G_{PDMS}, indicating that the diffusion of uncured siloxane oligomers was prevented by the PFPE layer. A narrow-scan XPS spectrum with a higher energy resolution [inset, Fig. 4.9(b)], however, reveals the Si2p peak, whose intensity is significantly smaller than that of G_{PDMS} [inset, Fig. 4.9(a)], meaning that the surface of G_{PFPE} is not

completely free of siloxane oligomers. I speculate that these oligomers are those that were dissolved in IPA during the dip-coating process and remained on the top surface of the PFPE-coated stamp, and that they can be further reduced or eliminated by more thorough rinsing after the dip-coating process. Nevertheless, the number of uncured oligomers on G_{PFPE} is sufficiently small that the charge transport between G_{PFPE} and its adjacent layer is substantially more efficient compared with the case of G_{PDMS}, as shown in the Section 4.2.4.

The contrast in the cleanliness of G_{PDMS} and G_{PFPE} is also evident in SEM and AFM images, shown in Fig. 4.10. An SEM image of G_{PDMS} on a Si substrate shows irregularly distributed dark regions [Fig. 4.10(a)], whereas that of G_{PFPE} on a Si substrate is almost featureless [Fig. 4.10(b)]. Considering that these images were obtained in the secondary electron mode and that the intensities of the Si2s and Si2p peaks in the XPS spectrum of G_{PDMS} were significantly higher than those of G_{PFPE}, I conclude that the dark regions are due to the nonconductive oligomers transferred from the stamp, consistent with my previous work [22]. This conclusion is further supported by a tapping-mode AFM image of a dark region of G_{PDMS} [Fig. 4.10(c)] revealing that G_{PDMS} in that region is covered with a very thin layer of, most likely, oligomers. Because of this layer, two features commonly observed in CVD-grown graphene samples — graphene multilayers indicated by white arrows and wrinkles indicated by blue arrows — are much less clear than those in the case of G_{PFPE} [Fig. 4.10(d)]. Small particles randomly distributed throughout the surface of G_{PFPE},

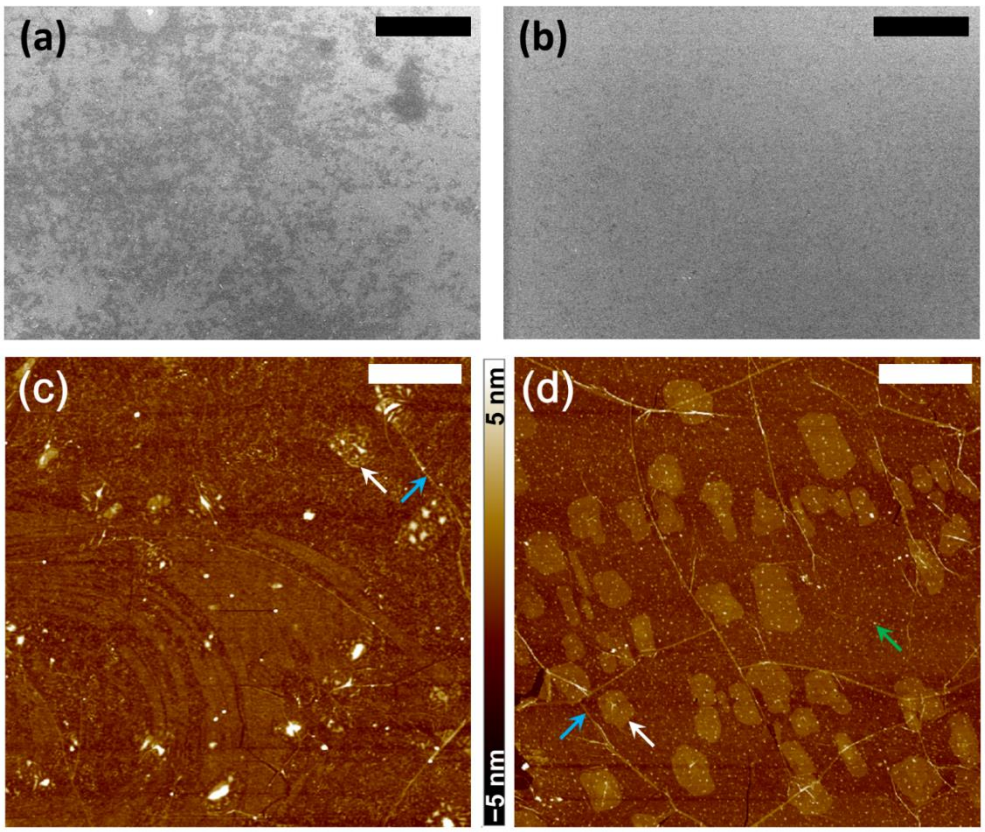

Figure 4.10 (a,b) Scanning electron microscopy and (c,d) atomic force microscopy images of a graphene monolayer transferred from (a,c) an uncoated PDMS stamp and (b,d) a PFPE-coated PDMS stamp. Scale bars in (a,b) and (c,d) are 25 and 2 µm, respectively.

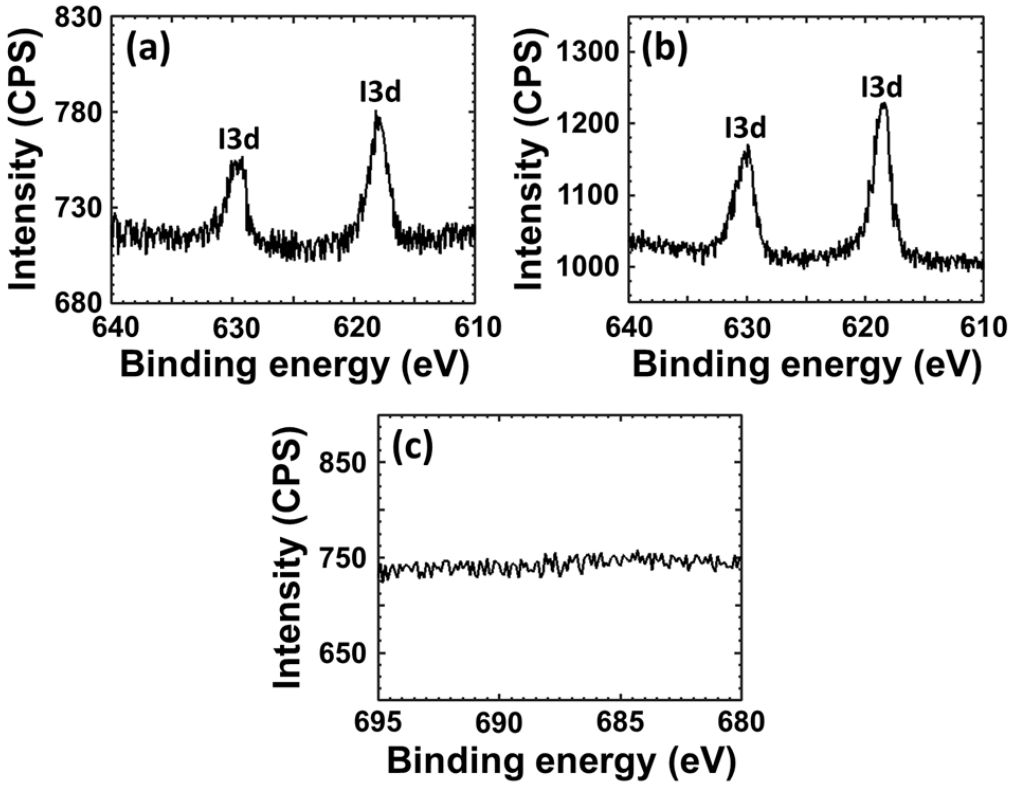

Figure 4.11 XPS spectra of the I3d peaks at 629.9 eV and 618.4 eV for a graphene monolayer on a PET film transferred from (a) a PFPE-coated PDMS stamp and (b) an uncoated PDMS stamp. (c) XPS spectrum of a graphene monolayer on a PET film transferred from a PFPE-coated PDMS stamp in a binding-energy range including 686 eV corresponding to the F1s electron.

indicated by a green arrow in Fig. 4.10(d), are most likely composed of ammonium iodide (NH_4I), an etchant for Au support layers used in wet transfer of graphene onto stamps [22], since the N1s peak at 400 eV [Fig. 4.11(b)] and the I3d peaks at 629.9 and 618.4 eV [Fig. 4.11(a)] were observed in the XPS spectra of G_{PFPE}. Therefore, these particles, which are also present on G_{PDMS} as inferred from the XPS spectra [Fig. 4.9(a) and Fig. 4.11(b)], did not originate from the PFPE-coated stamp, and can perhaps be eliminated by using a Au etchant based on a different chemistry. I also note that an XPS spectrum of G_{PFPE} near 686 eV does not show any signal related to the F1s electron [Fig. 4.11(c)], indicating that the unwanted transfer of the coating material, which has been previously reported for a stamp spin-coated with a fluorine resin [20,24], was prevented owing to the Si–O–Si covalent bond that strongly anchors PFPE molecules to the PDMS surface and links adjacent PFPEs.

4.2.4 Organic hole-only device with a graphene bottom electrode deposited by using the PFPE-coated PDMS stamp

For various graphene-based electronic devices, perhaps with an exception where the uppermost layer is composed of graphene, the top surfaces of graphene layers must be free of contaminants arising from graphene deposition processes, because surface contaminants can degrade the device performance. To show that G_{PFPE} satisfies this requirement, I fabricated an organic hole-only device with a G_{PFPE} bottom electrode — i.e., an organic device whose electrical current is dominantly determined by holes injected

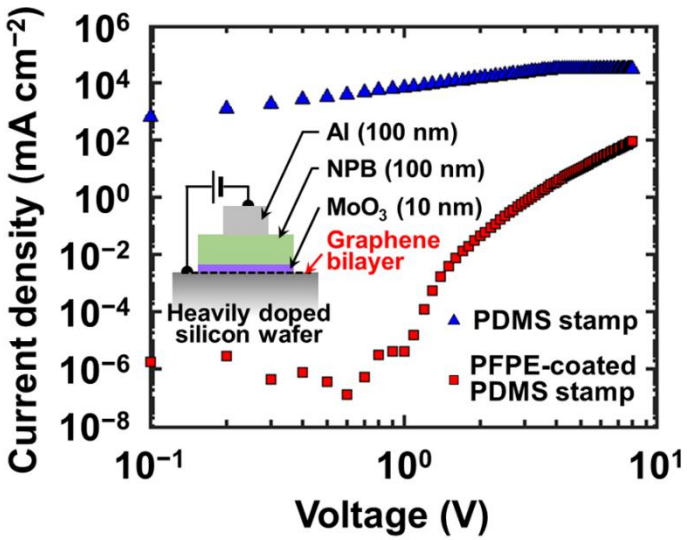

Figure 4.12 Current density–voltage (*J*–*V*) characteristics of organic hole-only devices whose graphene bottom electrodes were formed by using a PDMS stamp (blue triangles) and a PFPE-coated PDMS stamp (red squares). *J* was not allowed to exceed ~3×104 mA cm^{-2} by the instrument setting. The device structure is shown in the inset.

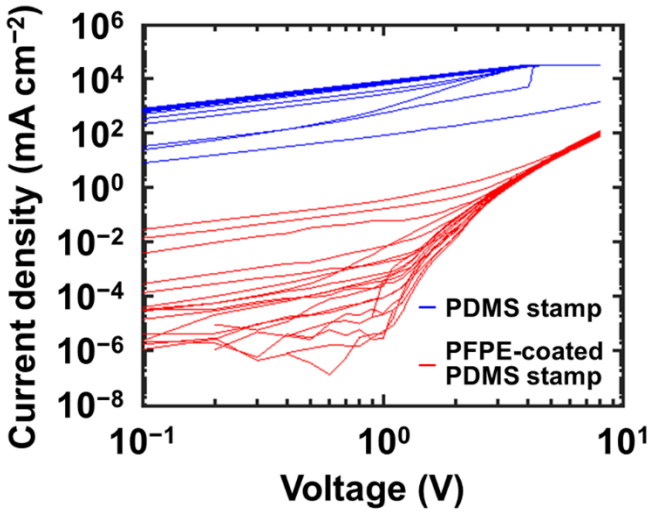

Figure 4.13 Current density–voltage (*J*–*V*) characteristics of NPB hole-only devices whose graphene bottom electrodes were formed by using a PDMS stamp (blue) and a PFPE-coated PDMS stamp (red). *J* was not allowed to exceed ~3×104 mA cm^{-2} by the instrument setting.

from its bottom electrode composed of G_{PFPE} — and compared its *J–V* characteristic with that of a same device with a G_{PDMS} bottom electrode. The device structure was heavily doped Si wafer/G_{PDMS} (or G_{PFPE}) bilayer/10 nm MoO_3/100 nm NPB/100 nm Al (Fig. 4.12, inset). To minimize the effects of charge transport in the lateral direction in the bottom electrode on the *J–V* characteristics, and thus, to clearly probe the impact of the cleanliness of the graphene surface on the hole injection at the graphene–MoO_3 interface, a heavily doped Si wafer was used as a substrate. Also, the possibility of hole injection from Si (not from graphene) in defect regions not covered by graphene was minimized by using a graphene bilayer formed by transferdepositing another graphene monolayer on G_{PFPE} (or G_{PDMS}). The MoO_3 layer was deposited onto the graphene bilayer to enhance the wetting of the graphene top surface by the NPB layer [34] and to ensure efficient hole injection into the NPB layer [35]. The devices were 2 mm in diameter, defined by cathode deposition through a shadow mask. Figure 4.12 compares the *J–V* characteristics of representative hole-only devices with the G_{PDMS} and G_{PFPE} bilayer electrode. For each type of holeonly devices, 20 devices were fabricated and the *J–V* characteristics of all devices are shown in Fig. 4.13. The device with the G_{PDMS} electrode shows an Ohmic behavior with very high conductivity ($\geq 10^{-5}$ S cm^{-1}), indicating that the Al electrode is in direct contact with the MoO_3 or the graphene layer in some regions of the device. This direct contact is likely to have been caused by the transferred oligomer residues at the graphene–MoO_3 and graphene–graphene interfaces,

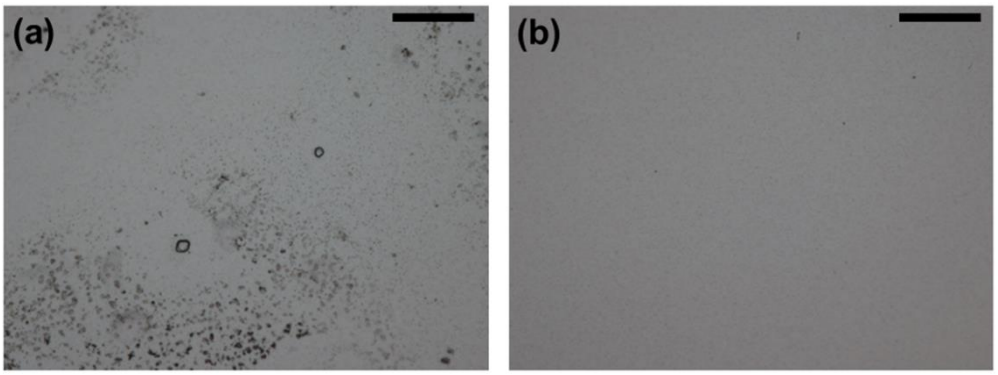

Figure 4.14 Optical microscopy images of the top surfaces of NPB hole-only devices whose graphene bottom electrodes were formed by using (a) a PDMS stamp and (b) a PFPE-coated PDMS stamp (b). Scale bar: 40 μm.

which locally disturbed the deposition of a continuous NPB layer. In fact, the optical microscopy observation of the G_{PDMS} device reveals irregularly distributed contamination [Fig. 4.14], clearly showing that G_{PDMS} cannot be used for devices where charge injection or extraction needs to occur at the top graphene surface. The device with the G_{PFPE} bilayer electrode, in contrast, shows the *J–V* characteristic of a hole-only device with non-Ohmic hole injection, with *J* rapidly increasing beyond a voltage of ~1 V. The significant improvement of the *J–V* characteristic of the G_{PFPE} device indicates that the surface cleanliness of G_{PFPE}, confirmed by the XPS, SEM, and AFM characterization, is sufficient to allow the formation of electronically functional interfaces at that surface. Therefore, the PFPE-coated PDMS stamp can expand the range of applications of dry-transferred graphene layers [22] to include devices where the top graphene surface is involved in charge injection or extraction. Such applications include a tandem OLED or solar cell whose interlayer contains a graphene layer, and the integration of organic optoelectronic devices with graphene electrodes.

4.2.5 Characteristics of red phosphorescent OLEDs fabricated by patterns transfer

The PFPE-coated PDMS stamp can be sufficiently used to fabricate phosphorescent OLEDs by organic-patterns transfer from the stamp to a target substrate, for which other contact-transfer methods fail. To demonstrate this, I fabricated red phosphorescent OLEDs whose structure is glass/ITO/

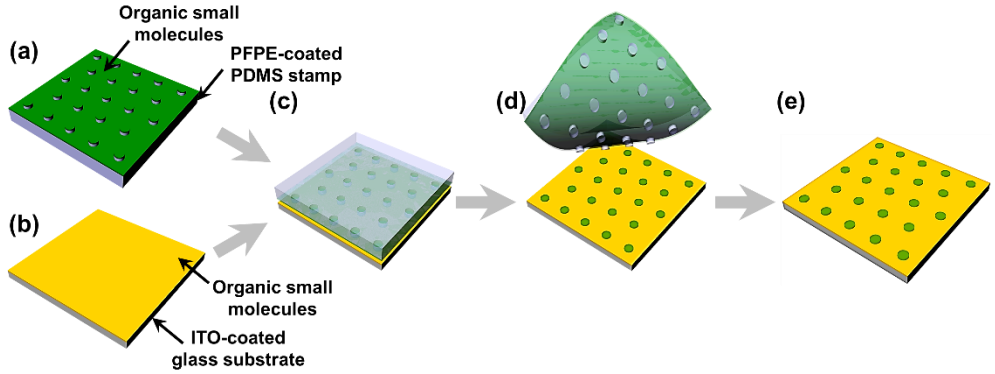

Figure 4.15 Illustration of the transfer-printing of organic small molecule layers on a PFPE-coated PDMS stamp with relief structures from the stamp onto an organic small molecule layer on an ITO-coated glass substrate. (a) A thermally deposited organic-small molecule layers on the PFPE-coated PDMS stamp with relief structures (a) and the ITO-coated glass substrate (b). (c) Placing the structure-faced stamp onto the substrate, and then keeping it on a hot plate at 75 ˚C with a pressure of ~0.5 MPa for 15 min. (d) Peeling off the stamp from the molecules/substrate. (e) Consequentially, the molecule patterns on the relief structures were transfer-printed onto the target substrate.

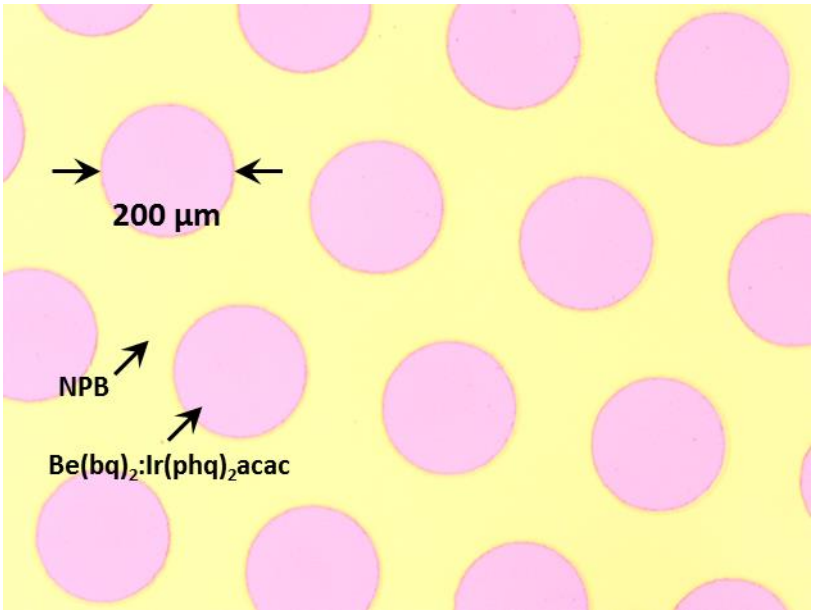

Figure 4.16 Optical microscope images of patterned $Be(bq)_2$:$Ir(phq)_2acac$ layers (thickness: 40 nm) on a 40-nm-thick NPB layer. The diameter of the patterns is 200 μm.

40 nm NPB/50 nm $Be(bq)_2$:$Ir(phq)_2acac$ (1.5 wt%)/0.5 nm LiF/100 nm Al [Fig. 4.15(a)], by transfer-printing of the $Be(bq)_2$:$Ir(phq)_2acac$ layer the experiments described in Fig. 5.1, followed by depositing the LiF/Al layer through a shadow mask with 110-μm-diameter circular openings by thermal evaporation in vacuum (~10^{-7} Torr). In Step (c) in Fig 4.15, the sample was placed on a hot plate at 75 ˚C for 15 min under a pressure of 0.5 MPa. The transfer-printed $Be(bq)_2$:$Ir(phq)_2acac$ patterns on a substrate coated a NPB layer have a sharp edges as shown in optical microscope image in Fig. 4.16. Figure 4.18 shows that the current density–voltage (*J*–*V*) and the external quantum efficiency–current density (η_{ext}–*J*) characteristics of transfer printed devices were compared with those of the control device, where all the layers were vacuum deposited. Although the shapes for the characteristics *J*–*V* are similar for all devices, the transfer printed device has a somewhat higher voltage at the same current density. For example, the voltage corresponding to J = 10 mA/cm^2 is 3.3 V for the control device and 3.7 V for the transfer printed device. The transfer printed device has a lower η_{ext} in the region of low current density. This can be improved by designing the transfer-printed interface to NPB−NPB instead of NPB−$Be(bq)_2$:$Ir(phq)_2acac$, as shown in Fig 4.17 and 4.18. When the work of adhesion (W) is measured, the values of NPB–$Be(bq)_2$ and NPB–NPB interface are 63.86 and 56.41 mJ/m^2. It is considered that the reason why the value of W at the NPB–$Be(bq)_2$ interface is higher than the value of W at the NPB–NPB inter-

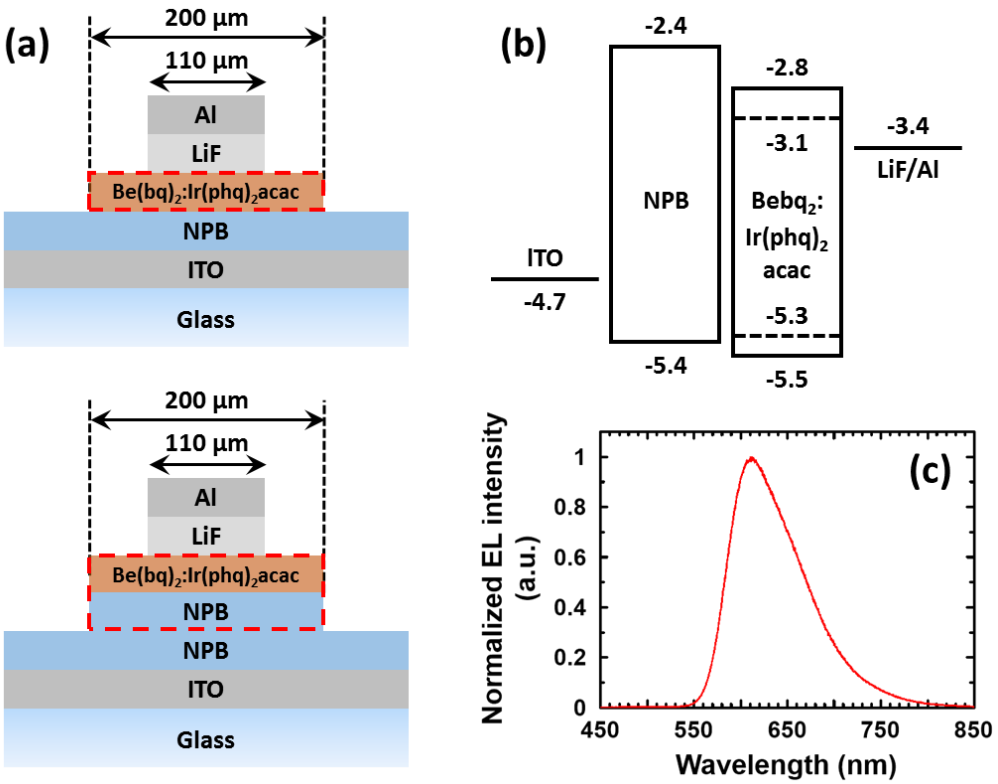

Figure 4.17 The device structure and the schematic energy-level diagram of the red phosphorescent OLED are shown in (a) and (b), respectively. (c) Normalized electroluminescence spectrum of the OLED (c).

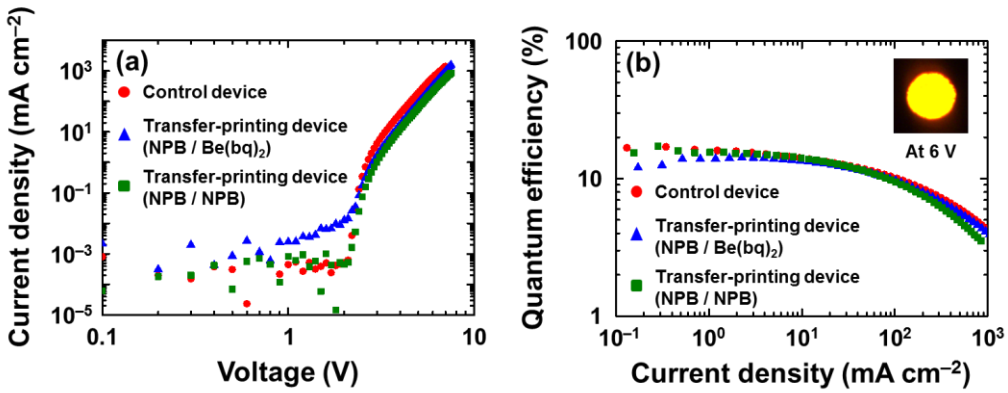

Figure 4.18 (a) Current density–voltage (*J*–*V*) and (b) external quantum efficiency–current density (η_{ext}–*J*) characteristics of organic light-emitting devices fabricated by transfer-printing 50 nm $Be(bq)_2$:$Ir(phq)_2acac$ patterns (blue triangles) and 5 nm NPB/50 nm $Be(bq)_2$:$Ir(phq)_2acac$ patterns (green squares) using PFPE-coated PDMS stamps with relief structures, compared with those of control devices where all layers were vacuum-deposited (red circles). The inset shows EL images of the device at 6 V.

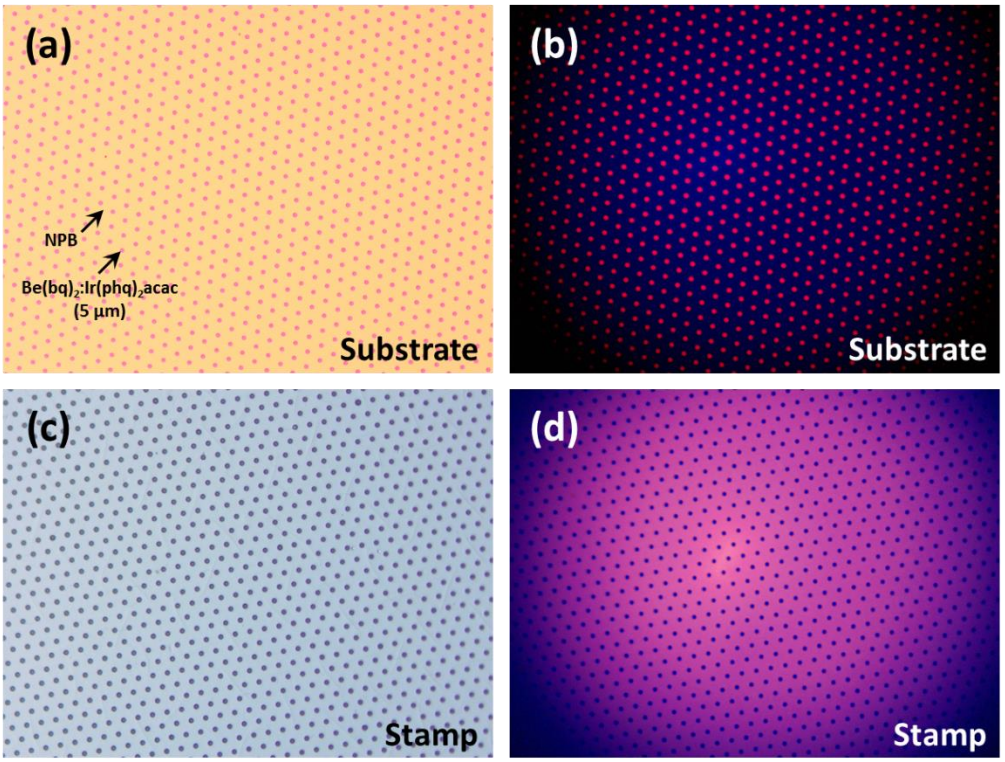

Figure 4.19 Organic patterns formed by a transfer-printing process. (a,c) Optical microscope images and (b,d) photoluminescence images of patterns of $Be(bq)_2$:$Ir(phq)_2acac$.

face but has the lower eqe characteristic is that the charge balance characteristic is improved.

4.2.6 Organic patterns formed by a transfer-printing process

To fabricate high-resolution OLEDs, the process of patterning organic small molecules into a feature size of several micrometers is essential. To show this, I transfer-printed a $Be(bq)_2$:$Ir(phq)_2$acac layer onto a NPB layer using the PFPE-coated PDMS stamp with relief structure of 5 μm. Fig. 4.19 is optical microscope image (a,c) and photoluminescence images (b,d) of the transfer-printed organic patterns. Not only the patterns were entirely formed on the NPB layer, but also the photoluminescence of the pattern did not exhibit degradation. When the stamp after the transfer process is observed, I can confirm that the organic material deposited on the relief structure completely transferred over the substrate.

4.3 Conclusions

Using the PFPE-coated stamps, I have fabricated two types of organic electronic devices — an Alq_3–NPB bilayer OLED and a NPB hole-only device with a bottom electrode composed of a graphene bilayer. The Alq_3–NPB OLED, fabricated by transferring a layer of Alq_3 from the PFPE-coated stamp onto a layer of NPB, has the performance comparable to a control device fabricated by sequential thermal evaporation in vacuum, which is, to

the best of my knowledge, the first demonstration that an organic–organic heterojunction formed by a layer transfer is electronically functional. Also, the NPB hole-only device with a graphene bilayer electrode deposited by sequential transfers of a graphene monolayer from a PFPE-coated stamp has a significantly enhanced *J–V* characteristic, compared to that fabricated using uncoated PDMS stamps.

In this Chapter, the stamps were unpatterned and the layers transferred from them were either unpatterned or patterned with a shadow mask to simplify the fabrication processes and focus on characterizing the properties of the transferred layers and the mechanically formed interfaces. In more practical applications requiring patterned active layers, they can be obtained by transferring them from PFPE-coated PDMS stamps with relief structures, which can be readily prepared by performing the dip-coating process described in this study with PDMS stamps molded from microfabricated masters [36] instead of PDMS stamps. As in previous demonstrations of stamp-based layer transfer [4,36], it is expected that the smallest feature size that can be obtained using the PFPE-coated PDMS stamp is primarily determined by the pattern resolution of the stamp, which is limited to be larger than ~1 μm by low Young's modulus of PDMS. A smaller feature size can be obtained by using a polymer with higher Young's modulus such as h-PDMS [37] instead of PDMS. In addition, as the feature size decreases below ~1 μm, it may be necessary to decrease the thickness of the PFPE layer, which can be controlled by adjusting the dipping time and/or the PFPE

concentration in the dipping solution.

Finally, I show that the characteristics of the phosphorescent OLEDs fabricated by transfer-printing of organic patterns are comparable to those of the control device, where all layers were thermally deposited in vacuum. I also demonstrated that the transfer-printing process using the PFPE-coated PDMS stamp can be used to provide a possible way for fabricating high-resolution OLEDs.

4.4 References

[1] W. M. Lackowski, P. Ghosh, and R. M. Crooks, Micron-scale patterning of hyperbranched polymer films by micro-contact printing, *J. Am. Chem. Soc.*, **121**, 1419 (1999).

[2] Y. Ka, H. Hwang, and C. Kim, Hybrid organic tandem solar cell comprising small-molecule bottom and polymer:fullerene top subcells fabricated by thin-film transfer, *Sci. Rep.*, **7**, 1942 (2017).

[3] H. Schmid, H. Wolf, R. Allenspach, H. Riel, S. Karg, B. Michel, and E. Delamarche, Preparation of metallic films on elastomeric stamps and their application for contact processing and contact printing, *Adv. Funct. Mater.*, **13**, 145 (2003).

[4] C. Kim, M. Shtein, and S. R. Forrest, Nanolithography based on patterned metal transfer and its application to organic electronic devices, *Appl. Phys. Lett*, **80**, 4051 (2002).

[5] K. S. Kim, Y. Zhao, H. Jang, S. Y. Lee, J. M. Kim, K. S. Kim, J. -H. Ahn, P. Kim, J. Y. Choi, and B. H. Hong, Large-scale pattern growth of graphene films for stretchable transparent electrodes, *Nature*, **457**, 706 (2009).

[6] G. -H. Lee, Y. -J. Yu, X. Cui, N. Petrone, C. -H. Lee, M. S. Choi, D. -Y. Lee, C. Lee, W. J. Yoo, K. Watanabe, T. Taniguchi, C. Nuckolls, P. Kim, and J. Hone, Flexible and transparent MoS_2 field-effect transistors on hexagonal boron nitride-graphene hetero-structures, *ACS Nano*, **7**, 7931 (2013).

[7] G. Plechinger, F. Mooshammer, A. Castellanos-Gomez, G. Steele, C. Schu¨ller, and T. Korn, Optical spectroscopy of interlayer coupling in artificially stacked MoS_2 layers, *2D Mater*., **2**, 034016 (2015).

[8] L. Kim, P. O. Anikeeva, S. A. Coe-Sullivan, J. S. Steckel, M. G. Bawendi, and V. Bulović, Contact printing of quantum dot light-emitting devices, *Nano Lett*., **8**, 4513 (2008).

[9] T. -H. Kim, K. -S. Cho, E. K. Lee, S. J. Lee, J. Chae, J. W. Kim, D. H. Kim, J. -Y. Kwon, G. Amaratunga, S. Y. Lee, B. L. Choi, Y. Kuk, J. M. Kim, and K. Kim, Full-colour quantum dot displays fabricated by transfer printing, *Nat*. *Photonics*, **5**, 176 (2011).

[10] T. Kraus, L. Malaquin, H. Schmid, W. Riess, N. D. Spencer, and H. Wolf, Nanoparticle printing with single-particle resolution, *Nat*. *Nanotechnol*., **2**, 570 (2007).

[11] V. Santhanam and R. P. Andres, Microcontact printing of uniform nanoparticle arrays, *Nano Lett*., **4**, 41 (2004).

[12] T. Takahashi, K. Takei, J. C. Ho, Y. -L. Chueh, Z. Fan, and A. Javey, Monolayer resist for patterned contact printing of aligned nanowire arrays, *J. Am. Chem. Soc*., **131**, 2102 (2009).

[13] C. H. Lee, D. R. Kim, and X. Zheng, Fabricating nanowire devices on diverse substrates by simple transfer-printing methods, *Proc. Natl. Acad. Sci. U.S.A*., **107**, 9950 (2010).

[14] C. M. Bruinink, C. Nijhuis, M. Peter, B. Dordi, O. Crespo-Biel, T. Auletta, A. Mulder, H. Schonherr, G. Vancso, J. Huskens, and D. Reinhoudt, Supramolecular microcontact printing and dip-pen nanolithography on molecular printboards, *Chem. Eur. J*., **11**, 3988 (2005).

[15] S. A. Lange, V. Benes, D. P. Kern, J. H. Ho¨rber, and A. Bernard, Microcontact printing of DNA molecules, *Anal. Chem*., **76**, 1641 (2004).

[16] S. J. Kang, B. Kim, K. S. Kim, Y. Zhao, Z. Chen, G. H. Lee, J. Hone, P. Kim, and C. Nuckolls, Inking elastomeric stamps with micro-patterned, single layer graphene to create high-performance OFETs, *Adv. Mater*., **23**, 3531 (2011).

[17] A. Rizzo, M. Mazzeo, M. Palumbo, G. Lerario, S. D'Amone, R. Cingolani, and G. Gigli, Hybrid light-emitting diodes from microcontact-printing double-transfer of colloidal semiconductor CdSe/ZnS quantum dots onto organic layers, *Adv. Mater*., **20**, 1886 (2008).

[18] A. Carlson, A. M. Bowen, Y. Huang, R. G. Nuzzo, and J. A. Rogers, Transfer printing techniques for materials assembly and micro/nanodevice fabrication, *Adv*. *Mater*, **24**, 5284 (2012).

[19] S. Yunus, C. de Crombrugghe de Looringhe, C. Poleunis, and A. Delcorte, Diffusion of oligomers from polydimethylsiloxane stamps in microcontact printing: surface analysis and possible application, *Surf*. *Interface Anal*., **39**, 922 (2007).

[20] J. Song, F. -Y. Kam, R. -Q. Png, W. -L. Seah, J. -M. Zhuo, G. -K. Lim, P. K. Ho, and L. -L. Chua, A general method for transferring graphene onto soft surfaces, *Nat*. *Nanotechnol*., **8**, 356 (2013).

[21] K. Glasmästar, J. Gold, A. -S. Andersson, D. S. Sutherland, and B. Kasemo, Silicone transfer during microcontact printing, *Langmuir*, **19**, 5475 (2003).

[22] S. Cha, M. Cha, S. Lee, J. H. Kang, and C. Kim, Low-temperature, dry transfer-printing of a patterned graphene monolayer, *Sci*. *Rep*., **5**, 17877 (2015).

[23] C. Kim, Y. Cao, W. O. Soboyejo, and S. R. Forrest, Patterning of active organic materials by direct transfer for organic electronic devices, *J*. *Appl*. *Phys*., **97**, 113512 (2005).

[24] J. H. Beck, R. A. Barton, M. P. Cox, K. Alexandrou, N. Petrone, G. Olivieri, S. Yang, J. Hone, and I. Kymissis, Clean graphene electrodes on organic thin-film devices via orthogonal fluorinated chemistry, *Nano Lett*., **15**, 2555 (2015).

[25] E. Lee, J. Kim, and C. Kim, Polymer tandem photovoltaic cells with molecularly intimate interfaces achieved by a thin-film transfer technique, *Sol. Energy Mater. Sol. Cells*, **105**, 1 (2012).

[26] K. R. Seddon, A. Stark, and M. -J. Torres, Influence of chloride, water, and organic solvents on the physical properties of ionic liquids, *Pure Appl. Chem.*, **72**, 2275 (2000).

[27] K. Shoyama, W. Sato, Y. Guo, and E. Nakamura, Effects of water on the forward and backward conversions of lead(II) iodide to methylammonium lead perovskite, *J. Mater. Chem. A*, **5**, 23815 (2017).

[28] P. A. Losio, R. U. Khan, P. Gu¨nter, B. K. Yap, J. S. Wilson, and D. D. Bradley, Singlet excimer electroluminescence within N,N′-di-1-naphthalenyl-N,N′-diphenyl-[1,1′-biphenyl]-4,4′-diamine based Diodes, *Appl. Phys. Lett.*, **89**, 041914 (2006).

[29] H. Sung, J. Lee, K. Han, J. -K. Lee, J. Sung, D. Kim, M. Choi, and C. Kim, Controlled positioning of metal nanoparticles in an organic light-emitting device for enhanced quantum efficiency, *Org. Electron.*, **15**, 491 (2014).

[30] C. E. Packard, K. E. Aidala, S. Ramanan, and V. Bulović, Patterned removal of molecular organic films by diffusion, *Langmuir*, **27**, 9073 (2011).

[31] C. F. Madigan and V. Bulović, Solid state solvation in amorphous organic thin films, *Phys. Rev. Lett.*, **91**, 247403 (2003).

[32] M. Xu and J. Xu, Real-time visualization of thermally activated degradation of the ITO/CuPC/NPB/Alq_3 stack used in one of the organic light-

emitting diodes, *J*. *Phys*. *D*: *Appl*. *Phys*., **37**, 1603 (2004).

[33] R. Hawaldar, P. Merino, M. Correia, I. Bdikin, J. Grácio, J. Méndez, J. Martín-Gago, M. K. Singh, Large-area high-throughput synthesis of monolayer graphene sheet by hot filament thermal chemical vapor deposition, *Sci*. *Rep*., **2**, 682, (2012).

[34] K. Xiao, W. Deng, J. K. Keum, M. Yoon, I. V. Vlassiouk, K. W. Clark, A. -P. Li, I. I. Kravchenko, G. Gu, E. A. Payzant, B. G. Sumpter, S. C. Smith, J. F. Browning, and D. B. Geohegan, Surface-induced orientation control of CuPc molecules for the epitaxial growth of highly ordered organic crystals on graphene, *J*. *Am*. *Chem*. *Soc*., **135**, 3680 (2013).

[35] J. Meyer, P. R. Kidambi, B. C. Bayer, C. Weijtens, A. Kuhn, A. Centeno, A. Pesquera, A. Zurutuza, J. Robertson, and S. Hofmann, Metal oxide induced charge transfer doping and band alignment of graphene electrodes for efficient organic light emitting diodes, *Sci*. *Rep*., **4**, 5380 (2014).

[36] C. Kim and S. R. Forrest, Fabrication of organic light-emitting devices by low-pressure cold welding, *Adv*. *Mater*., **15**, 541 (2003).

[37] T. W. Odom, J. C. Love, D. B. Wolfe, K. E. Paul, and G. M. Whitesides, Improved pattern transfer in soft lithography using composite stamps, *Langmuir*, **18**, 5314 (2002).

Chapter 5 Conclusions

5.1 Summary

Poly(dimethylsiloxane) (PDMS) is not a perfect material for transferring various materials. However, many researchers are using PDMS without sufficient consideration about whether it is going to be an issue for their works. Furthermore, the following serious problems with it have been overlooked: absorbing organic small molecules and remaining uncured oligomers of the PDMS on a target substrate. These problems are especially serious when the transferred layer is located inside an electronic device.

In this study, I introduced advantageous properties of a perfluoropolyether (PFPE) thin layer chemically anchored on a PDMS surface by a simple dip-coating process for neatly overcoming above limitations in a transfer process. The most notable feature of the PFPE layer is not only that it effectively blocks the diffusion of molecules in and out of the stamp but also that it does not itself remain as a residue. All of this is possible due to that the PFPE coating has strong adhesion to the PDMS surface and strong internal cohesion by a condensation reaction between them, for which other coating methods fail. Using a PFPE-coated PDMS stamp, I show that the quality of electronic functions at the transfer-bonded interface and the cleanliness of transferred layers are remarkably high. These results indicate that the PFPE-coated stamp possesses

the potential for expanding the applicability of patterning depositions of various materials with high-quality interfaces.

To summarize it more specifically, in *Chapter 2*, I have developed a low temperature, dry process capable of transfer-printing a patterned graphene monolayer grown on Cu foil on a target substrate. Two features distinct from the conventional wet-transfer method [1] — the use of a support layer composed of Au, instead of poly(methyl methacrylate), and the decrease in surface tension of the liquid bath on which a graphene–Au bilayer floats — allow one to obtain a graphene monolayer on a PDMS stamp without defects that would otherwise arise. Subsequently, the graphene is transfer-printed from the stamp onto a target substrate. In addition, with pre-transfer patterning of graphene on Cu foil using conventional patterning processes, this technique is capable of creating graphene monolayer patterns on materials that are easily degraded when exposed to high-temperature processes, organic solvents, or aqueous chemicals. Additionally, I found that the top surface of the transferred graphene was seriously contaminated by oligomers of the stamp. To solve this, in *Chapter 3*, I have developed a hybrid stamp composed of a PDMS bulk and PFPE coating obtained by simple dip-coating inducing a condensation reaction between PDMS and PFPE molecules as well as that between the adjacent PFPE molecules. The PFPE-coated stamp has the following properties ideal for material transfer techniques: the ability to prevent diffusion of small molecules, low surface energy, strong internal cohesion of the PFPE layer, and strong adhesion at the PFPE–PDMS interface. In *Chapter 4*, using the PFPE-coated

PDMS stamp, I fabricated two types of organic electronic devices that have a mechanically bonded interface in their interiors, representative of applications where, in addition to layer transfer itself, high quality of the transfer-bonded interface and a high degree of cleanliness of the top surface of the transferred layer are required. From this, the effectiveness and versatility of the PFPE-coated stamp are demonstrated. Additionally, I show that the characteristics of the phosphorescent OLEDs fabricated by transfer-printing of organic patterns are comparable to those of the control device, where all layers were thermally deposited in vacuum. This result is the first demonstration of fabricating a highly efficient phosphorescent OLED, which is composed of a commercially useful structure, by forming a pattern through a contact transfer process. I also demonstrated that the transfer-printing process using the PFPE-coated PDMS stamp can be used to provide a possible way for fabricating high-resolution organic patterns.

5.2 Further studies

5.2.1 Further applications of a contact-transfer process using PFPE-coated PDMS stamps

One of the most practical applications of using the PFPE-coated PDMS stamps in contact transfer is repairing damaged organic patterns in pixels on a high-resolution OLED panel. The following scenario can solve damages of organic layers on an OLED panel that can occur in the process of thermally depositing

the organic material. The damaged patterns after depositing of all the organic layers can be removed by absorbing them using the PDMS or by etching them using reactive ion etch in O_2. After that process is completed, thermally deposited organic layers on a PFPE-coated PDMS stamp are transfer-printed onto the region of the removed organic layers. This method is very cost effective to repair the locally generated defects on organic layers because it eliminates the need to throw away the entire OLED panel fabricated or to put the panel into an organic deposition process.

The PFPE-coated PDMS stamp demonstrated in this work is expected to be widely used in fabricating devices or systems composed of materials that can easily be degraded by a high temperature or wet process. Examples include integrated organic electronic devices, hybrid devices composed of organic semiconductors and inorganic materials such as QDs, NPs, and nanowires, and practical devices based on van der Waals heterostructures of 2D materials [2−7]. In addition, coating of PDMS with a PFPE layer achieved by simple dip-coating may contribute to the field of microfluidics such as micro-reactors based on organic solvents [8] and cell culture systems [9] by eliminating the undesired properties of bare PDMS.

5.2.2 Further modification of a PFPE-coated PDMS stamp

When organic patterns below feature size of 5 micrometers are required, they can be easily obtained using the PFPE-coated PDMS stamp with smaller relief structure is primarily determined by the pattern resolution of the stamp, which

is ~1 μm limited by low Young's modulus of PDMS. For the fundamental applications such as nano LEDs [10] and single-photon LEDs [11], a feature size of sub-micrometer can be obtained by using a polymer with higher Young's modulus such as *h*-PDMS [12] instead of PDMS. In addition, as the feature size decreases below ~1 μm, it may be necessary to decrease the thickness of the PFPE layer, which can be controlled by adjusting the dipping time and/or the PFPE concentration in the dipping solution.

The low surface energy of the PFPE-thin layer on the PDMS stamp is not suitable for all of the reliable transfer-printing process. For example, there are studies that low surface energy stamps are not suitable for printing of hydrophilic molecules from polar solvents, including bio-molecule like DNA's [13]. I note that PFPEs in this demonstration can be considered as a representative polymer for the low-surface-energy and diffusion-blocking layer satisfying the following conditions — it must be terminated as ethoxysilane functions and can be self-assembly form a dense and continuous film on the PDMS stamp without diffusing into the stamp — and hence can be replaced by other polymer when a film on the stamp with a higher surface energy in required.

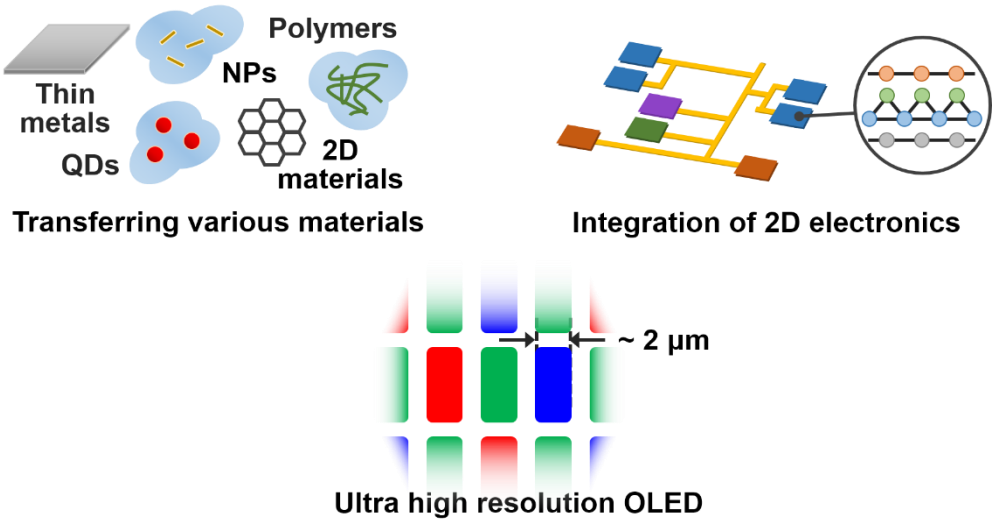

Figure 5.1. Summarization of further studies

5.3 References

[1] X. Li, W. Cai, J. An, S. Kim, J. Nah, D. Yang, R. Piner, A. Velamakanni, I. Jung, E. Tutuc, S. K. Banerjee, L. Colombo, and R. S. Ruoff, Large-area synthesis of high-quality and uniform graphene films on copper foils, *Science*, **324**, 1312 (2009).

[2] L. Kim, P. O. Anikeeva, S. A. Coe-Sullivan, J. S. Steckel, M. G. Bawendi, and V. Bulović, Contact printing of quantum dot light-emitting devices, *Nano Lett*., **8**, 4513 (2008).

[3] T. -H. Kim, K. -S. Cho, E. K. Lee, S. J. Lee, J. Chae, J. W. Kim, D. H. Kim, J. -Y. Kwon, G. Amaratunga, S. Y. Lee, B. L. Choi, Y. Kuk, J. M. Kim, and K. Kim, Full-colour quantum dot displays fabricated by transfer printing, *Nat*. *Photonics*, **5**, 176 (2011).

[4] J. Li, L. Xu, C. W. Tang, and A. A. Shestopalov, High-resolution organic light-emitting diodes patterned via contact printing, *ACS Appl*. *Mater*. *Interfaces*, **8**, 16809 (2016).

[5] H. Jin and J. C. Sturm, Super-high-resolution transfer printing for full-color OLED display patterning, *J*. *Soc*. *Inf*. *Disp*., **18**, 141 (2010).

[6] B. V. Lotsch, Vertical 2D heterostructures, *Annu*. *Rev*. *Mater*. *Res*., **45**, 85 (2015).

[7] P. J. Jeon, Y. T. Lee, J. Y. Lim, J. S. Kim, D. K. Hwang, and S. Im, Black phosphorus-zinc oxide nanomaterial heterojunction for p-n diode and junction field-effect transistor, *Nano Lett*., **16**, 1293 (2016).

[8] J. N. Lee, C. Park, and G. M. Whitesides, Solvent compatibility of poly (dimethylsiloxane)-based microfluidic devices, *Anal. Chem.*, **75**, 6544 (2003).

[9] L. J. Millet, M. E. Stewart, J. V. Sweedler, R. G. Nuzzo, and M. U. Gillette, Microfluidic devices for culturing primary mammalian neurons at low densities, *Lab Chip*, **7**, 987 (2007).

[10] M. Mikulics and H. Hardtdegen, Nano-LED array fabrication suitable for future single photon lithography, *Nanotechnology*, **26**,185302 (2015).

[11] A. Lohrmann, S. Pezzagna, I. Dobrinets, P. Spinicelli, V. Jacques, J. -F. Roch, J. Meijer, and A. M. Zaitsev, Diamond based light-emitting diode for visible single-photon emission at room temperature, *Appl. Phys. Lett.*, **99**, 251106 (2011).

[12] T. W. Odom, J. C. Love, D. B. Wolfe, K. E. Paul, and G. M. Whitesides, Improved pattern transfer in soft lithography using composite stamps, *Langmuir*, **18**, 5314 (2002).

[13] S. A. Lange, V. Benes, D. P. Kern, J. H. Ho¨rber, and A. Bernard, Micro-contact printing of DNA molecules, *Anal. Chem.*, **76**, 1641 (2004).

요 약 (국문초록)

낮은 표면 에너지와 확산 방지층으로 코팅된 하이브리드 도장의 개발 및 유기전자소자 제작에 대한 그 응용

차 석 균
융합과학부 나노융합전공
융합과학기술대학원
서울대학교

폴리디메틸실록산(PDMS)은 다양한 재료를 최종 기판으로 옮길 때 사용하는 소재로써 매우 널리 사용되어 왔다. 그러나 많은 연구자들이 오랫동안 이와 관련된 많은 연구들을 진행했음에도 불구하고, PDMS 도장 기반의 층 또는 패턴 전사 공정은 기계적으로 접합된 계면과 전사된 물질의 청결이 중요하지 않은 응용분야에서만 제한적으로 진행되었다. 이는 다음과 같은 PDMS 도장의 불리한 성질에 기인한다: (i) PDMS의 내부로 유기소분자의 흡수, (ii) PDMS의 경화되지 않은 올리고머에 의한 이동된 층의 오염. 이러한 문제가 해결된다면, 도장을 이용한 패턴된 물질 증착은 기존의 쉐도우 마스크 공정과 진공증착 공정으로 제작되는 유기전자소자 분야에서 다양하고 새로운 구조 및 소자를 제작할 수 있을 것이다.

본 연구에서는 PDMS와 퍼플루오르폴리에테르(PFPE) 분자뿐만 아니라 인접한 PFPE 분자들 사이의 응축 반응에 의해 유도된 PDMS 벌크 및 PFPE 코팅 층으로 구성된 하이브리드 도장을 개발하였다. PDMS 도장 위에 있는 PFPE 코팅 층의 핵심 역할은 PDMS의 경화되지 않은 실록산 올리고머가 전사 될 층 위로 이동하는 것을 막고 전사 될 층의 물질이 도장 내부로 흡수되는 것을 방지하는 것이다. 박막전사 과정에서 가지는 PFPE로 코팅된 PDMS 도장의 효율성과 다 기능성은 전사 공정으로 형성된 유기—유기 계면이 포함된 유기발광 다이오드와 상기 도장으로부터 전사된 그래핀 이중층으로 구성된 하부 전극을 갖는 유기 hole-only 소자를 제작함으로써 증명되었다. 그 결과 기계적으로 결합된 계면의 품질은 열 증발에 의해 형성된 동일한 계면의 품질과 비교하여 비슷한 수준이었다. 또한, 도장과 접촉한 전사 층의 상부 표면은 전하 캐리어를 주입 및 추출하기에 충분하였다. 본 연구에서 개발된 PFPE가 코팅된 도장은 고온 또는 습식 공정을 사용하여 구현하기가 특히 어려운 전자장치 또는 전자소자 제작에 널리 사용될 수 있을 것으로 예상된다. 가장 흥미로운 예는 가상 현실 어플리케이션에 필요하지만 현재의 쉐도우 마스크 기반 패터닝을 사용하여 제조하기 어려운 스마트 폰의 현재 디스플레이보다 훨씬 높은 해상도를

갖춘 풀 컬러 유기발광소자 (OLED) 디스플레이이다.

주요어: PDMS 도장, PFPE 코팅, 유기소분자 패턴 전사, 확산 차단층, 이종접합 계면

학 번: 2013-31258